Title
Molecular mechanisms of macrophage phagocytic decision-making

Author
Suter, Emily Coleen

Publication Date
2021

Peer reviewed|Thesis/dissertation

Molecular mechanisms of macrophage phagocytic decision-making

By

Emily Coleen Suter

A dissertation submitted in partial satisfaction of the

requirements for the degree of

Doctor of Philosophy

in

Bioengineering

in the

Graduate Division

of the

University of California, Berkeley

Committee in charge:

Professor Daniel A. Fletcher, Chair
Professor Ellen Robey
Professor Kole Roybal

Fall 2021

Abstract

Molecular mechanisms of macrophage phagocytic decision-making

By

Emily Coleen Suter

Doctor of Philosophy in Bioengineering

University of California, Berkeley

Professor Daniel A. Fletcher, Chair

Controlled and selective activation of immune cells is critical for ridding the body of disease-causing threats while limiting damage to healthy cells and maintaining normal tissue function. Though immune signaling can be initiated and mediated by soluble factors, many key immune responses require direct contact with a target to both evaluate the threat that it poses and initiate attack, if necessary. Macrophage phagocytosis is one such example of a contact-dependent effector function, in which macrophage Fc receptors (FcRs) directly engage with antigen-bound antibodies on a target cell. This drives FcR phosphorylation of intracellular ITAM motifs and initiates downstream signaling, ultimately leading to actin polymerization, membrane remodeling, and target engulfment. However, simultaneous to engagement of FcRs, inhibitory receptors—such as SIRPα—can bind their ligand on a target, shutting down phagocytosis through their intracellular ITIM motifs, despite the presence of activating signaling. While important for preventing auto-immune responses, these inhibitory checkpoints also reduce efficacy of tumor-targeting antibodies and other immunotherapies.

In the first Chapter of this dissertation, I probe how macrophages integrate contradictory signals from activating FcR-antibody and inhibitory SIRPα-CD47 interactions. Using reconstituted tumor cell-like target particles, I conclude that macrophage phagocytosis decisions are dictated by the ratio of activating ligand to inhibitory ligand over a range of absolute molecular densities. Lowering the antibody:CD47 reduces FcR phosphorylation due to inhibitory phosphatases recruited to CD47-bound SIRPα, thus preventing downstream phagocytic signaling from proceeding. I demonstrate that this ratiometric signaling is important in tumor cell phagocytosis and that it can be manipulated by blocking SIRPα engagement, demonstrating that this decision-making paradigm may be important for controlling macrophage phagocytosis in cancer immunotherapy.

In the next two Chapters, I discuss two strategies for probing and manipulating signaling at the macrophage-target interface. First, I probe the importance of ITAM and ITIM multiplicity on phagocytic receptors. By creating panels of synthetic receptors containing 0-4 ITAMs each, I conclude that increasing signaling motifs beyond two ITAMS does little to enhance phagocytosis and that additional ITAMs in series do not decrease inhibitory signaling. Second, I propose a

novel therapeutic strategy that leverages spatial reorganization of the phagocytic interface to overcome inhibitory signaling. Using synthetic receptors, I show that tethering a protein with a short extracellular domain to one with a large extracellular domain can lead to exclusion of the short protein from a cell interface due to size-dependent segregation of the tall protein. I then propose a system for linking short SIRPα to tall CD45 to drive exclusion of SIRPα from a macrophage-target interface and reduce inhibitory signaling.

Next, I zoom out from the single macrophage-target interface to look more wholistically at macrophage signal integration. Here, I ask whether engagement with many inhibitory targets can impact phagocytosis of activating targets. I conclude that high levels of SIRPα-CD47 engagement does not significantly impact phagocytosis of other targets, highlighting how macrophage decisions are made locally.

Lastly, in the final Chapter of this dissertation, I zoom into the phagocytic interface to examine phosphorylation of ITAM motifs at a single receptor level. ITAMs contain two tyrosines that become phosphorylated and subsequently engage with Syk kinase, and the phosphorylation state of the ITAM alters Syk binding kinetics. By using variation in these binding kinetics to readout ITAM state, I present a strategy for spatial mapping of ITAM phosphorylation. With ITAM phosphopeptides, I demonstrate the ability to kinetically distinguish between ITAM phosphorylation states. I then show how this kinetic variation can be implemented for mapping phosphorylation of endogenous FcRs in macrophages.

Table of Contents

Chapter 1: Introduction

Immune cell-target cell interfaces

Immune cells protect tissues and organs throughout the body against the destructive and toxic effects of pathogens and diseased cells. Importantly, the ability of the human immune system to reliably and accurately discern between healthy tissues and potentially dangerous foreign or diseased cells is critical to maintaining normal tissue function while ridding the body of threats (Charles A Janeway et al., 2001).

Initiation of immune response broadly occurs through one of two mechanisms: via soluble factors or direct contact (Bulati et al., 2020; Xie et al., 2013). Secreted signaling molecules from adjacent tissues—specifically cytokines and chemokines—can drive changes in immune receptor expression, activation, and cell migration to promote immune response. Alternatively, small molecules, proteins, or nucleic acids directly from a pathogen may also initiate immune response.

However, many critical immune effector functions require direct contact between an immune cell and a target cell or pathogen (Dustin, 2007, 2014). In general, this direct contact is facilitated by immune receptors engaging their complementary ligand on the target surface, which brings the immune cell and target membranes in close apposition to each other and creates a complex signaling hub through which the immune cell molecularly evaluates the threat to the target.

Macrophage phagocytosis

One example of contact-dependent effector functions is the process of macrophage phagocytosis. Macrophages—a type of innate immune cell that resides in most tissues—bind directly to antibody-opsonized particles through their Fc receptors (FcRs). Upon antibody engagement and clustering, FcRs become phosphorylated, which triggers downstream signaling, actin polymerization, and membrane remodeling (Flannagan et al., 2012). Formation of this phagocytic cup then further promotes FcR engagement such that the membrane extends around the target, ultimately leading to full target internalization and degradation.

However, in addition to activating FcRs, macrophage-target cell contacts can also include or be facilitated by inhibitory receptors, such as SIRPα, that prevent phagocytosis from occurring. These receptors are critical for preventing aberrant immune activation and avoiding auto-immune diseases (Logtenberg et al., 2020). Yet ligands to these inhibitory receptors have also been shown to be upregulated in various tumor types, enabling cancer cells to evade destruction by hijacking immune checkpoints and preventing activation. Yet, despite the crucial role of these receptors in modulating immune response and despite their growing importance for immunotherapeutic strategies, understanding how inhibitory receptors halt effector functions

such as phagocytosis is still very much an area of active research (Morrissey et al., 2020; Tsai et al., 2010; Tsai & Discher, 2008).

Cell-cell interfaces as signaling hubs

Engagement of immune receptors to their ligands on the target surface promotes immune-target engagement, formation of contact between two cells, and enrichment of immune receptors at the interface. Importantly, extracellular engagement of receptors also drives intracellular enrichment of signaling domains at the macrophage target interface, creating signaling hubs through which phagocytosis decisions are made (Belardi et al., 2020).

Two types of signaling domains primarily contribute to these decisions. First, immunoreceptor tyrosine-based activation motifs (ITAMs) on FcRs contain two tyrosine residues that, upon phosphorylation, bind to the cytoplasmic kinase Syk and initiate downstream phagocytic signaling (Crowley et al., 1997). Second, the immunoreceptor tyrosine-based inhibition motifs (ITIMs) on SIRPα contain a single tyrosine residue that recruits various phosphatases—most notably, Shp1—upon phosphorylation (Barclay & van den Berg, 2014).

While recent studies have advanced mechanistic understanding of activation (Bakalar et al., 2018; Freeman et al., 2016), ITIM signaling mechanisms and how ITIMs directly inhibit ITAM-mediated phagocytosis is still poorly characterized (Barrow & Trowsdale, 2006; Huang et al., 2003). What rules govern how many inhibitory molecules are required or where they must be located to shut down activation? Understanding where, when, and how contradictory phagocytic signals are integrated is critical for both mechanistic understanding of immune signaling and for manipulating and harnessing the inhibitory axis in clinical immunotherapeutic strategies.

Furthermore, it is not clear what role ITAM and ITIM multiplicity play in signal potency and signal integration within these hubs at macrophage-target interfaces. FcRs only have one ITAM per cytoplasmic chain, in contrast to some other ITAM-containing receptors such as the T-cell receptor complex, which has multiple chains with 3 ITAMs each. SIRPα and other inhibitory receptors, including multiple members of the sialic acid-binding SIGLEC family, contain multiple ITIM domains in their cytoplasmic tails (Crocker et al., 2007). What role this multiplicity plays in phagocytosis is largely unexplored, but a better understanding could help create a set of design rules useful in the budding field of engineering macrophages as cell therapies.

Spatial organization of phagocytosis

Beyond simply the presence and enrichment of ITAM and ITIM signaling domains, the local organization of molecules within a cell-cell contact can play a key role in signaling. Previous work from our lab demonstrated the importance of short antigen height in phagocytic interfaces, due to the requirement that the tall phosphatase CD45 be excluded for robust activation (Bakalar

et al., 2018). Interestingly, SIRPα also facilitates a short intermembrane height when engaging with its ligand, CD47, raising the question of whether it requires a similar separation from CD45 to be productively phosphorylated. This further prompts the question of whether co-localization of activating and inhibitory receptors, perhaps in part facilitated by CD45 exclusion, is important to understanding ITAM-ITIM signal competition.

Examination of the biophysical properties of molecules at immune interfaces also presents the potential to exploit spatial organization for therapeutic means. Movement of the tall extracellular domains from a short intermembrane gap could be harnessed to manipulate the location of other molecules as well. More specifically, linkage of a short inhibitory protein to a tall extracellular domain could remove inhibitory signaling from immune interfaces, rendering them less potent. Further work on biophysical characterization of immune interfaces as well as development of therapeutic molecules is needed to leverage this as a therapeutic strategy.

Experimental evidence to date indicates that spatial organization of activating and inhibitory receptors ultimately dictates the ability of their ITAMs and ITIMs to become and stay in a phosphorylated state. But exactly when and where tyrosines in these different signaling domains become phosphorylated within an expanding phagocytic interface is not well characterized. Development of a spatial map of phosphorylation could provide interesting insight into the connection between receptor clustering, phosphorylation, and signal potency.

Additionally, spatial organization of activation and inhibition is potentially important not just at a local interface but across the entirety of a cell. Macrophages within dense tissue can potentially engage with multiple adjacent cells simultaneously, and the ability to discriminate between cells and act selectively on only certain cells is important to maintaining proper tissue homeostasis. However, whether cellular interfaces impact macrophage signal interpretation and decision-making towards another interface is a completely unexplored question.

Reconstitution as strategy to model complex cellular systems

Many topics raised here involve probing signaling and organization at extremely complex cell-cell interfaces, making it difficult to isolate variables and understand mechanistic contributions of specific molecules. The ability to pare down these complex biological systems to controllable parts is critical to correctly identifying and characterizing key drivers of cellular behavior. *In vitro* reconstitution—the process of recreating simplified biological systems from synthetic or purified components—provides a powerful tool to quantitatively test molecular hypotheses (Liu & Fletcher, 2009). For example, reconstitution of a target cell-like particle, consisting of a glass bead coated a mobile lipid bilayer and functionalized with tumor markers, enables precise control of surface composition to tease out signaling interactions (Joffe et al., 2020). Additionally, other synthetic strategies, such as use of artificial receptors in live cells, or reductionist techniques, like the use of giant plasma membrane vesicles to emulate plasma membranes, enable the study of important immune processes in a more controlled and precise ways that enable mechanistic understanding.

Scope of this dissertation

This dissertation delves into many of the questions raised here regarding macrophage phagocytic signaling and macrophage-target interfaces. In Chapter 2, I explore what rules govern macrophage activation-inhibition signal integration, focusing on the interplay between activating FcR-antibody interactions and inhibitory SIRPα-CD47 interactions. I demonstrate that the ratio of antibody to CD47 is a key determinant to phagocytic efficiency because of its ability to shift relative ITAM:ITIM enrichment and the downstream competition between signaling molecules. In Chapter 3, I manipulate ITAM and ITIM number and order within a single receptor chain, demonstrating that additional ITAMs in series have little impact on phagocytic efficiency. In Chapter 4, I discuss the impact of peripheral inhibitory interactions on local phagocytic decision making, concluding that at least in the short term, the impact of these interactions is weak. In Chapter 5, I explore our ability to spatially manipulate molecular organization within an immune interface using inducible dimerization. In Chapter 6, I propose a single molecule kinetics strategy and present initial results on spatial mapping of ITAM phosphorylation within a phagocytic interface. In aggregate, this research represents a focused examination of the molecular mechanisms and spatial dependencies of phagocytic signaling and decision-making in macrophages that advance basic understanding and identify possible directions for new therapeutic strategies.

References

Bakalar, M. H., Joffe, A. M., Schmid, E. M., Son, S., Podolski, M., & Fletcher, D. A. (2018). Size-Dependent Segregation Controls Macrophage Phagocytosis of Antibody-Opsonized Targets. *Cell*, *174*(1), 131-142.e13. https://doi.org/10.1016/j.cell.2018.05.059

Barclay, A. N., & van den Berg, T. K. (2014). The Interaction Between Signal Regulatory Protein Alpha (SIRPα) and CD47: Structure, Function, and Therapeutic Target. *Annual Review of Immunology*, *32*(1), 25–50. https://doi.org/10.1146/annurev-immunol-032713-120142

Barrow, A. D., & Trowsdale, J. (2006). You say ITAM and I say ITIM, let's call the whole thing off: The ambiguity of immunoreceptor signalling. *European Journal of Immunology*, *36*(7), 1646–1653. https://doi.org/10.1002/eji.200636195

Belardi, B., Son, S., Felce, J. H., Dustin, M. L., & Fletcher, D. A. (2020). Cell–cell interfaces as specialized compartments directing cell function. *Nature Reviews Molecular Cell Biology*, *21*(12), 750–764. https://doi.org/10.1038/s41580-020-00298-7

Bulati, M., Miceli, V., Gallo, A., Amico, G., Carcione, C., Pampalone, M., & Conaldi, P. G. (2020). The Immunomodulatory Properties of the Human Amnion-Derived Mesenchymal Stromal/Stem Cells Are Induced by INF-γ Produced by Activated Lymphomonocytes and Are Mediated by Cell-To-Cell Contact and Soluble Factors. *Frontiers in Immunology*, *11*, 54. https://doi.org/10.3389/fimmu.2020.00054

Charles A Janeway, J., Travers, P., Walport, M., & Shlomchik, M. J. (2001). Principles of innate and adaptive immunity. *Immunobiology: The Immune System in Health and Disease. 5th Edition*. https://www.ncbi.nlm.nih.gov/books/NBK27090/

Crocker, P. R., Paulson, J. C., & Varki, A. (2007). Siglecs and their roles in the immune system. *Nature Reviews Immunology*, *7*(4), 255–266. https://doi.org/10.1038/nri2056

Crowley, M. T., Costello, P. S., Fitzer-Attas, C. J., Turner, M., Meng, F., Lowell, C., Tybulewicz, V. L. J., & DeFranco, A. L. (1997). A Critical Role for Syk in Signal Transduction and Phagocytosis Mediated by Fcγ Receptors on Macrophages. *The Journal of Experimental Medicine*, *186*(7), 1027–1039.

Dustin, M. L. (2007). Cell adhesion molecules and actin cytoskeleton at immune synapses and kinapses. *Current Opinion in Cell Biology*, *19*(5), 529–533. https://doi.org/10.1016/j.ceb.2007.08.003

Dustin, M. L. (2014). The immunological synapse. *Cancer Immunology Research*, *2*(11), 1023–1033. https://doi.org/10.1158/2326-6066.CIR-14-0161

Flannagan, R. S., Jaumouillé, V., & Grinstein, S. (2012). The cell biology of phagocytosis. *Annual Review of Pathology*, *7*, 61–98. https://doi.org/10.1146/annurev-pathol-011811-132445

Freeman, S. A., Goyette, J., Furuya, W., Woods, E. C., Bertozzi, C. R., Bergmeier, W., Hinz, B., van der Merwe, P. A., Das, R., & Grinstein, S. (2016). Integrins Form an Expanding Diffusional Barrier that Coordinates Phagocytosis. *Cell*, *164*(1), 128–140. https://doi.org/10.1016/j.cell.2015.11.048

Huang, Z.-Y., Hunter, S., Kim, M.-K., Indik, Z. K., & Schreiber, A. D. (2003). The effect of phosphatases SHP-1 and SHIP-1 on signaling by the ITIM- and ITAM-containing Fcγ receptors FcγRIIB and FcγRIIA. *Journal of Leukocyte Biology*, *73*(6), 823–829. https://doi.org/10.1189/jlb.0902454

Joffe, A. M., Bakalar, M. H., & Fletcher, D. A. (2020). Macrophage phagocytosis assay with reconstituted target particles. *Nature Protocols*, *15*(7), 2230–2246. https://doi.org/10.1038/s41596-020-0330-8

Liu, A. P., & Fletcher, D. A. (2009). Biology under construction: In vitro reconstitution of cellular function. *Nature Reviews Molecular Cell Biology*, *10*(9), 644–650. https://doi.org/10.1038/nrm2746

Logtenberg, M. E. W., Scheeren, F. A., & Schumacher, T. N. (2020). The CD47-SIRPα Immune Checkpoint. *Immunity*, *52*(5), 742–752. https://doi.org/10.1016/j.immuni.2020.04.011

Morrissey, M. A., Kern, N., & Vale, R. D. (2020). CD47 Ligation Repositions the Inhibitory Receptor SIRPA to Suppress Integrin Activation and Phagocytosis. *Immunity*, *53*(2), 290-302.e6. https://doi.org/10.1016/j.immuni.2020.07.008

Tsai, R. K., & Discher, D. E. (2008). Inhibition of "self" engulfment through deactivation of myosin-II at the phagocytic synapse between human cells. *The Journal of Cell Biology*, *180*(5), 989–1003. https://doi.org/10.1083/jcb.200708043

Tsai, R. K., Rodriguez, P. L., & Discher, D. E. (2010). Self inhibition of phagocytosis: The affinity of 'Marker of Self' CD47 for SIRPα dictates potency of inhibition but only at low expression levels. *Blood Cells, Molecules & Diseases*, *45*(1), 67–74. https://doi.org/10.1016/j.bcmd.2010.02.016

Xie, J., Tato, C. M., & Davis, M. M. (2013). How the immune system talks to itself: The varied role of synapses. *Immunological Reviews*, *251*(1), 65–79. https://doi.org/10.1111/imr.12017

Chapter 2: Antibody:CD47 ratio regulates macrophage phagocytosis through competitive receptor phosphorylation

Emily C. Suter[1,2], Eva M. Schmid[1], Andrew R. Harris[1,3], Erik Voets[4], Brian Francica[5], Daniel A. Fletcher[1,2,6,7,*,†]

[1]Department of Bioengineering, University of California Berkeley, Berkeley CA, USA
[2]UC Berkeley/UC San Francisco Graduate Group in Bioengineering, Berkeley, CA, USA
[3]Department of Mechanical and Aerospace Engineering, Carleton University, Ottawa, Ontario, Canada
[4]Aduro Biotech Europe, Oss, Netherlands
[5]Aduro Biotech Inc., Emeryville, CA, USA
[6]Division of Biological Systems and Engineering, Lawrence Berkeley National Laboratory, Berkeley, CA, USA
[7]Chan Zuckerberg Biohub, San Francisco, CA, USA
*Address for correspondence: fletch@berkeley.edu
[†]Lead Contact

Abstract

Cancer immunotherapies often modulate macrophage effector function by introducing either targeting antibodies that activate Fc gamma receptors or blocking antibodies that disrupt inhibitory SIRPα-CD47 engagement. Yet how these competing signals are integrated is poorly understood, raising questions about how to effectively titrate immune responses. Here we find that macrophage phagocytic decisions are regulated by the ratio of activating ligand to inhibitory ligand over a broad range of absolute molecular densities. Using both endogenous and chimeric receptors, we show that activating:inhibitory ligand ratios of at least 10:1 are required to promote phagocytosis of model antibody-opsonized CD47-inhibited targets and that lowering this ratio reduces FcγR phosphorylation due to inhibitory phosphatases recruited to CD47-bound SIRPα. We demonstrate that ratiometric signaling is critical for phagocytosis of tumor cells and can be modified by blocking SIRPα, indicating that balancing targeting and blocking antibodies may be important for controlling macrophage phagocytosis in cancer immunotherapy.

Introduction

Macrophages play a critical role in cancer immunotherapy by recognizing and destroying antibody-opsonized cells. The clinical success of therapeutic antibodies, including anti-CD20 clearance of chronic lymphocytic leukemia cells (Chu et al., 2018; VanDerMeid et al., 2018) and anti-CD38 clearance of multiple myeloma (van de Donk & Usmani, 2018), has been attributed in part to macrophage destruction of tumor cells via antibody-dependent cellular phagocytosis (ADCP). However, potent inhibitory molecules found on tumor cells, such as the ubiquitous "marker of self" CD47, can dampen the pro-phagocytic effect of therapeutic antibodies (Okazawa et al., 2005; Oldenborg et al., 2000). Though the SIRPα-CD47 inhibitory checkpoint is critically important for avoiding destruction of healthy cells, it is commonly hijacked by tumor cells, which can upregulate CD47 expression from 2 to 6 times normal surface expression to avoid recognition and destruction (Willingham et al., 2012).

Disrupting the SIRPα-CD47 inhibitory checkpoint has become an important immunotherapeutic target in recent years (Feng et al., 2019), with antibodies that block SIRPα and CD47 intended to increase macrophage effector function. Promising clinical and mouse studies have shown that CD47 blockade therapies can bolster the efficacy of therapeutic antibodies (Chao et al., 2010; Majeti et al., 2009; Theocharides et al., 2012; Weiskopf et al., 2016), though concerns remain about the potential for off-target effects. Since high concentrations of a blocking antibody are best for disrupting the SIRPα-CD47 inhibitory checkpoint but low antibody concentrations are best for minimizing off-target effects, doses must be found that are neither ineffective nor dangerous. While this can be done empirically (Feng et al., 2019), understanding the molecular mechanisms underlying macrophage decision-making is important for designing effective and safe combination immunotherapies.

Recent work on macrophage FcγR activation has helped to clarify the molecular mechanisms responsible for antibody-dependent phagocytosis (Bakalar et al., 2018; Freeman et al., 2016), but

how CD47 binding activates SIRPα and how SIRPα counteracts FcγR signaling remain active areas of research. Recently, Morrissey et al. demonstrated that SIRPα-CD47 binding inhibits macrophage integrin activation (Morrissey et al., 2020). Previously, Tsai et al. showed that dephosphorylation of non-muscle myosin IIA was a key component of CD47-mediated shutdown of macrophages (Tsai & Discher, 2008). However, it remains possible that a more direct interaction between activating and inhibitory receptors could dictate phagocytic signaling.

Here, we quantitatively evaluate macrophage phagocytic decision-making by systematically varying pro-phagocytic antibody and anti-phagocytic CD47 in a reconstituted target system. We find that the ratio of activating and inhibitory ligands, rather than their absolute number, determines macrophage phagocytosis, with an antibody:CD47 ratio of 10:1 necessary to overcome inhibition in the model system. We show that this ratio-dependent behavior is exhibited by both endogenous and chimeric receptors and that shifting this ratio changes SIRPα-mediated FcγR phosphorylation. Finally, we demonstrate that the activation:inhibition ratio is critical for tumor cell phagocytosis, indicating the effectiveness of inhibitory checkpoint immunotherapies will depend on the relative number of antigens and CD47 on target tumor cells.

Results

Ratio of Antibody:CD47 drives phagocytosis in a reconstituted target assay

To study competition between inhibitory SIRPα and activating FcγR signals, we used reconstituted cell-like target particles consisting of silica beads coated in fluorescent supported lipid bilayers (SLBs). Briefly, Ni-NTA-conjugated lipids in the SLB enabled controlled attachment of His-tagged CD47 (inhibitory ligand), and the target particles were opsonized by binding anti-biotin IgG to biotinylated lipids (activating ligand) (Figure 1a). Importantly, the fluidity of the SLB facilitates the binding and subsequent enrichment of membrane-bound proteins on the target (Joffe et al., 2020). After protein attachment, target particles were added to RAW 264.7 macrophage-like cell line and phagocytosis was measured by quantifying internalized target particle fluorescence using confocal microscopy. We found that target particles coated only in antibody were engulfed, but addition of CD47 reduced phagocytosis to background (no protein) levels, confirming that this inhibitory axis can be reconstituted in our model system (Figure 1b).

We next investigated how macrophage phagocytosis depends on ligand density and whether phagocytosis stops when CD47 reaches a threshold density on the target surface. Antibody and CD47 are attached to the target particle orthogonally, enabling us to precisely control the numbers of activating and inhibitory ligands presented to the macrophage. To verify these numbers, we measured surface densities of fluorescently-labeled CD47 and antibody on target particles using flow cytometry before every assay (Figure S1a). Importantly, estimated macrophage SIRPα and FcγR receptors are in excess of their corresponding ligands on the target particle surface.

We first measured sensitivity to ligand density by creating a panel of target particles combining three different antibody surface densities (150, 300, and 600 molecules/μm^2), each with five different CD47 surface densities (0, 4, 10, 20, 50 molecules/μm^2, Figure 1c). For comparison, CD47 surface density on red blood cells is approximately 250 molecules/μm^2 (Mouro-Chanteloup et al., 2003). We found that phagocytosis scaled inversely with CD47 surface density and did not exhibit a step function at a specific CD47 density, as would be expected for threshold-governed behavior (Figure 1d). Target particles with the highest antibody density overcame CD47 inhibition better than those with lower antibody densities, indicating that phagocytosis was responding to both CD47 and antibody densities. Indeed, by replotting the data as a function of CD47:antibody ratio, we see that phagocytosis is highly sensitive to small changes in relative CD47:antibody densities rather than absolute molecule numbers (Figure 1d).

To more directly test this ratio hypothesis, we mixed antibody and CD47 in ratios varying from 1:1 to 50:1, and then serially diluted them prior to adding proteins to SLB-coated beads (Figure 1e). This enabled us to create target particles with a fixed ratio of molecules but vary the absolute numbers of those molecules by over 100-fold (Figure S1b). We find that target particles with the same ratio of molecules yield similar levels of phagocytosis across a wide range of surface densities. We note, however, that phagocytosis can be sensitive to absolute molecule numbers when measured densities of antibody or CD47 become extremely low (<20 molecules/μm^2 anti-biotin antibody and <2 molecules/μm^2 CD47). For dilution series in which the first dilution shows lower phagocytosis than subsequent dilutions, we hypothesize that an excess of antibody saturates FcγRs, effectively lowering the bound antibody:CD47 ligand ratio and reducing phagocytosis.

SIRPα-CD47 binding drives exclusion of CD45 and co-localizes with bound FcγRs

We next investigated how the ratio of antibody:CD47 governs phagocytosis by studying the composition of the interface between a macrophage and target particle. To improve quantification of interfacial organization and density, we used TIRF microscopy to image macrophages undergoing frustrated phagocytosis on SLB-coated glass coverslips containing the same tunable concentrations of antibody and CD47 as the target particles used above (Figure 2a).

We first tested whether receptor engagement at the interface was proportional to ligand ratio by dropping cells on to planar SLBs with varying antibody:CD47 ratios and measuring enrichment within the macrophage footprint (Figure 2b). We found that average enrichment within the footprint scales with the ratio of ligands present on the SLB, indicating that binding of the two ligand-receptor pairs is independent of each other (i.e. local enrichment of one does not inhibit enrichment of the other) (Figure 2c).

Next, we examined how the size of bound SIRPα-CD47 compared with the size of bound antibody-FcγR. We previously found that macrophage phagocytosis is dependent on size-based segregation of the inhibitory phosphatase CD45 from the antibody-bound FcγR (Bakalar et al., 2018). Specifically, FcγR binding to an antibody targeting the membrane, which creates a membrane-membrane gap of approximately 12 nm (estimated from crystal structures (Bakalar et al., 2018; Lu et al., 2011)), results in efficient phagocytosis due to maximum exclusion of CD45 (Bakalar et al., 2018). This activating interface gap matches with the approximate size of SIRPα-

CD47 interaction (~13 nm estimated by crystal structure (Hatherley et al., 2009)). This would allow bound SIRPα-CD47 to be remain in the gap formed by a short phagocytic interface after CD45 is excluded, potentially inhibiting phagocytosis. To test this prediction, we assessed co-localization of the two binding pairs, FcγR-antibody and SIRPα-CD47, using TIRF microscopy of RAW 264.7 cells and giant plasma membrane vesicles (GPMVs) from RAW cells (Sezgin et al., 2012), which do not have an active cytoskeleton. In both the RAW cells and GPMVs, SIRPα-CD47 and FcγR-antibody were enriched and co-localized in the footprint, indicating that these two opposing pathways can co-exist at an interface due to their similarity in size (Figure 2d, 2g).

Size-dependent segregation of CD45 from the small gap created by FcγR engagement with antibodies is required for sustained phosphorylation of tyrosine residues in immunoreceptor tyrosine-based activation motifs (ITAMs) on activating FcγRs (Bakalar et al., 2018). ITAMs are phosphorylated by cytoplasmic membrane-anchored kinase Lyn—a member of the Src family kinases—which remains present within an FcγR-antibody interface due to its lack of extracellular domain (Figure 2e). Lyn is also believed to phosphorylate tyrosines on the immunoreceptor tyrosine-based inhibition motifs (ITIMs) of SIRPα, given previous evidence that Lyn can phosphorylate other ITIM-containing receptors and that depletion of Lyn leads to decreased SIRPα phosphorylation (Abram & Lowell, 2008; Scapini et al., 2009). However, the mechanism by which SIRPα phosphorylation is regulated is not well understood.

We hypothesized that phosphorylation of SIRPα ITIMs when engaged with CD47 is similarly regulated by size-dependent exclusion of CD45, which would prevent dephosphorylate Lyn-phosphorylated ITIMs. To investigate this, we imaged GPMVs from RAW 264.7 cells on SLBs containing CD47 but not antibody and saw dramatic exclusion of CD45 from interfaces established by only SIRPα-CD47, as quantified by Pearson's correlation analysis (Figure 2f, 2g). This observation indicates that SIRPα-CD47 binding creates a small enough gap to exclude CD45 and that exclusion of CD45 does not require FcγR engagement.

We next tested whether CD45 exclusion results in increased tyrosine phosphorylation at the interface between macrophages and target particles coated in antibody, CD47, or both ligands (Figure 2h). Using phosphotyrosine immunostaining (not specific to ITAMs or ITIMs), we expected to detect an increase in phosphorylation at target interfaces with both CD47 and antibody, compared to antibody alone, due to the presence of both phosphorylated ITAMs and ITIMs. Surprisingly, phosphorylation at the target particle interface dropped significantly with the addition of CD47 despite similar levels of antibody on the two target particle populations (Figure 2i). This unexpected result raised the question of why phosphorylation is reduced rather than increased when CD45 is excluded in the presence of CD47.

SIRPα enrichment decreases phosphorylation at the macrophage-target interface

Our phosphorylation results indicated that not only were phosphorylated SIRPα ITIMs not contributing to total phosphorylation at the particle interface, but that phosphorylation of the antibody-bound FcγR ITAMs was also decreasing. To better quantify this, we immunostained macrophages for phosphotyrosine after allowing them to interact with target particles coated with increasing antibody:CD47 ratios. Normalizing the average pixel intensity of the phosphotyrosine

antibody by the anti-biotin antibody intensity, we find that the level of phosphorylation per anti-biotin antibody at the interface goes down with increasing CD47 (Figure 3a), indicating that there is proportionally less phosphorylation for each ITAM at the macrophage-target interface when CD47 is present. We confirmed that this decrease in phosphorylation is not caused by diminished particle engagement due to CD47, nor is the average level of phosphorylation dependent on the number of particles engaged to a cell (Figure S2a-c). While our results suggest that the phosphotyrosine antibody is reporting ITAM phosphorylation, we note that immunostaining may also pick up phosphorylation of additional downstream components of the activation pathway. Despite this, our phosphorylation data shows a titratable decrease of activation pathway phosphorylation with increasing CD47.

To test whether we see a similar result over the entire macrophage-target interface, we fixed and stained macrophages on SLBs with and without CD47. Again we saw proportionally less phosphorylation per antibody enriched in the interface in the presence of CD47 (Figure S2d-e).

Close proximity of ITIM-associated phosphatases decreases FcγR phosphorylation

We speculated that decreasing phosphorylation in the presence of CD47 did not occur because CD45 was less excluded at the interface where bound SIRPα-CD47 and antibody-FcγR co-localize but rather because soluble phosphatases bind to phosphorylated ITIM domains at the interface (Kharitonenkov et al., 1997; Veillette et al., 1998). Previous work has shown that recruitment of phosphatases SHP1, SHP2, and SHIP to phosphorylated ITIMs is a key regulator of their phosphatase activity (Binstadt et al., 1996; Burshtyn et al., 1997; Neel et al., 2003). SHP1—the most widely studied and directly implicated in down-regulation of macrophage activation—is recruited to phosphorylated SIRPα via its tandem N-terminal SH2 domains and has been shown to dephosphorylate a range of targets, including ITAMs and other substrates of Syk kinase (Frank et al., 2004; Kant et al., 2002). In synthetic peptide studies, SHP1 preferentially dephosphorylates ITAM-like targets (Frank et al., 2004), and in cells, overexpression of SHP1 reduces phosphorylation of activating FcγRIIA, dramatically decreasing Syk activation (Huang et al., 2003).

Based on this, we hypothesize that SHP1 dephosphorylates adjacent ITAMs after binding to SIRPα, suppressing FcγR activation. To test whether SHP1 is recruited to the macrophage-target particle interface when CD47 is present, we created an ITIM phosphorylation sensor by replacing the phosphatase domain of SHP1 with GFP (Figure S3a). This sensor serves to both visualize SHP1 recruitment and also demonstrate SIRPα phosphorylation, which was hard to capture with phosphotyrosine immunostaining. We first dropped RAW cells stably expressing this sensor onto SLBs coated in different concentrations of CD47 or antibody and quantified the SHP1-GFP sensor intensity within the footprint (Figure 3b, S3b). We found that SHP1 sensor recruitment to SLB interfaces containing only CD47 was greater than to those with only antibody, with SHP1 increasing as CD47 surface density increased from 250 to 2500 molecules/μm^2. As expected, SHP-1 sensor recruitment decreased upon addition of Src family kinase inhibitor PP2, which should prevent Lyn kinase phosphorylation of ITIMs (Figure S3c).

We next investigated whether co-localization of ITIMs and ITAMs at the interface between the macrophage and target particle reduced ITAM signaling. We speculated that the presence of

SHP1 on nearby ITIMs could dephosphorylate ITAMs and reduce FcγR activation by shutting down recruitment of Syk kinase, which drives phosphorylation of downstream targets leading to phagocytosis (Crowley et al., 1997; Fütterer et al., 1998; Tsang et al., 2008). To test this, we added macrophages to SLBs with different antibody:CD47 ratios and measured the signal from a fluorescent Syk sensor, which we previously developed to monitor phosphorylated ITAMs in real time (Bakalar et al., 2018) (Figure 3c, left). Adding 250 molecules/μm^2 of CD47 to the bilayer decreased the amount of Syk sensor recruited, and adding 2500 molecules/μm^2 decreased recruitment even further (Figure 3c, right, light bars).

To investigate whether the presence of CD47 on the target surface altered Syk and SHP1 binding kinetics, we created a second version of each sensor that replaced the GFP or mCherry with photoactivatable mEOS, which is converted from GFP to RFP with UV stimulation. The ability to convert only a small number of mEOS sensor molecules to RFP reduces background of the sensor and enables single molecule imaging. Macrophages expressing either the Syk-EOS or SHP1-EOS sensor were imaged while bound to SLBs coated in antibody, CD47, or both, and images were then analyzed to quantify molecule dwell times (Figure S3e, Supplementary Video S1, S2). We found that dwell times did not change significantly for either Syk-EOS or SHP1-EOS on different SLB compositions (Figure S3f, S3g). However, the number of binding events dropped significantly for Syk-EOS on CD47-coated SLBs and for SHP1-EOS on antibody-coated SLBs, despite similar sensor expression levels (Figure 3d, S3h). Importantly, Syk-EOS binding events also decreased significantly on SLBs containing both antibody and CD47, providing further evidence that CD47 engagement reduces local FcγR phosphorylation.

Model of ITIM-ITAM negative feedback captures ratio-dependent FcγR phosphorylation

We next developed a model of SHP1 recruitment, FcγR phosphorylation, and Syk recruitment to examine whether the observed ratio-dependent phagocytosis (as observed in Figure 1d) could be explained by negative feedback. The simple kinetic model includes parallel pathways of activation and inhibition (Figure 3e, Table S1) that are based on receptor-ligand binding, which drives receptor phosphorylation and subsequent binding of downstream effectors, SHP1 or Syk. Our model assumes that binding drives receptor enrichment and CD45 exclusion, enabling receptor phosphorylation.

We tested two versions of the model, one in which activation and inhibition are interacting and one in which they are not. In the 'non-interacting' version, the pathways proceed independently, with no SHP1 negative feedback on FcγR ITAM phosphorylation. In the 'interacting' version, activation and inhibition pathways are connected by a single integration point, dephosphorylation of FcγR ITAMs by SIRPα-bound SHP1 (Figure 3e). Constants used in the model were obtained from the literature, when available (Barua et al., 2012; Brooke et al., 2004; Li et al., 2007; Ren et al., 2011; Selner et al., 2014), and others were estimated (Table S2). The model is initiated with defined concentrations of unbound CD47, antibody, SIRPα, FcγR, SHP1, and Syk. FcγR-bound Syk is used as a proxy for phagocytosis since its localization to the target interface is known to be required for activation pathway signaling (Crowley et al., 1997; Kiefer et al., 1998). As expected, the 'non-interacting' model shows that FcγR-bound Syk is insensitive to varying ratio of CD47:antibody concentrations (Figure 3f), while the 'interacting' model shows that SHP1 is

able to dephosphorylate FcγR ITAMs, resulting in a sharp decrease of FcγR-bound Syk with increasing CD47:antibody ratio.

To experimentally test the 'non-interacting' model in cells, we incubated macrophages with target particles coated in a range of CD47:antibody ratios (as in Figure 3a) either with or without SHP1/2 inhibitor NSC-87877, which has previously been shown to be specific (Chen et al., 2006). Addition of the inhibitor should prevent SHP1 from dephosphorylating FcγRs and other activation pathway components, allowing phosphorylation to remain high at the target interface. Consistent with our 'non-interacting' model, we found that the amount of phosphorylation per antibody is higher than the control in the presence of inhibitor for each CD47:antibody ratio (Figure 3g), highlighting the key role SIRPα-bound phosphatases play in shutting down phagocytosis. We next tested the effect of SHP1/2 inhibition on Syk recruitment by dropping cells onto SLBs with varying CD47:antibody ratios in the absence or presence of NSC-87877. With the inhibitor, Syk sensor recruitment stayed constant with or without CD47 on the SLB, as expected from the 'non-interacting' model (Figure 3c, right panel, dark bars). To test the functional impact of SHP1 inhibition, we compared phagocytosis by wild-type macrophages to those expressing low or high levels of our SHP1-GFP sensor and found that cells expressing high SHP1-GFP phagocytose more efficiently in the presence of CD47 than wild-type or SHP1-GFP low-expressing macrophages (Figure S3d). As expected, expression of the phosphatase-free SHP1-GFP sensor reduced the amount of active phosphatase at the target interface, thereby reducing local dephosphorylation of FcγRs.

Both the ITIM phosphorylation and Syk recruitment data point to a model of macrophage decision-making in which small changes in CD47:antibody ratio drive shifts in relative enrichment of SIRPα and FcγRs (Figure 3h). This changing SIRPα enrichment alters the relative density of ITIM-bound phosphatases, which can then rapidly and effectively dephosphorylate nearby ITAMs to stop phagocytosis.

ITAM:ITIM ratio dictates phagocytosis levels independent of extracellular binding domain

The critical parameter in our model is the number of antibody-bound FcγRs relative to the number of CD47-bound SIRPα, which we abstract as the ratio of ITAM:ITIM enriched at a target interface. We wondered whether this ratio-dependent phagocytosis was specific to the competition between FcγRs and SIRPα or whether any receptor with an ITAM or ITIM would behave similarly.

To test this, we created a chimeric receptor containing the intracellular ITAM-containing portion of FcγRIIA and the Syn18 leucine zipper sequence as the extracellular binding domain (Thompson et al., 2012) (Figure S4a). As a ligand for the chimeric receptor, we used the complementary SynZip motif, Syn17, attached to three repeats of FNIII domain (Fibcon), which we used previously as a tool for modulating extracellular protein height (Bakalar et al., 2018), along with a His-tag for attachment to the SLB (Syn17-F3L). Upon binding, the chimeric receptor should create a membrane gap similar to that of SIRPα-CD47, approximately 13 nm. Using target particles coated in Syn17-F3L, we found that the chimeric receptors drove efficient phagocytosis that was specific to the FcγRIIA ITAM motif (Figure S4b). When CD47 and Syn17-F3L were added in varying ratios on target particles, we found that the chimeric receptor

responded in a titratable way to activation:inhibition ratio, very similar to the endogenous receptors (Figure 4a).

To investigate whether ITAMs from other receptors also exhibit ratio-dependent signaling, we created additional chimeric receptors featuring the intracellular signaling regions of the CD3 ζ-chain of the T-cell receptor complex and FcεRI γ-chain (Figure S4a). Each receptor construct was identical, with the exception of the signaling domain. We found that macrophages expressing each chimeric receptor responded similarly to Syn17-3L alone on the target surface (Figure S4c) and that each receptor responded similarly to a titration of CD47, suggesting that ratio dominates phagocytosis independent of receptor identity (Figure 4b). Interestingly, the ratio of Syn17 to CD47 required to achieve phagocytosis over background was nearly identical to that of antibody to CD47, approximately 10:1, indicating that ratiometric signaling through synthetic receptors mimics that through endogenous FcγRs.

To determine if similar rules exist for ITIM-containing domains, we next created a chimeric SIRPα receptor to compete against the activation signal of endogenous FcγRs. The inhibitory receptor design was the same as the activation chimeric receptors, except for replacing ITAM-containing domains with SIRPα's ITIM-containing intracellular region (Figure S4a). We found that the chimeric SIRPα response is also titratable with ratio similar to the endogenous SIRPα (Figure 4c). Additional inhibitory chimeric receptors featuring the ITIMs of CD22, FcγRIIB, and PD-1 also showed ratio-dependent phagocytosis behavior (Figure 4d). Interestingly, we observed that macrophage phagocytosis with the chimeric SIRPα never fully decreased to zero in response to the now inhibitory Syn17-F3L ligand. We attribute this elevated background engulfment to the high affinity of Syn17-F3L to the Syn18 receptor, independent of the inhibitory signaling (Figure S4e). Taken together, these experiments with chimeric receptors demonstrate that ratio-dependent phagocytic signaling is generalizable to other ITAM and ITIM signaling domains.

We used the same chimeric SIRPα receptor to test how spatial segregation of activation from inhibition influenced phagocytic decision making. To do so, we measured receptor co-localization and compared phagocytosis of particles coated in antibody plus different concentrations of either a short inhibitory ligand (Syn17-F3L, as used previously) or a tall ligand (Syn17-F5L, which includes two additional Fibcon repeats). Using SLB experiments, we found that Syn17-F5L was significantly segregated from the antibody, unlike the Syn17-F3L ligand, which colocalized with antibody (Figure S4f, S4g). When normalized to cells expressing a non-signaling Syn18-GFP control, particles coated in low density of Syn17-F5L were phagocytosed more efficiently on average than those with Syn17-F3L, indicating that segregation of inhibition rendered it less potent (Figure S4h) and that co-localization of activation and inhibition is important for shutting down phagocytosis in certain density regimes.

Ratio-dependent phagocytosis of tumor cells can be shifted using blocking antibodies

Finally, we tested whether our model of ratio-dependent signaling was applicable to live tumor cells. Tumor cell surfaces are notably more complex than the two-component reconstituted target particles used in our assays so far and therefore may be subject to additional inhibitory interactions that complicate efforts to overcome inhibitory signaling (Feng et al., 2019).

To conduct tumor cell phagocytosis assays, we used mouse bone marrow derived macrophages (BMDMs) and the mouse colon adenocarcinoma cell line MC38, both of which have been used in previously published tumor cell eating experiments (Morrissey & Vale, 2019; Xu et al., 2017). MC38 cells were stably expressing human HER2 protein (MC38-hHER2), a well-characterized tumor antigen over-expressed in 15-30% of breast cancers (Iqbal & Iqbal, 2014). We opsonized the MC38-hHER2 cells with a mouse anti-hHER2 antibody, which was modified from the clinical hHER2-targeting antibody Trastuzumab (McKeage & Perry, 2002). The opsonized tumor cells were incubated with BMDMs for 30 minutes before imaging (Figure 5a). Importantly, we estimate that macrophage FcγR and SIRPα receptors are in excess of their corresponding ligands on MC38 cells.

In order to shift the activation:inhibition ratio we chose to vary the activation signal by titrating the anti-hHER2 antibody, while CD47-SIRP interaction stayed constant. This strategy was informed by clinical evidence that efficacy of tumor growth inhibition is correlated to HER2 opsonization levels (McLarty et al., 2009). Over an anti-hHER2 concentration range of 0.01 - 5 μg/mL, we see a clear increase in tumor cell phagocytosis, consistent with an increased activation:inhibition ratio (Figure 5b). The highest concentration (5 μg/mL) showed a slight decrease in phagocytosis, potentially due to excess anti-hHER2 antibody in solution saturating unbound FcγRs and preventing their engagement with anti-hHER2 on the tumor cell. To confirm that increased opsonization is accompanied by changes in receptor phosphorylation, we fixed BMDMs interacting with MC38-hHER2 cells and immunostained them for phosphotyrosine. Consistent with our reconstituted target particle experiments, we find that phosphorylation is concentrated at the interface and that regions of antibody enrichment correlate with high levels of phosphorylation (Figure 5c).

Both BMDMs and RAW 264.7 cells exhibit a similar sensitivity to antibody:CD47 ratios on reconstituted target particles (Figure S5a), consistent with BMDMs and RAW cells having similar ratios of FcγR:SIRPα, roughly 2:3 and 1:2, respectively, despite having different absolute numbers of receptors (Figure S5b). From surface measurements of MC38-hHER2 cells, we estimated 26,100 hHER2 molecules/cell and 30,100 CD47 molecules per cell. Surprisingly, at antibody saturation of hHER2, this yields an activation:inhibition ratio of approximately 1:1, much lower than the 10:1 required for our reconstituted target particles. This difference in ratio may be due to many reasons, including differences in antibody affinity and partial segregation of SIRPα-CD47 from antibody-bound FcγR resulting from the size of HER2, suggesting that the optimal ratio must be determined for each specific antibody and antigen.

Finally, we asked if we could shift the activation-inhibition ratio to improve phagocytic efficiency at lower anti-hHER2 antibody concentrations by blocking SIRPα-CD47 interactions and tipping the balance towards activation. To test this, we utilized SIRPα antibody 18a, which was developed by Aduro Biotech to bind mouse SIRPα and block CD47 engagement. We found that adding 5 μg/mL of 18a antibody over multiple dilutions of anti-hHER2 antibody systematically raised phagocytosis levels for each concentration of anti-hHER2 (Figure 5d), indicating that phagocytosis of tumor cells is, like the reconstituted target particles, dependent on antibody:CD47 ratios. This data also suggests that SIRPα-CD47 is a primary means of inhibition for these tumor cells, since ratiometrically blocking this interaction increases phagocytosis significantly.

Discussion

Immune cells, including macrophages, make important effector function decisions by directly interacting with target cells. Receptor engagement, enrichment, and signaling at cell-cell contacts are critical for determining the response to a target, and understanding these steps at a mechanistic level has the potential to inform efforts to harness macrophage effector functions for therapeutic purposes. This is especially the case when there is competition between inhibitory and activating cues. Here, we ask how macrophages process activating signals from antibodies and inhibitory signals from CD47 on target particles. We show quantitatively that the activating and inhibitory signals are integrated in a ratio-dependent manner, with approximately 10 antigen-bound antibodies required to overcome one CD47. Since each antibody-bound activating FcγR brings one or two ITAMs to the synapse while each CD47-bound SIRPα brings three ITIMs, our findings estimate that phagocytosis proceeds when there are at least 2-3 ITAMs for every ITIM.

In order to obtain a mechanistic picture of how macrophages respond to complex stimuli, we examine ligand densities across a regime in which macrophages transition between inhibition and activation of phagocytosis. Ultimately, macrophage decision making comes down to a race between phosphorylation and dephosphorylation of receptors, with Syk and SHP1 in direct competition. Subtle changes in ligand ratio drive changes in relative recruitment of SHP1 (and other phosphatases such as SHP2 and SHIP) to ITIMs, which rapidly shuts down activation by dephosphorylating nearby ITAMs. Importantly, SHP1 likely dephosphorylates ITIMs as well, as evidenced by low phosphorylation measurements at the interface between macrophages and targets, even in the presence of high SIRPα-CD47 engagement. This suggests that the phosphatase feedback acts not only to shut down activation but also to quickly turn off inhibition, returning the cell to a neutral state, poised to respond to the next potential target. A similar negative feedback model was proposed for PD-1, in which SHP2 phosphatase recruited to phosphorylated PD-1 clusters suppresses T cell receptor activation (Yokosuka et al., 2012). As such, we speculate that trans-dephosphorylation of activating pathways by proximal phosphatases may be a shut-off mechanism universal to all ITIM motifs.

Interestingly, it appears that the SIRPa-CD47 inhibitory checkpoint recruits SHP1 when CD45 is excluded from the interface, presumably because the gap formed drives size-dependent exclusion of CD45 as originally proposed for T cell receptor activation (Davis & van der Merwe, 2006). Our previous work showed that antigen size is critical for effective ADCP, with shorter antigens more efficiently excluding CD45, which in turn allows increased ITAM phosphorylation (Bakalar et al., 2018). We speculate that the similarity in height of SIRPα-CD47 and FcγR-antibody-antigen is not coincidental but rather has evolved specifically to shut down phagocytosis at its most efficient point if markers of self are detected. Our findings point to the possibility that CD45's main role is to maintain non-interacting macrophages in an "off" state by preventing both activating and inhibitory signaling. Exclusion of CD45 upon close contact with a target then enables engaged and enriched receptors of either pathway to signal, with FcγR and SIRPα signaling interpreted ratiometrically.

In our model of macrophage FcγR activation, co-localization of SIRPα-CD47 and FcγR-antibody binders not only reinforces CD45 exclusion but also provides SHP1 access to phosphorylated ITAMs. Our data using different heights of Syn17 ligand suggests that size-dependent segregation of inhibitory signaling can decrease its effectiveness. Consistent with this idea, a study in NK cells found that the inhibitory KIR2DL1-HLAC interaction was most potent when its height was matched to that of the activating NKG2D-MICA receptor-ligand pair (Köhler et al., 2010).

Our data also implies that the most important node for integrating activating versus inhibitory signaling is the receptors themselves. In NK cells, it has been suggested that Vav1 acts as an integrative node for inhibition triggered by inhibitory KIR receptors (Stebbins et al., 2003). However, macrophages lacking Vav1 are still able to phagocytose (Hall et al., 2006). In fact, many commonly cited players in downstream phagocytosis signaling can be removed without preventing productive FcγR-mediated phagocytosis, including WAVE and Rho proteins (Caron & Hall, 1998; Kheir et al., 2005). This suggests that phagocytosis, which makes use of a complex activation network, is not dependent on a single integrator downstream of the receptors. Instead, signal integration at the membrane enables more direct and localized response to engaged receptors, which may be particularly important when a macrophage is simultaneously interacting with multiple target cells (Dushek et al., 2012). Dephosphorylation of FcγR ITAMs by phosphatases recruited to SIRPα ITIMs may be further modulated by downstream processes that have been previously associated with CD47 on targets, including myosin phosphorylation and integrin activation (Morrissey & Vale, 2019; Tsai & Discher, 2008).

To show the relevance of our ratiometric model beyond reconstituted target particles, we demonstrated that live tumor cell phagocytosis follows the same requirement for ratiometric activating:inhibitory signaling. Though tumor cells have a far more complex cell surface, our study indicates that careful characterization of receptor and ligand densities on both immune and tumor cells may be important considerations for immunotherapies. More specifically, designing individualized therapeutic dosing informed by surface densities of tumor antigen, CD47, SIRPα, and FcγR could help to optimize results for specific cancers that involve macrophage effector function.

Interestingly, we saw that the ratio of activating:inhibitory ligand necessary for phagocytosis was much lower in tumor cell experiments than in our reconstituted system, approximately a 1:1 ratio versus a 10:1 ratio, respectively. This difference could be due to variation in antibody affinity towards the antigen or the FcγR, leading to different enrichment profiles and potentially higher activation. CD47 may also be less accessible to SIRPα in the crowded environment of tumor cell membranes than in our reconstituted target particle experiments, leading to lower receptor engagement and reduced inhibition. In addition, hHER2 is estimated to stand 11 nm above the cell membrane (Bakalar et al., 2018), meaning hHER2-antibody-FcγR would be expected to have a greater height than bound CD47-SIRPα, potentially leading to size-dependent spatial separation of activating and inhibitory signals and reducing the ability of SHP1 to dephosphorylate adjacent ITAMs. Our tumor cell eating experiments may also involve more stable macrophage-target interface facilitated by receptor-ligand interactions not present in the reconstituted system. Though T-cell immunological synapse adhesion and stability has been

extensively studied (Dustin, 2007; Graf et al., 2007; Philipsen et al., 2013), the impact of macrophage interface stability on signaling efficiency has not yet been completely characterized.

Though extracellular binding domains of immune receptors have been honed for target specificity and affinity, we believe the ratiometric signaling model we propose here may be broadly relevant to ITAM-dependent signaling in different cell types. In previous work in NK cells, overexpression of inhibitory Ly49 ligands on model tumor cells was able to shut down NKG2D-mediated activation in an expression-dependent manner, suggesting that relative amounts of the activating and inhibitory ligands were important in that system (Malarkannan, 2006). Additionally, previous work in microglia has shown that complement receptor CD11b requires ITAM-containing adapter protein DAP12 (Wakselman et al., 2008), indicating that not only could ITAM:ITIM ratio be important in complement-mediated phagocytosis but also to non-immunoreceptor (e.g., integrin) signaling as well. Probing whether ratio-dependent competition of activating and inhibitory signaling is widely applicable to diverse immune cell types is a question for future investigation that will require measurement of effector function over a range of absolute receptor surface densities.

Acknowledgements

The authors would like to thank Fletcher Lab members, especially Carmen Chan and Aaron Joffe, for useful feedback and technical consultation; Cancer Research Laboratory Flow Cytometry Facility for cell sorting; Portnoy Lab of UC Berkeley for providing BMDMs. We are grateful to Aduro Biotech—specifically Andrea van Elsas, Meredith Leong, Sander van Duijnhoven, and Sanne Spijkers—for support, discussions, and supplying a range of reagents used in this study. This work was supported by the NIH R01 GM134137 (DAF), the Immunotherapeutics and Vaccine Research Initiative at UC Berkeley (DAF), the Miller Institute for Basic Research (DAF), and the Chan Zuckerberg Biohub (DAF). ECS was funded by an NSF-GRFP fellowship.

Author Contributions

ECS, EMS, ARH, and DAF contributed to study conception and design. ECS executed reconstitution experiments and modeling, and EMS executed tumor cell experiments and surface characterization. ECS and EMS analyzed and interpreted data. EV and BF provided reagents as well as scientific and therapeutic expertise. ECS wrote the manuscript with extensive input from EMS and DAF.

Figures

Figure 1.

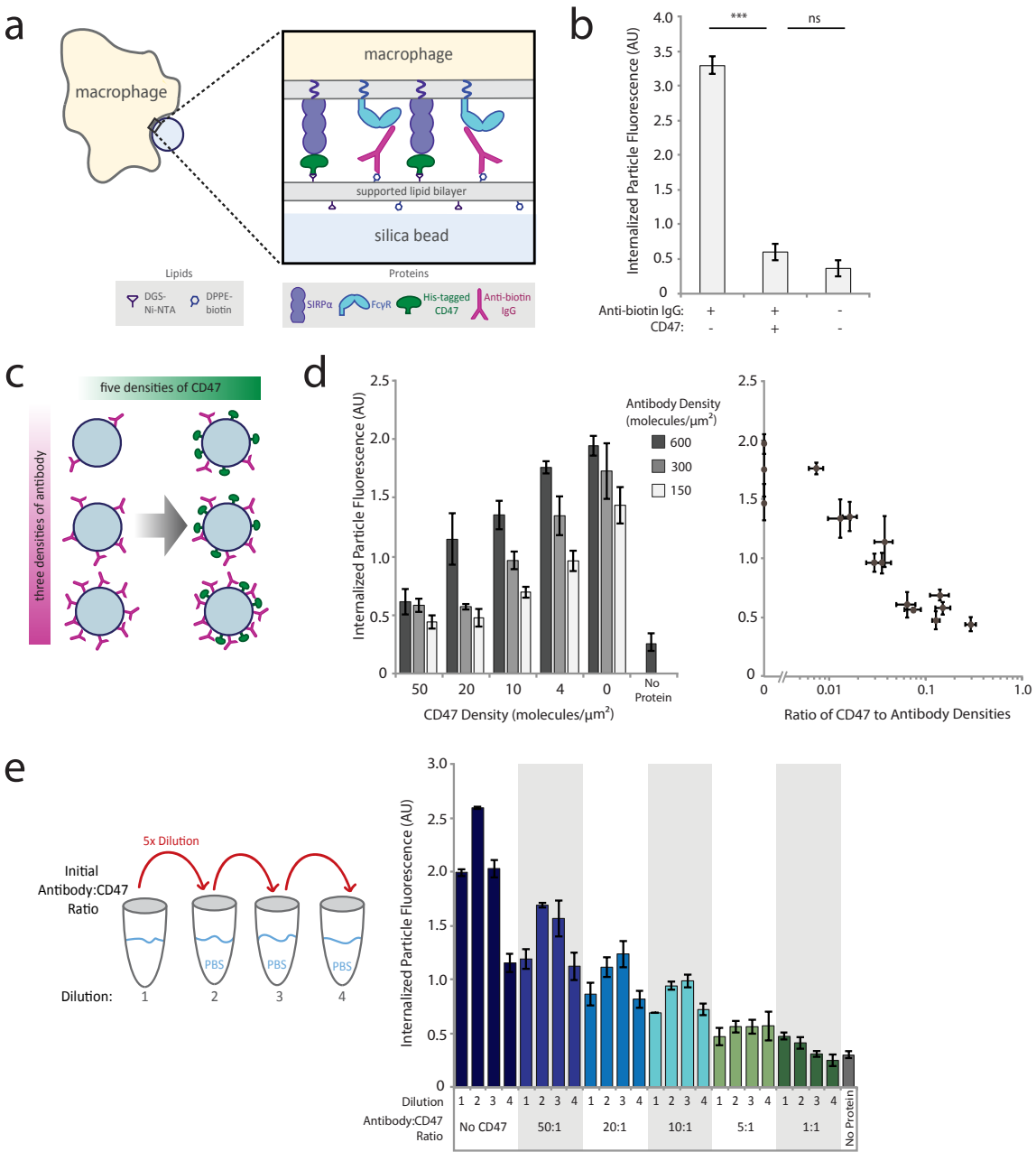

Figure 1. Phagocytosis is dependent on ratio of activating antibody to inhibitory CD47

(a) Experimental setup of phagocytosis assay of cell-like target particles by RAW 264.7 macrophages.

(b) Quantification of average internalized SLB-coated target particle fluorescence shows phagocytosis of protein-coated targets as compared to empty (lipid-only) targets. Each condition is the average of three independent experiments representing a total of >300 cells. Bars represent mean ± s.e.m. Conditions were compared with two-tailed student's *t* test, with (***) denoting $p<0.001$.

(c) Experimental setup of target particles with different anti-biotin IgG and CD47 densities. SLB-coated particles were incubated with 15 different combinations of anti-biotin IgG and CD47 concentrations, in addition to a no protein (lipid only) control.

(d) Internalized target particle fluorescence quantification for conditions outlined in (c) (left panel). Data replotted as a function of CD47:antibody ratio (right panel). Each condition is the average of three independent experiments representing a total of >300 cells. Bars represent mean ± s.e.m.

(e) Different anti-biotin IgG to CD47 ratios were created at high concentration, then serially diluted 5-fold three times, creating a total of four concentrations for each ratio. Internalized target particle fluorescence was quantified for phagocytosis of each particle ratio. Each condition is the average of three independent experiments representing a total of >300 cells. Bars represent mean ± s.e.m.

Figure 2.

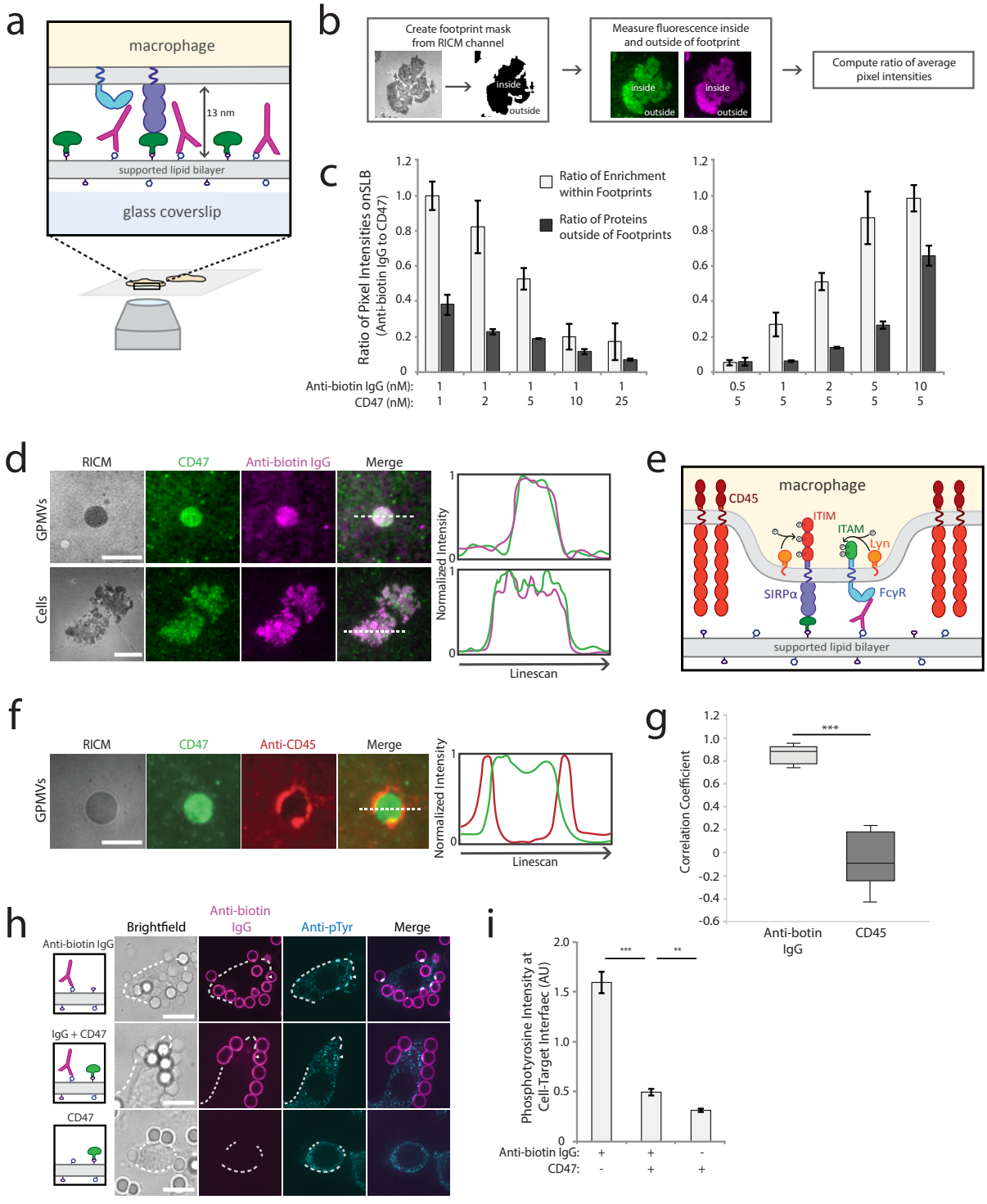

Figure 2. SIRPα-CD47 co-localizes with FcγR-antibody complexes and excludes CD45

(a) Experimental setup of TIRF imaging of macrophages on SLB.

(b) Workflow to quantify enrichment of CD47 and anti-biotin IgG on an SLB within a RAW 264.7 macrophage cell footprint. SLBs with variable concentrations of anti-biotin IgG (magenta) and CD47 (green) were created, and cell footprints were identified from RICM images. Average ratio of pixel intensities (anti-biotin IgG:CD47) was quantified inside and outside footprints.

(c) Average ratio of anti-biotin IgG and CD47 pixel intensities for SLBs of varying composition. Each condition is the average of three independent experiments representing a total of >200 footprints. Bars represent mean ± s.e.m.

(d) Representative TIRF fluorescent images of RAW 264.7 macrophages or GPMVs generated from RAW 264.7 cells on a planar SLB. SLBs were coated with 1 nM anti-biotin IgG (magenta) and 5 nM CD47 (green). Linescans of representative images show co-localization of anti-biotin IgG and CD47 in cell and GPMV footprints. Scale bar is 5 μm for GPMVs and 10 μm for cell footprints.

(e) FcγR ITAM and SIRPα ITIM phosphorylation by Lyn kinase upon CD45 phosphatase exclusion.

(f) Representative TIRF fluorescent image of GPMVs from RAW 264.7 macrophages labeled with anti-CD45 (red) on an SLB with CD47 (green). Linescan of representative image shows CD45 exclusion from interface. Scale bar is 5 μm.

(g) Pearson's correlation coefficient comparing CD47 localization with anti-biotin IgG (Figure 2d) and CD47 with localization with CD45 (Figure 2f) in RAW 264.7 macrophage GPMV footprints. Each condition represents >30 GPMV footprints. Conditions were compared with two-tailed student's *t* test, with (***) denoting $p<0.001$.

(h) Fluorescent confocal images of fixed RAW 264.7 macrophages interacting with target particles. Top row shows macrophages interacting with particles coated only in 1 nM anti-biotin IgG (magenta). Middle row shows particles coated in 1 nM anti-biotin antibody plus 50 nM CD47, and the bottom row shows particles coated only in 50 nM CD47. Phosphorylation visualized via anti-phosphotyrosine (cyan). Cell outlines are shown by white dotted lines. Scale bar is 10 μm.

(i) Quantification of anti-phosphotyrosine signal at particle-macrophage interfaces. Each condition is the average of three independent experiments representing a total of >100 cell-bead interfaces. Bars represent mean ± s.e.m. Conditions were compared with two-tailed student's *t* test, with (**) denoting $p<0.01$ and (***) denoting $p<0.001$.

Figure 3.

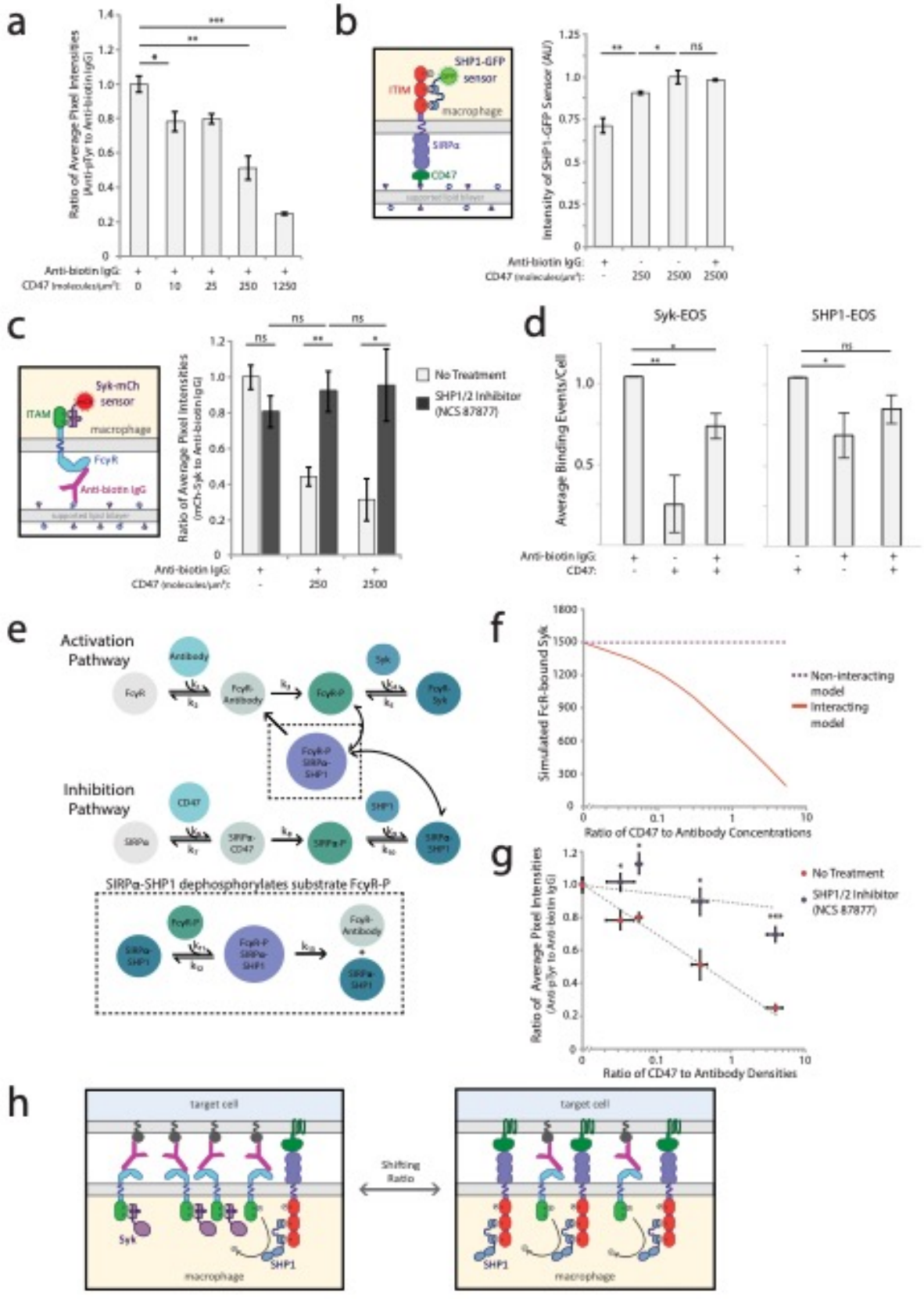
a
b
c
d
e
f
g
h
SHP1-GFP sensor
ITIM
macrophage
SIRPα
CD47
supported lipid bilayer
Syk-mCh sensor
FcγR
Anti-biotin IgG
No Treatment
SHP1/2 Inhibitor (NCS 87877)
Syk-EOS
SHP1-EOS
Activation Pathway
Inhibition Pathway
SIRPα-SHP1 dephosphorylates substrate FcγR-P
Non-interacting model
Interacting model
Ratio of CD47 to Antibody Concentrations
Ratio of CD47 to Antibody Densities
target cell
Shifting Ratio
Syk
SHP1

Figure 3. SIRPα-bound SHP1 dephosphorylates activation pathway to inhibit phagocytosis

(a) Quantification of the ratio of anti-phosphotyrosine to anti-biotin IgG fluorescence at macrophage-bead interfaces. RAW 264.7 macrophages interacting target particles coated with a fixed density of anti-biotin IgG (300 molecules/μm^2) and variable CD47 (0-1250 molecules/μm^2). Each condition is the average of 3 independent experiments representing a total of >150 particle-cell interfaces. Bars represent mean ± s.e.m. Conditions were compared with two-tailed student's *t* test, with (*) denoting $p<0.05$, (**) denoting $p<0.01$, and (***) denoting $p<0.001$.

(b) Schematic of SHP1-GFP sensor for detection of phosphorylated SIRPα (left panel). Average SHP1-GFP fluorescence signal within cell footprints was quantified for cells on SLBs coated with different CD47 densities (0, 250, 2500 molecules/μm^2) with and without anti-biotin IgG (300 molecules/μm^2) (right panel). Each condition is the average of 3 independent experiments representing a total of >100 macrophage footprints. Bars represent mean ± s.e.m. Conditions were compared with two-tailed student's *t* test, with (*) denoting $p<0.05$ and (**) denoting $p<0.01$.

(c) Schematic of Syk-mCh sensor for detecting phosphorylated FcγRs. RAW 264.7 cells expressing Syk-mCh sensor were imaged on SLBs coated with anti-biotin IgG (300 molecules/μm^2) and a range of CD47 densities (0, 250, 2500 molecules/μm^2). Average fluorescence signal within the cell footprint was measured for anti-biotin IgG and Syk-mCh, and the ratio of Syk-mCh to anti-biotin IgG was quantified for each cell. Cell footprint fluorescence was measured for cells with no pre-treatment (light gray bars) and treatment with SHP1/2 phosphatase inhibitor NSC-87877 (dark gray bars). Each condition is the average of 3 experiments representing a total of >200 cell footprints. Bars represent mean ± s.e.m. Conditions were compared with two-tailed student's *t* test, with (*) denoting $p<0.05$ and (**) denoting $p<0.01$.

(d) Normalized average Syk-EOS (left) and SHP1-EOS (right) binding events per cell for RAW macrophages on SLBs containing anti-biotin IgG (300 molecules/μm^2), CD47 (2500 molecules/μm^2), or both. Each condition is the average of 3 independent experiments representing a total of >50 macrophage footprints. Bars represent mean ± s.e.m. Conditions were compared with two-tailed student's *t* test, with (*) denoting $p<0.05$ and (**) denoting $p<0.01$.

(e) Schematic of computational model combining activating (top) and inhibitory (bottom) pathways. SIRPα-SHP1 dephosphorylation of FcγR captured in the black dotted inset represents the "interacting" version of the model.

(f) "Interacting" and "non-interacting" models were initiated with a fixed antibody concentration and variable CD47 concentrations, yielding a range of CD47:antibody ratios. Each model for each ratio condition was run until steady state was reached, and FcγR-bound Syk was plotted.

(g) Ratio of anti-phosphotyrosine to anti-biotin IgG at macrophage-target interfaces was measured for a range of CD47:antibody ratios on target particles (as described in (a)).

Quantification was done with and without pre-treatment of macrophages with SHP1/2 phosphatase inhibitor NSC-87877. Each condition is the average of 3 independent experiments representing a total of >150 particle-cell interfaces. Dots represent mean ± s.e.m. Conditions were compared with two-tailed student's *t* test, with (*) denoting $p<0.05$ and (***) denoting $p<0.001$.

(h) Schematic of SHP1-facilitated shutoff of activation pathway. In the absence of CD47, FcγR ITAMs are phosphorylated and bind Syk kinase, promoting phagocytosis. Upon CD47 engagement and SIRPα ITIM phosphorylation, SHP1 phosphatase is brought in close proximity to phosphorylated ITAMs, enabling their dephosphorylation.

Figure 4.

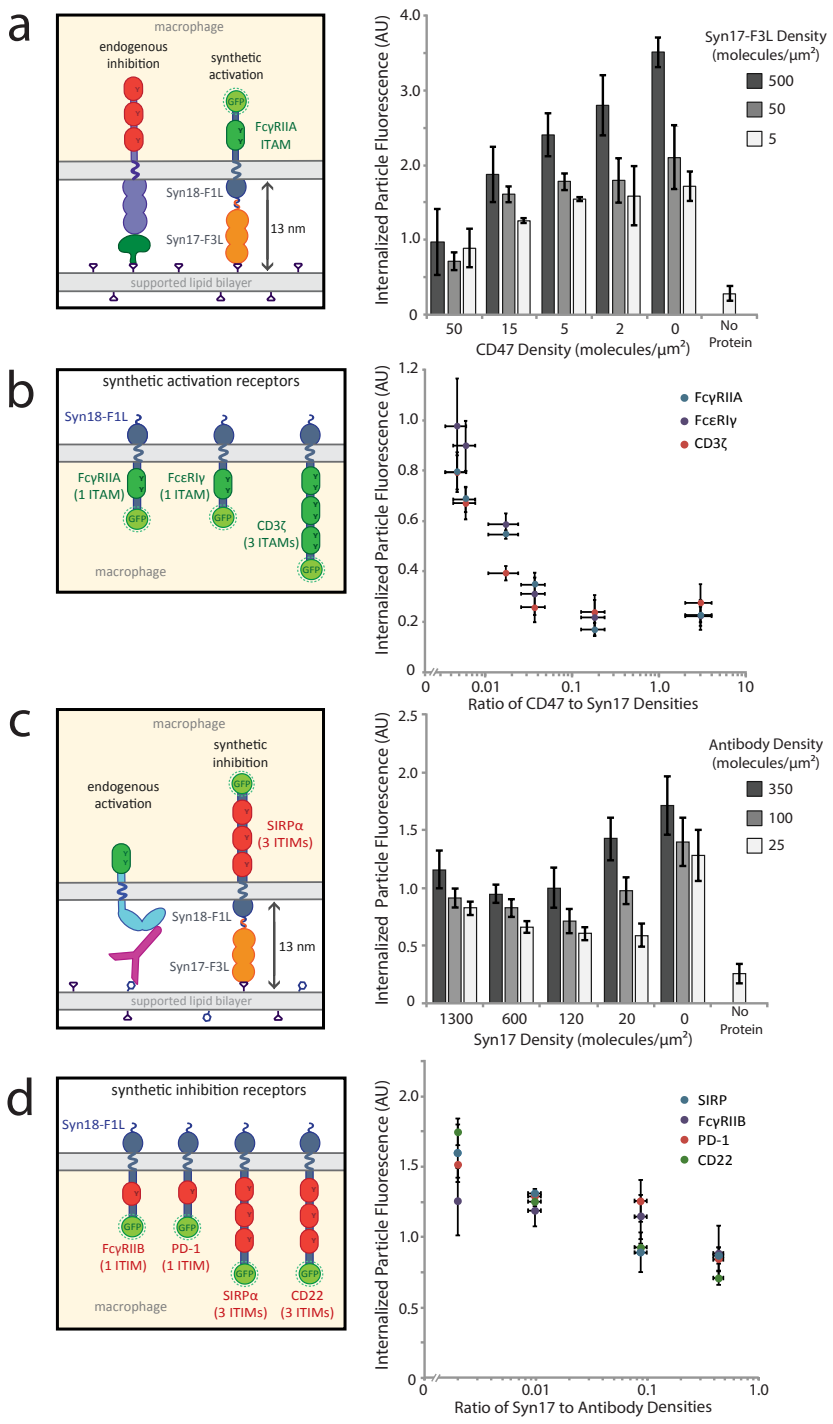
a
macrophage
endogenous inhibition
synthetic activation
FcγRIIA ITAM
Syn18-F1L
Syn17-F3L
13 nm
supported lipid bilayer
Internalized Particle Fluorescence (AU)
Syn17-F3L Density (molecules/μm²)
500
50
5
CD47 Density (molecules/μm²)
No Protein
b
synthetic activation receptors
Syn18-F1L
FcγRIIA (1 ITAM)
FcεRIγ (1 ITAM)
CD3ζ (3 ITAMs)
macrophage
FcγRIIA
FcεRIγ
CD3ζ
Ratio of CD47 to Syn17 Densities
c
macrophage
synthetic inhibition
endogenous activation
SIRPα (3 ITIMs)
Syn18-F1L
Syn17-F3L
13 nm
supported lipid bilayer
Antibody Density (molecules/μm²)
350
100
25
Syn17 Density (molecules/μm²)
No Protein
d
synthetic inhibition receptors
Syn18-F1L
FcγRIIB (1 ITIM)
PD-1 (1 ITIM)
SIRPα (3 ITIMs)
CD22 (3 ITIMs)
macrophage
SIRP
FcγRIIB
PD-1
CD22
Ratio of Syn17 to Antibody Densities

Figure 4. Ratio of activation to inhibition governs phagocytosis in a synthetic context

(a) Target particles coated in varying ratios of CD47 to Syn17-F3L were incubated with RAW 264.7 macrophages stably expressing the synthetic activating receptor Syn18-F1L-TM-FcγRIIA-GFP. Each condition is the average of three independent experiments representing a total of >300 cells. Bars represent mean ± s.e.m.

(b) RAW 264.7 macrophages stably expressing synthetic receptors containing three different ITAM-containing signaling motifs: FcγRIIA, CD3ζ, and FcεRI γ-chain. Phagocytosis was quantified for target particles with a range of CD47:Syn17-F3L ratios. Each condition is the average of three independent experiments representing a total of >300 cells. Dots represent mean ± s.e.m.

(c) Target particles containing varying ratios of Syn17-F3L to anti-biotin IgG were incubated with RAW 264.7 macrophages stably expressing synthetic inhibitory receptor Syn18-F1L-TM-SIRPα-GFP. Each condition is the average of three independent experiments representing a total of >300 cells. Bars represent mean ± s.e.m.

(d) RAW 264.7 macrophages stably expressing synthetic receptors containing four different ITIM-containing signaling motifs: FcγRIIB, SIRPα, PD-1, and CD22. Phagocytosis was quantified for target particles with a range of Syn17-F3L:anti-biotin IgG ratios. Each condition is the average of three independent experiments representing a total of >300 cells. Dots represent mean ± s.e.m.

Figure 5.

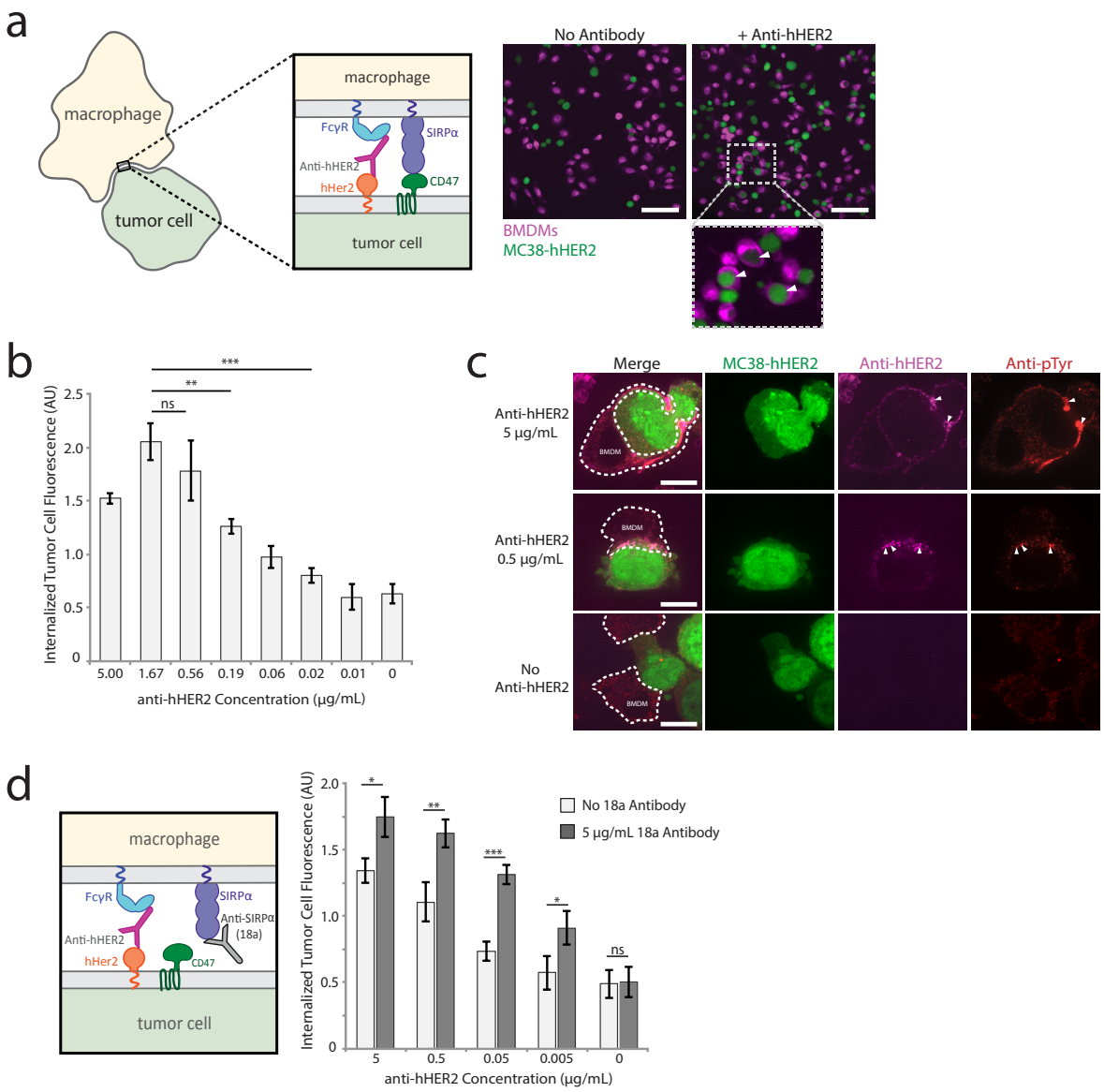
a
macrophage
tumor cell
macrophage
FcγR
SIRPα
Anti-hHER2
hHer2
CD47
tumor cell
No Antibody
+ Anti-hHER2
BMDMs
MC38-hHER2
b
Internalized Tumor Cell Fluorescence (AU)
***
**
ns
2.5
2.0
1.5
1.0
0.5
0
5.00
1.67
0.56
0.19
0.06
0.02
0.01
0
anti-hHER2 Concentration (μg/mL)
c
Merge
MC38-hHER2
Anti-hHER2
Anti-pTyr
Anti-hHER2
5 μg/mL
Anti-hHER2
0.5 μg/mL
No
Anti-hHER2
BMDM
d
macrophage
FcγR
SIRPα
Anti-hHER2
Anti-SIRPα
(18a)
hHer2
CD47
tumor cell
Internalized Tumor Cell Fluorescence (AU)
2.0
1.5
1.0
0.5
0
*
**
***
*
ns
No 18a Antibody
5 μg/mL 18a Antibody
5
0.5
0.05
0.005
0
anti-hHER2 Concentration (μg/mL)

Figure 5. Tumor cell phagocytosis is dictated by activation-inhibition ratio

(a) Representative confocal images of bone marrow derived macrophages (BMDMs, magenta) incubated with MC38-hHER2 cells (green) either with or without tumor targeting anti-hHER2 antibody opsonization. White arrows within inset indicate phagocytosed MC38-hHER2 cells. Scale bar is 50 μm.

(b) Quantification of MC38-hHER2 tumor cell phagocytosis by BMDMs. MC38-hHER2 tumor cells were opsonized with a range of anti-hHER2 antibody concentrations (0-5 μg/mL). Each condition is the average of 3 independent experiments representing >150 total cells. Bars represent mean ± s.e.m. Conditions were compared with two-tailed student's *t* test, with (**) denoting $p<0.01$ and (***) denoting $p<0.001$.

(c) Fluorescent confocal images of fixed BMDMs engaging with MC38-hHER2 cells (green) opsonized with different concentrations of anti-hHER2 antibody (0, 0.5, 5 μg/mL, magenta). Phosphorylation visualized via anti-phosphotyrosine (red). BMDM outlines are shown in white dotted lines. Areas of high anti-hHER2 enrichment are highlighted with white arrows. Scale bar is 5 μm.

(d) Anti-SIRPα blocking antibody 18a interrupting SIRPα binding to CD47 (left panel). MC38-hHER2 cells incubated with a range of anti-hHER2 antibody concentrations (0-5 μg/mL) were added to BMDMs in the presence or absence of 5 μg/mL 18a antibody. Average tumor cell phagocytosis was quantified (right panel). Each condition is the average of 3 independent experiments representing >150 total cells. Bars represent mean ± s.e.m. Conditions were compared with two-tailed student's *t* test, with (*) denoting $p<0.05$, (**) denoting $p<0.01$, and (***) denoting $p<0.001$.

STAR Methods

RESOURCE AVAILABILITY

Lead Contact

Further information and requests for resources and reagents should be directed to and will be fulfilled by the lead contact, Daniel Fletcher (fletch@berkeley.edu).

Materials Availability

- Plasmids generated in this study can be obtained from the Lead Contact.
- There are restrictions to the availability of reagents obtained through Aduro Biotech. These reagents MC38 cells expressing hHER2, as well as anti-SIRPα antibody clone 18a and mouse IgG1 anti-hHER2 antibody. Anti-SIRPα clone p84 and anti-CD47 antibody MIAP 301 were obtained from Aduro Biotech, but are commercially available.

Data and Code Availability

- Data reported in this paper will be shared by the lead contact upon request.
- This paper does not report original code.
- Any additional information required to reanalyze the data reported in this paper is available from the lead contact upon request.

EXPERIMENTAL MODEL AND SUBJECT DETAILS

All cell lines tested negative for mycoplasma as verified by Mycoalert detection kit (Lonza).

RAW 264.7 macrophage cell culture

RAW 264.7 murine male macrophage-like cell line was obtained from the UC Berkeley Cell Culture Facility. Cells were cultured in RPMI 1640 media (Corning) supplemented with 10% heat-inactivated fetal bovine serum (HI-FBS, Thermo Fisher Scientific) and 1% Pen-Strep (Thermo Fisher Scientific) in non-tissue culture-treated 10 cm dishes (VWR) at 37°C, 5% CO_2.

Bone marrow derived macrophage cell culture

Bone marrow derived macrophages (BMDMs) from male C57BL/6 (B6) mice were a kind gift from the Portnoy Lab (UC Berkeley). BMDMs were grown in RPMI 1640 media supplemented with 10% HI-FBS and 1% Pen-Strep at 37°C. BMDMs were used in experiments within 24 hours of thawing.

MC38 cell culture

MC38 female murine colon adenocarcinoma cells stably expressing human HER2 (referred to as MC38-hHER2) were obtained from Aduro Biotech. MC38-hHER2 cells were grown in RPMI 1640 media supplemented with 10% HI-FBS and 1% Pen-Strep at 37°C.

HEK 293T cell culture

Human embryonic kidney (HEK) 293T cells were obtained from the Cell Culture facility at UC San Francisco. Cells were cultured in DMEM media (Thermo Fisher Scientific) supplemented with 10% HI-FBS and 1% Pen-Strep at 37°C.

METHOD DETAILS

Preparation of cell-like reconstituted target particles

Cell-like reconstituted target-particles were generated according to previously published protocol (Joffe, A. et al., 2020), summarized in the following sections.

Formation of small unilamellar vesicles (SUVs)

SUVs were prepared by rehydrating a lipid film composed primarily of POPC (1-palmitoyl-2-oleoyl-sn-glycero-3-phosphocholine, Avanti Polar Lipids), doped with 0.5% of Biotinyl Cap PE (1,2-dioleoyl-sn-glycero-3-phosphoethanolamine-N-(cap biotinyl), Avanti Polar Lipids), 1% DGS-Ni-NTA (1,2-dioleoyl-sn-glycero-3-[(N-(5-amino1-carboxypentyl)iminodiacetic acid)succinyl] with nickel salt, Avanti Polar Lipids), and 0.4% LISS-Rhodamine (1,2-dioleoyl-sn-glycero-3-phosphoethanolamine-N-(lissamine rhodamine B sulfonyl), Avanti Polar Lipids) in pure deionized H_2O. The rehydrated solution was vortexed briefly and then sonicated using a tip-sonicator at 20% power pulsing off and on for 3 minutes. SUVs were then filtered through a 200 nm PTFE filter (Millipore). SUV solutions were stored at 4°C and used within 48 hours of preparation to avoid phospholipid oxidization.

Formation of cell-like target particles

40 μL of 4.07 μm silica beads (Bangs Laboratories) were cleaned using a 3:2 mixture of H_2SO_4:H_2O_2 (Piranha) for 30 minutes while sonicating. Cleaned beads were spun down at 1000 x g and washed 3 times with 1 mL pure water before being resuspended in 400 μL of water. Cleaned beads were stored at room temperature. To form SLBs, 40 μL of SUVs was added to 160 μL of MOPS buffer (25 mM MOPS (3-(N-morpholino)propanesulfonic acid), Thermo Fisher Scientific), 125 mM NaCl, pH 7.4), along with 20 μL of clean bead slurry. The mixture was incubated at room temperature for 15 minutes while rotating continuously. Coated beads (also referred to as target particles) were spun down at 50 x g for 1 minute, and 200 μL of the solution was removed and replaced with PBS (Corning).

Addition and quantification of protein on particles

AlexaFluor647-labeled anti-biotin mouse IgG (clone BK-1/39, Thermo Fisher Scientific) and AlexaFluor488-labeled His-tagged recombinant mouse CD47 (SinoBiological) were diluted in PBS to appropriate concentrations for target particle experiments. 50 μL of SLB-coated beads was added to 50μL of protein dilution, and beads were incubated at room temperature for 20 minutes with continuous rotation.

SLB and protein-coated target particles were diluted in PBS and analyzed using an Attune NxT flow cytometer (Thermo Fisher Scientific). Target particles were compared to calibrated beads with known numbers of AlexaFluor488 and AlexaFluor647 fluorophores (Quantum MESF Kits, Bangs Laboratories), which enabled calculate of protein surface density.

Fluorescent labeling of proteins
His-tagged recombinant mouse CD47 (as well as proteins and antibodies noted later) was labeled using AlexaFluor488 NHS Ester (Succinimidyl Ester, Thermo Fisher Scientific) reconstituted in anhydrous DMSO (dimethylsulfoxide, Sigma Aldrich). Dye was mixed with protein at a 5x molar ratio (dye:protein ratio was 5:1) and incubated at room temperature for 1 hour. Excess dye was removed by purifying protein over NAP-5 columns (GE Healthcare). Labeling was confirmed using NanoDrop 2000c (Thermo Fisher).

Imaging techniques

All live cells were maintained at 37°C, 5% CO2 with a stage top incubator (Okolab) during imaging. For confocal microscopy, cells were imaged with a spinning disk confocal microscope (Eclipse Ti, Nikon) with a spinning disk (Yokogawa CSU-X, Andor), CMOS camera (Zyla, Andor), and either a 20x objective (Plano Fluor, 0.45NA, Nikonor a 60x objective (Apo TIRF, 1.49NA, oil, Nikon). For total internal reflection fluorescence (TIRF) microscopy, cells were imaged with TIRF microscope (Eclipse Ti, Nikon), 60x objective (Apo TIRF, 1.49NA, oil, Nikon) and EMCCD camera (iXON Ultra, Andor). Both microscopes were controlled with Micro-Manager. Images were analyzed and prepared using FIJI (Schindelin, J. et al., 2012).

Phagocytosis assays

Target particle phagocytosis assay
35,000 macrophages were seeded in wells of a tissue-culture flat-bottom 96-well plate (Falcon) in 100 μL of RPMI 1640 medium. Post-seeding, cells were incubated at 37°C for 3-4 hours prior to target particle addition. 100 μL of target particles were prepared for each well with appropriate protein concentrations, and 95 μL of the 100 μL were added. Macrophages were incubated with target particles at 37°C for exactly 20 minutes. During those 20 minutes, the remaining 5μL were diluted in 250 μL of PBS and immediately measured using flow cytometry as previously described.

After incubation, wells were washed twice with PBS to remove excess particles. PBS containing 1 μM of CellTracker Green (CMFDA, Thermo Fisher Scientific) and 10 μM Hoechst 33342 (Thermo Fisher Scientific) was added to wells to stain the cytoplasm and nuclei, respectively. Wells were imaged after 10 minutes of staining using a spinning-disk confocal microscope (Nikon) at 20x. Images were acquired in an automated grid pattern at the same location within each well to reduce bias in image acquisition. For each well, at least 100 cells were imaged. Images were than analyzed using a custom CellProfiler (v2.1.1, Broad Institute (Carpenter, A.E. et al., 2006)) project program to identify single cells and quantify the internalized target particle fluorescence intensity (of LISS-Rhodamine lipid) within each cell. Average internalized fluorescence per cell was calculated per condition. Independent replicates were conducted on different days, and replicates were normalized to average eating for all conditions to control for day-to-day variation.

Target particle binding assay
To assess particle engagement, macrophages were seeded in 96-well plates and target particles were prepared as with the phagocytosis assay. Upon addition of target particles to macrophage

wells, the 96-well plate was incubated at 4°C for 30 minutes to enable binding but prevent engulfment. Cells were then rinsed of excess beads and stained with 1 μM of CellTracker Green (CMFDA, Thermo Fisher Scientific) and 10 μM Hoechst 33342 (Thermo Fisher Scientific) while kept on ice. Images were acquired and analyzed using a custom CellProfiler (v2.1.1) project program to identify bound beads. Average number of bound beads per cell was calculated per condition. Independent replicates were conducted on different days, and replicates were normalized to average eating for all conditions to control for day-to-day variation.

Tumor cell phagocytosis assay
After thawing and resuspending in RPMI 1640 medium, BMDMs were incubated with 1 μM of CellTracker Deep Red (Thermo Fisher Scientific) at room temperature for 10 minutes. Cells were washed 2 times in PBS to remove excess dye, resuspended in RPMI 1640 medium and seeded at 40,000 cells per well in a tissue-culture flat-bottom 96-well plate. Cells were incubated at 37°C overnight (approximately 18 hours prior to tumor cell addition).

MC38-hHER2 cells were incubated in 1 μM Cell Tracker Green in PBS for 10 minutes at room temperature. Cells were washed 2 times in PBS to remove excess dye, and then resuspended in RPMI 1640 media. AlexaFluor647-labeled anti-hHER2 antibody (mouse IgG2a isotype targeting clinical Trastuzumab hHER2 epitope, Aduro Biotech) was serially diluted with MC38-hHER2 cells to achieve appropriate final concentrations for opsonization. MC38-hHER2 cells were coated in anti-hHER2 antibody dilutions 20 minutes prior to addition to BMDMs wells. When applicable, 18a antibody (SIRPα-blocking antibody, Aduro Biotech) was added directly to seeded BMDMs 20 minutes prior to MC38-hHER2 cell addition. 40,000 MC38-hHER2 cells (in 100 μL) were added to each well of 40,000 BMDMs to achieve a 1:1 ratio.

MC38-hHER2 cells were incubated with BMDMs for exactly 30 minutes. Wells were washed 2 times with PBS to remove excess MC38-hHER2 cells. Wells were imaged using the same microscope and automated technique as the target particle phagocytosis assay. Images were analyzed using a CellProfiler program that identified single BMDM cells and quantified the internalized MC38-hHER2 fluorescence intensity (CellTracker Green) within each BMDM cell. Average internalized fluorescence per cell was calculated per condition. Independent replicates were conducted on different days, and replicates were normalized to average eating for all conditions to control for day-to-day variation.

Generation of cell lines

Design of synthetic receptors
The alpha helical SYNZIP Syn18-Syn17 binding pair was chosen due to its antiparallel orientation (Thompson et al., 2012). For each synthetic receptor design, the 41 amino acid sequence of Syn18 was placed N-terminally to one FNIII domain (Jacobs et al., 2012) to control the height above the membrane of the synthetic receptor protein (Figure S2a). The extracellular part was followed by the transmembrane domain of mouse SIRPα (Accession #P97797, amino acid 374-394), followed by intracellular regions of FcγRIIA (Accession #P12318, amino acid 240-317), CD3ζ (Accession #24161, amino acid 52-164), FcεRI γ-chain (Accession #P20491, amino acid 45-86), SIRPα (Accession #P97797, amino acid 395-513), CD22 (Accession #P35329, amino acid 722-862), PD-1 (Accession #Q02242, amino acid 191-288), and FcγRIIB

(Accession #P08101, amino acid 232-330). A C-terminal GFP facilitated cell sorting and validated receptor localization. The entirety of each of the annotated intracellular domains was ordered as a separate gene fragment (Integrated DNA Technologies) and each complete receptor was cloned into pHR lentiviral expression vector (Clontech). Each region of the protein was amplified using PCR and fragments were combined using Gibson assembly.

Design of Syk and SHP1 sensors
mCh-Syk live phosphosensor was designed and utilized as previously published (Bakalar et al., 2018).

SHP1 interacts with phosphorylated SIRPα through interaction with its tandem SH2 domains. We created a sensor that specifically localizes to phosphorylated ITIMs by fusing the two SH2 domains of SHP1 to GFP to enable visualization of intracellular localization of the expressed protein. SH2 domain sequences were obtained from Addgene (pGEX-SHP-1(NC)-SH2, A #46496 (Machida et al., 2007)) and a linker region (GGGSGGGS) was placed between the SH2 domains and GFP. The sensor was cloned into pHR lentiviral expression vector under control of low-expression UBC promoter and high-expression SFFV promoter.

Additional mEOS constructs were created using Syk and SHP1 SH2 domains as described above. Each was cloned into pHR lentiviral expression vector under control of low-expression UBC promoter.

Generation of stable cell lines
HEK293T cells were grown to 70% confluency in a 6-well tissue-culture plate, and 160 ng pDM2.G (Clontech), 1.3 μg CMV 8.91 (Clontech), and 1.5 μg of target vector were transfected using TransIT-293T transfection reagent (Mirus Bio). Viral supernatant was collected 60 hours after transfection and spun at 1000 x g to remove HEK293T cells and used immediately. 1 mL of lentiviral supernatant was added to $5x10^5$ RAW 264.7 macrophages with 4 μg/mL of hexadimethrine bromide (Millipore) and cells were spinoculated at 300 x g for 30 minutes at room temperature. Cells were resuspended and plated into a 10 cm non-tissue-culture dish. Cells were sorted via fluorescence-activated cell sorting using an Aria Fusion cell sorter (Becton Dickinson) and the sorted population was expanded for use. For cell lines expressing synthetic receptors, function of Syn18 receptors was confirmed using AlexaFluor647-labeled soluble Syn17-F3L (see "Purification of Syn17-F3L").

Purification of Syn17-F3L

Design of Syn17-F3L and Syn17-F5L
To create the Syn18 receptor ligands, the 42-amino acid sequence of Syn17 (Thompson et al., 2012) was followed by three or five repeats of the synthetic FNIII domain (Jacobs et al., 2012). Three Fibcon repeats were used to achieve a receptor-ligand interaction height that corresponds to FcγR-antibody, and five repeats were used to intentionally increase receptor-ligand height. Finally, a C-terminal His-10 allowed for attachment to Ni-NTA lipids. Each region of the protein was amplified via PCR and fragments were combined using Gibson assembly into pET28 vector (Millipore) for expression in *E. coli*.

Syn17-F3L and Syn17-F5L protein expression and purification
Syn17-F3L or Syn17-F5L was expressed in Rosetta DE3 competent cells (Millipore). Cells were grown at 37°C to OD = 0.8 and expression was induced with 0.3 mM IPTG (Isopropyl b-D-1-thiogalactopyranoside, Calbiochem) overnight at 18°C. Cells were pelleted and resuspended in 25 mM HEPES pH 7.4 (4-(2-hydroxyethyl)-1-piperazineethanesulfonic acid, Thermo Fisher Scientific), 150 mM NaCl, 0.5 mM TCEP (tris(2-carboxyethyl)phosphine, Thermo Fisher Scientific) and 10 mM imidazole (Thermo Fisher Scientific), and lysed. After centrifugation, lysate was affinity purified using Cobalt-charged His-Trap Chelating column (GE Healthcare) through imidazole gradient elution. Peak fractions were gel-filtered using Superdex 200 column (GE Healthcare) into 25 mM HEPES pH 7.4, 150 mM NaCl, 0.5 mM TCEP. Protein was then labeled with AlexFluor647 NHS Ester (Thermo Fisher Scientific) as described in "Fluorescent labeling of proteins".

SLB TIRF imaging and quantification

Formation of planar SLBs
To image footprints of macrophages and GPMVs, planar SLBs were formed onto coverslips via fusion of SUVs to RCA-cleaned glass coverslips. PDMS (Polydimethylsiloxane, Sylgard) placed atop RCA-cleaned glass formed the imaging chamber, and 50 μL of MOPS buffer and 50 μL of non-fluorescent SUV solution were added. The SUVs were incubated for 20 minutes at room temperature. Excess SUVs were then removed by gently washing 5x with 60 μL of PBS. Appropriate antibody or CD47 dilutions were prepared, 60 μL were added to the washed SLB and incubated for 20 minutes. Excess protein was removed by gently washing the SLB 2x with PBS. The fluidity of proteins on the SLB was confirmed by using a spinning-disk confocal (Nikon) to examine diffusion of labeled molecules after photobleaching a small region of interest.

GPMV formation
GPMVs were made according to the protocol outlined by Sezgin et al (Sezgin et al., 2012). RAW 264.7 macrophages were seeded in a 6-well plate (Falcon). After adhering, they were rinsed with 1 mL GPMV buffer (10 nM HEPES (4-(2-hydroxyethyl)-1-piperazineethanesulfonic acid), 150 mM NaCl, 2 mM $CaCl_2$, pH 7.4) before addition of 1 mL of vesiculation buffer (GPMV buffer plus 25 mM PFA (paraformaldehyde, Electron Microscopy Services) and 2 mM DTT (1,4-dithiothreitol, Anaspec). Cells were incubated for 1 hour at 37°C and GPMVs were collected by removing supernatant from cells.

TIRF imaging of GPMV and cell interfaces
Macrophages or GPMVs were added directly to planar SLBs containing AlexaFluor647-labeled anti-biotin IgG, AlexaFluor488-labeled CD47, or both. Cells or GPMVs were allowed to settle for 20 minutes prior to imaging. Engaged GPMVs or cells were located and identified using reflection interference contrast microscopy (RICM). Images were acquired using RICM and TIRF microscopy for all relevant fluorescent channels. When applicable, CD45 was labeled with 10 nM anti-CD45 antibody (clone 30-F11 Brilliant Violet 421, BioLegend).

Quantification of TIRF images

Images were quantified by identifying ROIs in RICM so as to not bias analysis by segmenting on a fluorescent channel. RICM images were flattened using a background (no cells or GPMV) image, then outlines of SLB-bound cells or GPMVs were identified. Fluorescence inside and outside these ROI outlines was measured and averaged for each fluorescent channel. The outside background measurement was subtracted from the average signal inside of the footprint. This was implemented using an automated custom macro in FIJI (Schindelin, J. et al., 2012). Data was processed and analyzed using Python 3.5 (python.org).

Single molecule imaging and quantification
Macrophages expressing SHP1-EOS and Syk-EOS were incubated on planar SLBs containing unlabeled anti-biotin IgG, CD47, or both. Cells were allowed to settle for 20 minutes prior to imaging. Cells were imaged for EOS expression using 488 nm excitation in TIRF. Single molecules were then converted to RFP using 50 ms pulse of 405 nm light. Timelapse images were acquired every 30 ms using a 561 nm excitation. Timelapse images were then analyzed using MatLab TrackNTrace package (Stein & Thiart, 2016) and a custom Matlab script to identify binding events and quantify molecule dwell times.

Staining and quantification of phosphotyrosine

Fixation of macrophages with target particles
To stain for phosphotyrosine at macrophage-target interfaces, macrophages were seeded into 8-well imaging chambers with a coverslip glass bottom (Cellvis) and allowed to adhere for at 3-4 hours. If applicable, cells were treated with 3 μM SHP1/2 phosphatase inhibitor (NSC-87877, Sigma-Aldrich) for 20 minutes prior to target particle addition. Target particles coated in non-fluorescent SLBs plus AlexaFluor647-labeled anti-biotin IgG and/or AlexaFluor488-labeled CD47 were added to the seeded cells. After exactly 10 minutes at 37°C, cells were fixed for 10 minutes with 4% PFA in PBS. Cells were then permeabilized using 0.2% Tween-20 (Thermo Fisher Scientific) for 10 minutes and rinsed twice with PBS. Non-specific binding was blocked with 3% (w/v) bovine serum albumin (BSA, ChemCruz) in PBS with 0.5 g/mL Fc Block (BD Biosciences) for 30 minutes. Phosphotyrosine antibody (P-Y-1000 MultiMab, Cell Signaling Technology 8954S) was added to cells at 1:500 dilution in 1% BSA and incubated at room temperature for 1 hour. Cells were rinsed twice with 1% BSA, then incubated with a secondary antibody (AlexaFluor546-labeled goat anti-rabbit IgG, Invitrogen A11010) at a dilution of 1:1000 in 1% BSA for 1 hour at room temperature. Cells were washed twice with PBS before fluorescence and brightfield imaging with spinning-disk confocal microscope.

Interfaces between cells and bound (but not internalized) target particles were manually identified using brightfield images. Average pixel intensity within the interface was quantified using an automated custom macro in ImageJ.

Fixation and quantification of macrophages on SLB
To stain phosphotyrosine within footprints, macrophages were dropped onto a planar SLB and incubated at 37°C for 10 minutes. After exactly 10 minutes, cells were fixed and stained according to "Fixation of macrophages with beads." Cells were imaged using RICM and TIRF imaging, and fluorescence within the footprint was measured as described in "Quantification of TIRF images."

Fixation of BMDMs with tumor cells
To stain phosphotyrosine at BMDM-MC38 interfaces, 60,000 BMDMs were seeded into 8-well imaging chambers with a coverslip glass bottom. 40,000 MC38-hHER2 cells were incubated with various concentrations of AlexaFluor647-labeled anti-hHER2 antibody for 20 minutes at room temperature with continuous rotation. Opsonized MC38-hHER2 cells were added to BMDMs and incubated at 37°C for exactly 10 minutes. Cells were fixed and stained according to "Fixation of macrophages with beads."

Modeling

Activation and inhibition pathways were modeled using a set of 13 differential equations. Each equation represented a molecular species in the model, and the mass balance equations calculated species concentration change per unit time. Equations were implemented using Python 3.5 using *SciPy* software package functions for numerically solving ODEs (scipy.org). Simulations were run for 200 time points, a sufficient time to consistently reach steady state values for all species. Antibody concentrations were initiated from 1000 to 5000, and CD47 concentrations between 0 and 10000.

Measurement of cell surface densities

BMDM, RAW 264.7, or MC38-hHER2 cells were resuspended at a density of 300,000 cells/mL in PBS with 5% FBS. On RAW 264.7 cells, Mouse Fc Block (rat anti-mouse CD16/CD32, BD Biosciences 553142) and p84 (provided by Aduro Biotech) were used to label FcγRs and SIRPα, respectively. On BMDMs, Fc Block and 18a with mutant Fc tail to prevent FcγR binding (provided by Aduro Biotech) were used to label FcγRs and SIRPα, respectively. On MC38-hHER2 cells, anti-hHER2 (mouse Fc Trastuzumab) and MIAP 301 (both provided by Aduro Biotech) were used to label hHER2 and CD47, respectively. Antibodies were labeled using AlexFluor647 NHS Ester (Thermo Fisher Scientific) (see "Fluorescent labeling of proteins"). Each antibody was added at a top concentration of 50 μg/mL, then serially diluted 4-fold into 8 sequential samples. This yielded a final range of 0.01 to 50 μg/mL antibody. Each antibody concentration was mixed with 30,000 cells and incubated at 4°C for 30 minutes to prevent internalization. Cells were washed twice by spinning for 5 minutes at 300 x g, removing supernatant, and replacing with PBS. Fluorescence of antibodies bound to cell surface was immediately measured on an Attune NxT flow cytometer. Surface antibodies were quantified using calibrated fluorescent beads.

QUANTIFICATION AND STATISTICAL ANALYSIS
All statistical analysis was performed in Python 3.5 using *SciPy* software package functions. The number of cells, particles, and interfaces quantified per experiment are indicated for each figure in the figure legend. In general, significance was based on a two-sample Student's t-test for the mean values of experimental replicates, where *$p<0.05$, **$p<0.01$, and ***$p<0.001$. Statistical details of data presented are indicated in figure legends.

Supplementary Information

Supplemental Figure 1.

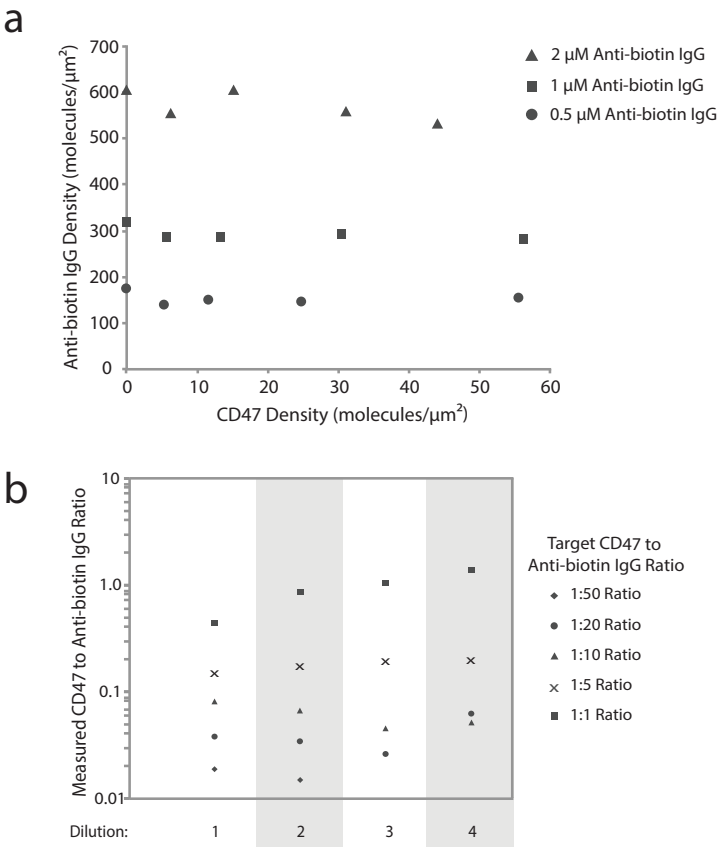

Figure S1. Quantification of bead surface densities of antibody and CD47. Related to Figure 1.

(a) Example target particle surface density data from phagocytosis assay summarized in Figure 1b. SLB-coated target particles were coated in different concentrations of AlexaFluor647-labeled anti-biotin IgG and AlexaFluor488-labeled CD47. Target particle fluorescence was measured via flow cytometry and compared to calibrated beads to calculate surface densities for each protein.

(b) Example target particle surface density data from phagocytosis assay summarized in Figure 1c. Target ratios of CD47 and anti-biotin IgG were created, then serially diluted 5-fold 3 times (for a total of 4 dilutions). Note that conditions that have no CD47 added or data points in which CD47 was diluted past detectable limits are not plotted.

Supplemental Figure 2.

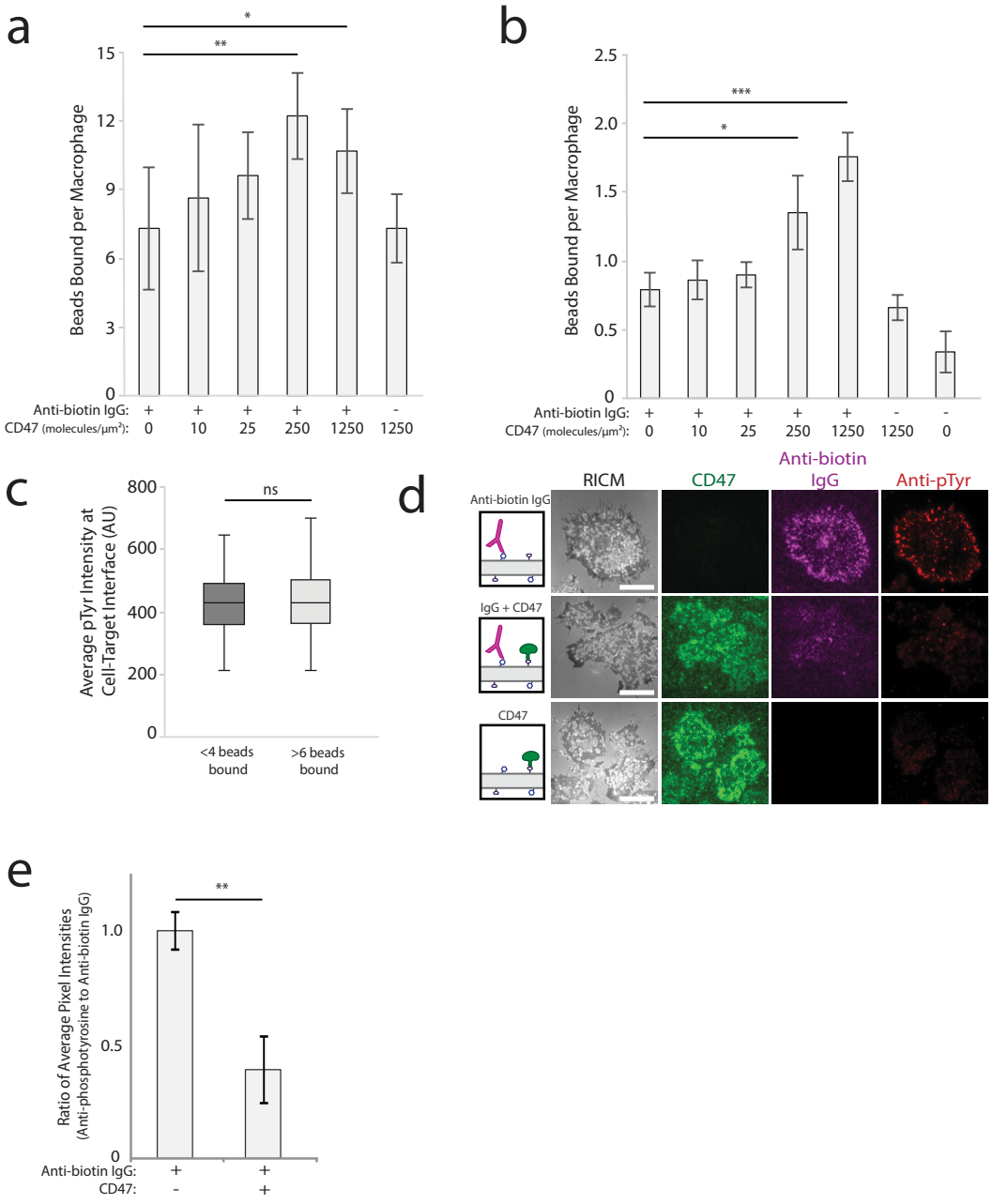

Figure S2. Measurement of binding and phosphorylation at immune interface. Related to Figures 2 and 3.

(a) Average number of beads bound to RAW 264.7 macrophages quantified in Figure 3a. Beads coated in anti-biotin IgG (300 molecules/μm^2) and CD47 (10-1250 molecules/μm^2) were incubated with macrophages for 10 minutes prior to fixation. Each condition is the average of 3 independent experiments representing a total of >40 cells. Bars represent mean ± s.e.m. Conditions were compared with two-tailed student's *t* test, with (*) denoting $p<0.05$ and (**) denoting $p<0.01$.

(b) Beads coated in anti-biotin IgG (300 molecules/μm^2) and CD47 (10-1250 molecules/μm^2) were incubated with RAW 264.7 macrophages at 4°C for 30 minutes to prevent phagocytosis, and bound beads were quantified. Each condition is the average of three independent experiments representing a total of >200 cells. Bars represent mean ± s.e.m. Conditions were compared with two-tailed student's *t* test, with (*) denoting $p<0.05$ and (***) denoting $p<0.001$.

(c) RAW 264.7 macrophages quantified in Figure 3a were partitioned into high engagement (>6 beads bound) and a low engagement (<4 beads bound) groups, and the average pTyr signal at bead interfaces was averaged for each group. Each condition represents >50 cell-target interfaces. Bars represent mean ± s.e.m. Conditions were compared with two-tailed student's *t* test, with (**) denoting $p<0.01$.

(d) RAW 264.7 macrophages were dropped onto SLBs coated in AlexaFluor647-labeled anti-biotin IgG (magenta), AlexaFluor488-labeled CD47 (green), or both. Cells were imaged using RICM and TIRF microscopy. Scale bar is 5 μm.

(e) The fluorescence ratio of anti-phosphotyrosine to anti-biotin IgG was quantified for each footprint. Each condition is the average of >50 footprints. Bars represent mean ± s.e.m. Conditions were compared with two-tailed student's *t* test, with (**) denoting $p<0.01$.

Supplemental Figure 3.

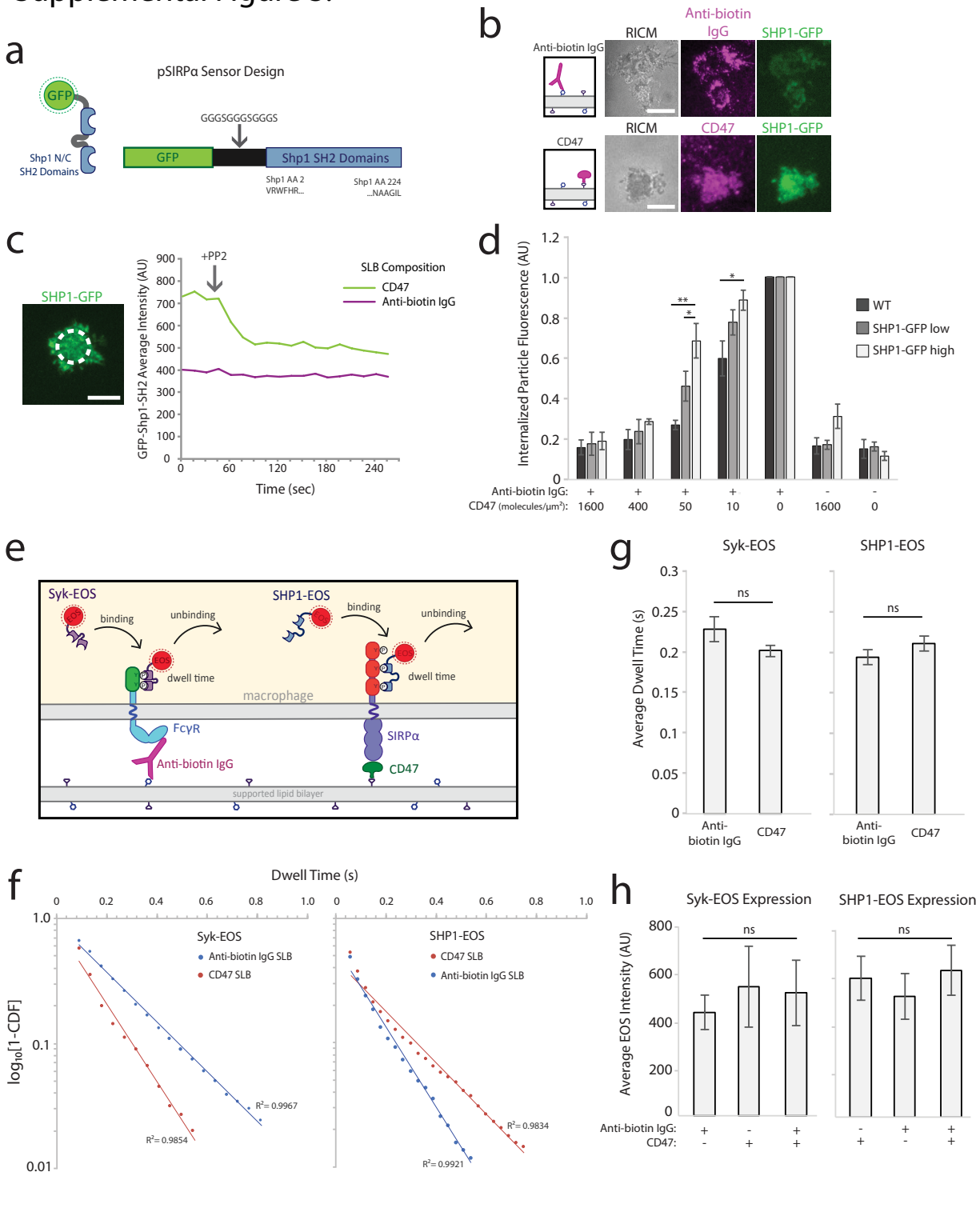

Figure S3. Design and measurement of phosphorylation sensors. Related to Figure 3.

(a) Design of SHP1-GFP sensor for phosphorylated SIRPα. GFP was linked to the tandem SH2 domains of SHP1, which bind to phosphorylated ITIMs in the cytoplasmic tail of SIRPα.

(b) Representative TIRF and RICM images of RAW 264.7 cells expressing SHP1-GFP (green) on SLBs containing either anti-biotin IgG only or CD47 only (each labeled with AlexaFluor647, magenta). Scale bar is 10 μm.

(c) Effect of addition of 1μM Src family kinase inhibitor PP2 on SHP1-GFP sensor intensity. Src family kinase Lyn is responsible for phosphorylation of SIRPα, and decreasing SIRPα phosphorylation prevents SHP1 binding. Sensor intensity over time was measured in region indicated by white circle. Scale bar is 10 μm.

(d) Phagocytosis was quantified for target particles with a range of CD47:antibody densities with RAW 264.7 macrophages stably expressing SHP1-GFP at high or low levels. Each condition is the average of three independent experiments representing a total of >300 cells. Bars represent mean ± s.e.m. Conditions were compared with two-tailed student's *t* test, with (*) denoting $p<0.05$ and (**) denoting $p<0.01$.

(e) Binding of Syk-EOS and SHP1-EOS to their preferred targets, phosphorylated FcγR and SIRPα, respectively. Binding events and molecule dwell times were quantified from TIRF timelapse images.

(f) Cumulative distribution function for SHP1-EOS (left) and Syk-EOS (right) dwell times. RAW 264.7 cells stably expressing SHP1-EOS and Syk-EOS were dropped onto SLBs coated in either anti-biotin IgG (300 molecules/μm^2) or CD47 (500 molecules/μm^2).

(g) Average dwell time for Syk-EOS and SHP1-EOS was quantified from binding event dwell times quantified in Figure S3e. Each condition is the average of three independent experiments representing a total of >3000 binding events per condition. Bars represent mean ± s.e.m. Conditions were compared with two-tailed student's *t* test.

(h) SHP1-EOS and Syk-EOS expression of cells quantified in Figure 3d. Expression was assessed by quantifying average GFP intensity in cell footprint. Each condition is the average of 3 independent experiments representing a total of >50 macrophage footprints. Bars represent mean ± s.e.m. Conditions were compared with one-way ANOVA statistical test.

Supplemental Figure 4.

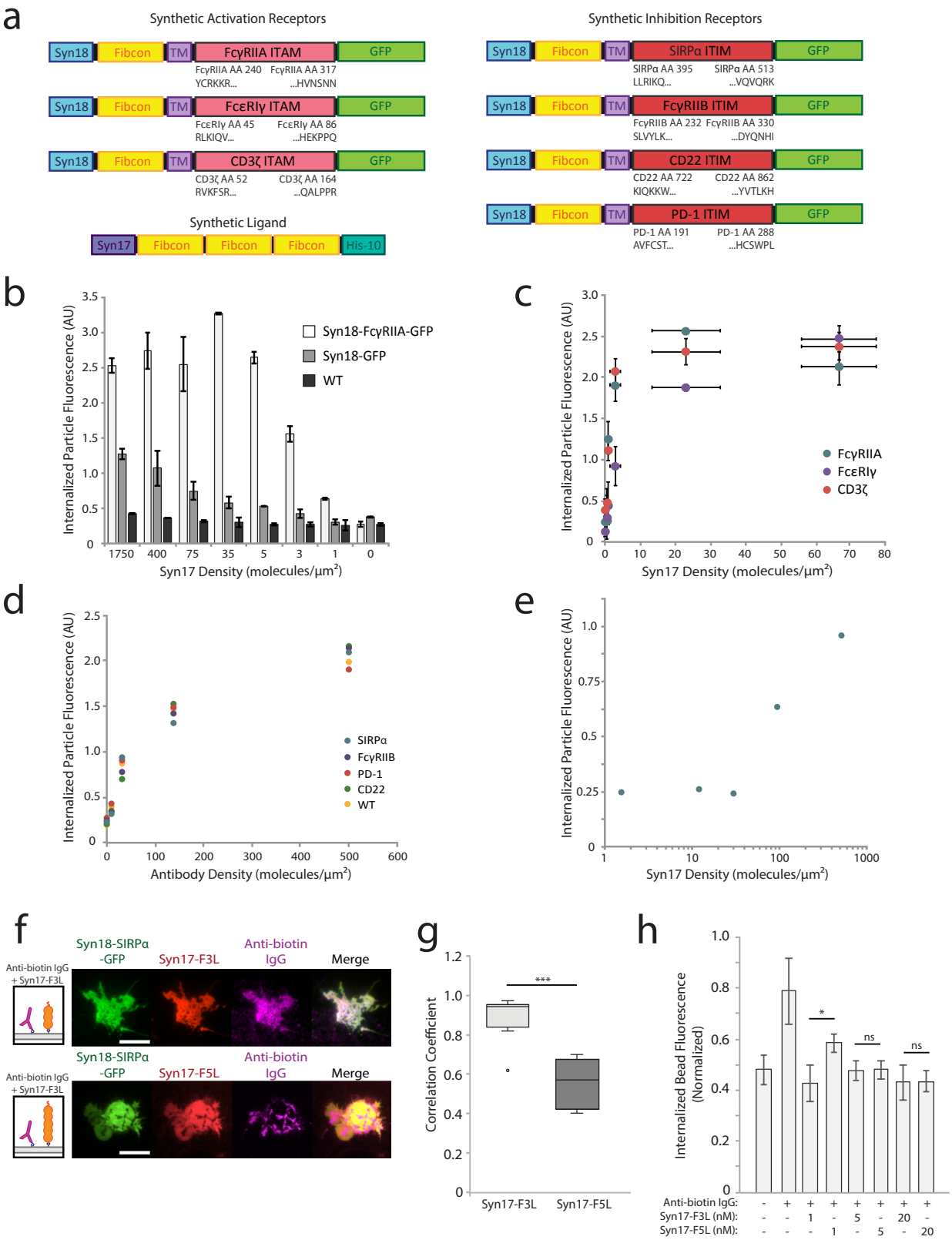

Figure S4. Validation of ITAM- or ITIM-containing synthetic receptors. Related to Figure 4.

(a) Schematic of synthetic chimeric receptor constructs. Synthetic activation receptors signaled via FcγRIIA, FcεRI γ-chain, and CD3 ζ-chain ITAM-containing intracellular domains. Synthetic inhibition receptors signaled via FcγRIIB, PD-1, SIRPα, and CD22 ITIM-containing intracellular domains.

(b) Target particles with varying surface densities of Syn17-F3L (0-1750 molecules/μm^2) were incubated with RAW 264.7 macrophages stably expressing Syn18-FcγRIIA-GFP receptor (light gray bars) and non-signaling Syn18-GFP (medium gray bars), as well as wild type macrophages (WT, dark gray bars). Average phagocytosis was quantified. Each condition is the average of three independent experiments representing a total of >300 cells. Bars represent mean ± s.e.m.

(c) Phagocytosis of Syn17-3L-coated target particles with macrophages expressing different Syn18 activating receptors. RAW 264.7 macrophages independently express Syn18 receptors containing FcγRIIA, FcεRI γ-chain, and CD3 ζ-chain intracellular signaling motifs. Target particles coated with increasing Syn17-F3L densities (0-75 molecules/μm^2) were simultaneously added to each receptor cell line, and average phagocytosis was quantified in the absence of an inhibitory ligand. Each condition is the average of three independent experiments representing a total of >300 cells. Dots represent mean ± s.e.m.

(d) Phagocytosis of anti-biotin IgG coated target particles by macrophages expressing different Syn18 inhibitory receptors. RAW 264.7 macrophages independently express Syn18 receptors containing FcγRIIB, PD-1, SIRPα, and CD22 intracellular signaling motifs. Target particles coated with increasing anti-biotin IgG surface densities (0-500 molecules/ μm^2) were simultaneously added to each receptor cell line as well as WT macrophages, and average phagocytosis was quantified in the absence of an inhibitory ligand. Each condition is the average of >100 cells.

(e) Phagocytosis of Syn17-F3L coated target particles by macrophages expressing Syn18-SIRPα-GFP. Phagocytosis was quantified for target particles coated in increasing densities of Syn17-F3L (0-500 molecules/μm^2) in the absence of an activating ligand. Each condition is the average of >100 cells.

(f) Representative TIRF images of RAW 264.7 cells expressing Syn18-SIRPα-GFP (green) on SLBs containing anti-biotin IgG (magenta) plus either Syn17-F3L or Syn17-F5L (red). Scale bar is 10 μm.

(g) Pearson's correlation coefficient comparing anti-biotin IgG localization with either Syn17-F3L or Syn17-F5L. Conditions were compared with two-tailed student's *t* test, with (***) denoting $p<0.001$.

(h) Phagocytosis of target particles coated in anti-biotin IgG and different concentrations of Syn17 ligand was quantified for Syn18-SIRPα-GFP macrophages. Phagocytosis levels of Syn18-SIRPα-GFP expressing cells were normalized to non-signaling Syn18-GFP expressing cells to

account for the impact of increased steric bulk of the Syn17-F5L on anti-biotin IgG accessibility. Each condition is the average of three independent experiments representing a total of >300 cells. Bars represent mean ± s.e.m. Conditions were compared with two-tailed student's *t* test, with (*) denoting $p<0.05$.

Supplemental Figure 5.

a

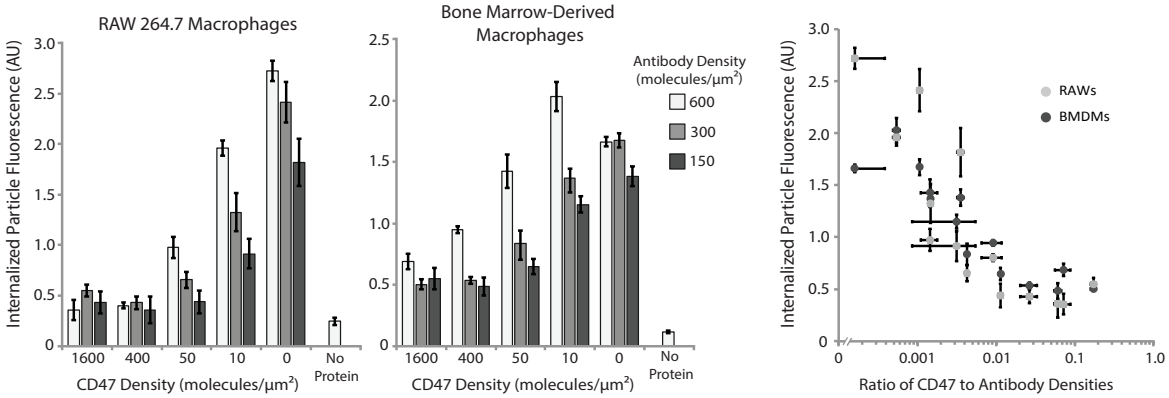

b

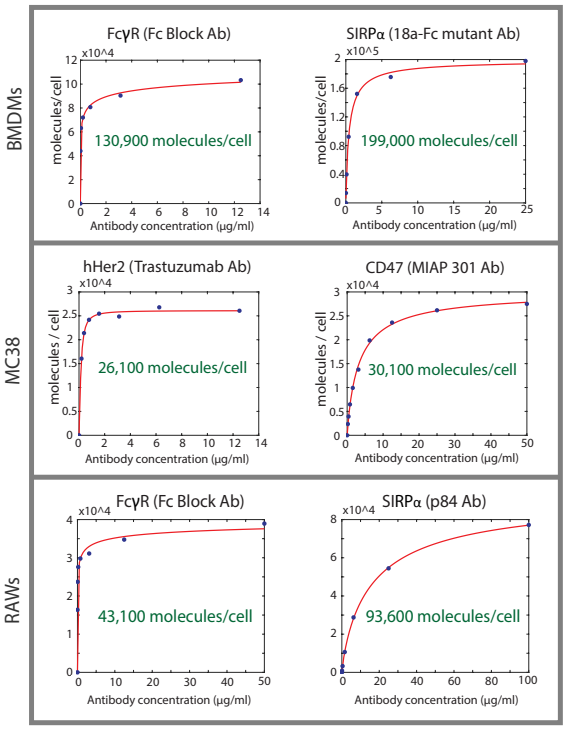

Figure S5. Characterization of BMDM phagocytosis and cell surface densities. Related to Figure 5.

(a) Phagocytosis comparison between RAW 264.7 macrophages and BMDMs. To create a panel of target particle compositions, three different anti-biotin IgG surface densities (150, 300, 600 molecules/μm^2) were combined with five different CD47 densities (0-1600 molecules/μm^2), plus an additional no protein (lipid only) control. All 16 different target particle densities were simultaneously added to RAWs and BMDMs, and average phagocytosis was quantified (left and center panels). Data replotted as a function of CD47:antibody ratio (right panel). Each condition is an average of 3 independent experiments representing >200 total cells. Bars represent mean ± s.e.m.

(b) Measurements of surface densities on RAW 264.7 macrophages, BMDMs, and MC38-hHER2 tumor cells. AlexaFluor647-labeled antibodies for FcγRs (Fc Block), SIRPα (18a Fc mutant and p84), hHER2 (anti-hHER2), and CD47 (MIAP 301) were increased to receptor saturating concentrations and measured via flow cytometry. Number of molecules per cell was estimated by fitting a Hill equation to each antibody titration and calculating y_{max}.

Supplemental Table 1.

Equations implemented in interacting kinetic model
(p denotes phosphorylated state)

$$\frac{\partial}{\partial t}[FcR] = -k_1[Ab][FcR] + k_2[FcR - Ab]$$

$$\frac{\partial}{\partial t}[FcR - Ab] = k_1[Ab][FcR] - k_2[FcR - Ab] - k_3[FcR - Ab] + k_{13}[SIRP\alpha - Shp1 - FcR_p]$$

$$\frac{\partial}{\partial t}[Ab] = -k_1[Ab][FcR] + k_2[FcR - Ab]$$

$$\frac{\partial}{\partial t}[FcR_p] = k_3[FcR - Ab] - k_4[FcR_p][Syk] + k_5[FcR - Syk] - k_{11}[SIRP\alpha - Shp1][FcR_p] + k_{12}[SIRP\alpha - Shp1 - FcR_p]$$

$$\frac{\partial}{\partial t}[FcR - Syk] = k_4[FcR_p][Syk] - k_5[FcR - Syk]$$

$$\frac{\partial}{\partial t}[Syk] = -k_4[FcR_p][Syk] + k_5[FcR - Syk]$$

$$\frac{\partial}{\partial t}[SIRP\alpha] = -k_6[SIRP\alpha][CD47] + k_7[SIRP\alpha - CD47]$$

$$\frac{\partial}{\partial t}[CD47] = -k_6[SIRP\alpha][CD47] + k_7[SIRP\alpha - CD47]$$

$$\frac{\partial}{\partial t}[SIRP\alpha - CD47] = k_6[SIRP\alpha][CD47] - k_7[SIRP\alpha - CD47] - k_8[SIRP\alpha - CD47]$$

$$\frac{\partial}{\partial t}[SIRP\alpha_p] = k_8[SIRP\alpha - CD47] - k_9[SIRP\alpha_p][Shp1] + k_{10}[SIRP\alpha - Shp1]$$

$$\frac{\partial}{\partial t}[SIRP\alpha - Shp1] = k_9[SIRP\alpha_p][Shp1] - k_{10}[SIRP\alpha - Shp1] - k_{11}[SIRP\alpha - Shp1][FcR_p] + k_{12}[SIRP\alpha - Shp1 - FcR_p] + k_{13}[SIRP\alpha - Shp1 - FcR_p]$$

$$\frac{\partial}{\partial t}[Shp1] = -k_9[Shp1][SIRP\alpha_p] + k_{10}[SIRP\alpha - Shp1]$$

$$\frac{\partial}{\partial t}[SIRP\alpha - Shp1 - FcR_p] = k_{11}[SIRP\alpha - Shp1][FcR_p] - k_{12}[SIRP\alpha - Shp1 - FcR_p] - k_{13}[SIRP\alpha - Shp1 - FcR_p]$$

Table S1. Differential equations implemented for interacting kinetic model. Related to Figure 3.

Equations were simulated in Python 3.5.

Supplemental Table 2.

Rate Constant	Value	Citation	Notes
k_1	8.2 x10^3 $M^{-1}s^{-1}$	Li et al, 2007	
k_2	5.7 x10^{-3} s^{-1}	Li et al, 2007	
k_3	0.15 s^{-1}	Barua et al, 2012	Estimated from value for unphosphorylated Lyn
k_4	1.8 x10^5 $M^{-1}s^{-1}$	Barua et al, 2012	
k_5	0.3 s^{-1}	Barua et al, 2012	
k_6	2 x10^5 $M^{-1}s^{-1}$	Brooke et al, 2004	
k_7	5.3 s^{-1}	Brooke et al, 2004	
k_8	0.15 s^{-1}	Barua et al, 2012	Same as k_3; Assumes no ITAM vs. ITIM preference
k_9	1.8 x10^6 $M^{-1}s^{-1}$	Barua et al, 2012	Estimate from other SFKs
k_{10}	0.1 s^{-1}	Barua et al, 2012	
k_{11}	1.8 x10^5 $M^{-1}s^{-1}$	Ren et al, 2011	Estimated from k_d value
k_{12}	5 s^{-1}	Ren et al, 2011	
k_{13}	66 s^{-1}	Selner et al, 2014	Measured value for peptide w/I at Y -2 position

Table S2. Rate constants utilized in phagocytosis kinetic model. Related to Figure 3.
Constants that were estimated from published values are noted.

SUPPLEMENTAL VIDEOS

Video S1. Representative TIRF timelapse image of SHP1-EOS. Related to Figure 3.
RAW 264.7 macrophages expressing SHP1-EOS were incubated on SLBs coated in CD47, then stimulated with 405 nm light pulse. Timelapse images of SHP1-EOS binding events were taken using 561 nm excitation light. The timecourse of the video is 10 seconds.

Video S2. Representative TIRF timelapse image of Syk-EOS. Related to Figure 3.
RAW 264.7 macrophages expressing Syk-EOS were incubated on SLBs coated in anti-biotin IgG, then stimulated with 405 nm light pulse. Timelapse images of Syk-EOS binding events were taken using 561 nm excitation light. The timecourse of the video is 10 seconds.

References

Abram, C. L., & Lowell, C. A. (2008). The diverse functions of Src family kinases in macrophages. *Frontiers in Bioscience : A Journal and Virtual Library*, *13*, 4426–4450.

Bakalar, M. H., Joffe, A. M., Schmid, E. M., Son, S., Podolski, M., & Fletcher, D. A. (2018). Size-Dependent Segregation Controls Macrophage Phagocytosis of Antibody-Opsonized Targets. *Cell*, *174*(1), 131-142.e13. https://doi.org/10.1016/j.cell.2018.05.059

Barclay, A. N., & van den Berg, T. K. (2014). The Interaction Between Signal Regulatory Protein Alpha (SIRPα) and CD47: Structure, Function, and Therapeutic Target. *Annual Review of Immunology*, *32*(1), 25–50. https://doi.org/10.1146/annurev-immunol-032713-120142

Barua, D., Hlavacek, W. S., & Lipniacki, T. (2012). A Computational Model for Early Events in B Cell Antigen Receptor Signaling: Analysis of the Roles of Lyn and Fyn. *The Journal of Immunology*, *189*(2), 646–658. https://doi.org/10.4049/jimmunol.1102003

Binstadt, B. A., Brumbaugh, K. M., Dick, C. J., Scharenberg, A. M., Williams, B. L., Colonna, M., Lanier, L. L., Kinet, J.-P., Abraham, R. T., & Leibson, P. J. (1996). Sequential Involvement of Lck and SHP-1 with MHC-Recognizing Receptors on NK Cells Inhibits FcR-Initiated Tyrosine Kinase Activation. *Immunity*, *5*(6), 629–638. https://doi.org/10.1016/S1074-7613(00)80276-9

Brooke, G., Holbrook, J. D., Brown, M. H., & Barclay, A. N. (2004). Human Lymphocytes Interact Directly with CD47 through a Novel Member of the Signal Regulatory Protein (SIRP) Family. *The Journal of Immunology*, *173*(4), 2562–2570. https://doi.org/10.4049/jimmunol.173.4.2562

Burshtyn, D. N., Yang, W., Yi, T., & Long, E. O. (1997). A Novel Phosphotyrosine Motif with a Critical Amino Acid at Position −2 for the SH2 Domain-mediated Activation of the Tyrosine Phosphatase SHP-1. *Journal of Biological Chemistry*, *272*(20), 13066–13072. https://doi.org/10.1074/jbc.272.20.13066

Caron, E., & Hall, A. (1998). Identification of Two Distinct Mechanisms of Phagocytosis Controlled by Different Rho GTPases. *Science*, *282*(5394), 1717–1721. https://doi.org/10.1126/science.282.5394.1717

Carpenter, A.E. et al. (2006). CellProfiler: Image analysis software for identifying and quantifying cell phenotypes. *Genome Biology*, *7*.

Chao, M. P., Alizadeh, A. A., Tang, C., Myklebust, J. H., Varghese, B., Gill, S., Jan, M., Cha, A. C., Chan, C. K., Tan, B. T., Park, C. Y., Zhao, F., Kohrt, H. E., Malumbres, R., Briones, J., Gascoyne, R. D., Lossos, I. S., Levy, R., Weissman, I. L., & Majeti, R. (2010). Anti-CD47 antibody synergizes with rituximab to promote phagocytosis and eradicate non-Hodgkin lymphoma. *Cell*, *142*(5), 699–713. https://doi.org/10.1016/j.cell.2010.07.044

Chen, L., Sung, S.-S., Yip, M. L. R., Lawrence, H. R., Ren, Y., Guida, W. C., Sebti, S. M., Lawrence, N. J., & Wu, J. (2006). Discovery of a Novel Shp2 Protein Tyrosine Phosphatase Inhibitor. *Molecular Pharmacology*, *70*(2), 562–570. https://doi.org/10.1124/mol.106.025536

Chu, C. C., VanDerMeid, K. R., Elliott, M. R., Baran, A. M., Barr, P. M., & Zent, C. S. (2018). Antibody-dependent cellular phagocytosis is responsible for efficacy of anti-CD20

monoclonal antibody therapy in chronic lymphocytic leukemia. *The Journal of Immunology*, *200*(1 Supplement), 56.4-56.4.

Crowley, M. T., Costello, P. S., Fitzer-Attas, C. J., Turner, M., Meng, F., Lowell, C., Tybulewicz, V. L. J., & DeFranco, A. L. (1997). A Critical Role for Syk in Signal Transduction and Phagocytosis Mediated by Fcγ Receptors on Macrophages. *The Journal of Experimental Medicine*, *186*(7), 1027–1039.

Davis, S. J., & van der Merwe, P. A. (2006). The kinetic-segregation model: TCR triggering and beyond. *Nature Immunology*, *7*(8), 803–809. https://doi.org/10.1038/ni1369

Dushek, O., Goyette, J., & van der Merwe, P. A. (2012). Non-catalytic tyrosine-phosphorylated receptors. *Immunological Reviews*, *250*(1), 258–276. https://doi.org/10.1111/imr.12008

Dustin, M. L. (2007). Cell adhesion molecules and actin cytoskeleton at immune synapses and kinapses. *Current Opinion in Cell Biology*, *19*(5), 529–533. https://doi.org/10.1016/j.ceb.2007.08.003

Feng, M., Jiang, W., Kim, B. Y. S., Zhang, C. C., Fu, Y.-X., & Weissman, I. L. (2019). Phagocytosis checkpoints as new targets for cancer immunotherapy. *Nature Reviews Cancer*, *19*(10), 568–586. https://doi.org/10.1038/s41568-019-0183-z

Frank, C., Burkhardt, C., Imhof, D., Ringel, J., Zschörnig, O., Wieligmann, K., Zacharias, M., & Böhmer, F.-D. (2004). Effective Dephosphorylation of Src Substrates by SHP-1. *Journal of Biological Chemistry*, *279*(12), 11375–11383. https://doi.org/10.1074/jbc.M309096200

Freeman, S. A., Goyette, J., Furuya, W., Woods, E. C., Bertozzi, C. R., Bergmeier, W., Hinz, B., van der Merwe, P. A., Das, R., & Grinstein, S. (2016). Integrins Form an Expanding Diffusional Barrier that Coordinates Phagocytosis. *Cell*, *164*(1), 128–140. https://doi.org/10.1016/j.cell.2015.11.048

Fütterer, K., Wong, J., Grucza, R. A., Chan, A. C., & Waksman, G. (1998). Structural basis for syk tyrosine kinase ubiquity in signal transduction pathways revealed by the crystal structure of its regulatory SH2 domains bound to a dually phosphorylated ITAM peptide11Edited by D. Rees. *Journal of Molecular Biology*, *281*(3), 523–537. https://doi.org/10.1006/jmbi.1998.1964

Graf, B., Bushnell, T., & Miller, J. (2007). LFA-1-mediated T cell costimulation through increased localization of TCR/class II complexes to the cSMAC and exclusion of CD45 from the immunological synapse. *Journal of Immunology (Baltimore, Md. : 1950)*, *179*(3), 1616–1624.

Hall, A. B., Gakidis, M. A. M., Glogauer, M., Wilsbacher, J. L., Gao, S., Swat, W., & Brugge, J. S. (2006). Requirements for Vav Guanine Nucleotide Exchange Factors and Rho GTPases in FcγR- and Complement-Mediated Phagocytosis. *Immunity*, *24*(3), 305–316. https://doi.org/10.1016/j.immuni.2006.02.005

Hatherley, D., Graham, S. C., Harlos, K., Stuart, D. I., & Barclay, A. N. (2009). Structure of Signal-regulatory Protein α: A link to antigen receptor evolution. *Journal of Biological Chemistry*, *284*(39), 26613–26619. https://doi.org/10.1074/jbc.M109.017566

Huang, Z.-Y., Hunter, S., Kim, M.-K., Indik, Z. K., & Schreiber, A. D. (2003). The effect of phosphatases SHP-1 and SHIP-1 on signaling by the ITIM- and ITAM-containing Fcγ receptors FcγRIIB and FcγRIIA. *Journal of Leukocyte Biology*, *73*(6), 823–829. https://doi.org/10.1189/jlb.0902454

Iqbal, N., & Iqbal, N. (2014). Human Epidermal Growth Factor Receptor 2 (HER2) in Cancers: Overexpression and Therapeutic Implications. *Molecular Biology International*, *2014*. https://doi.org/10.1155/2014/852748

Jacobs, S. A., Diem, M. D., Luo, J., Teplyakov, A., Obmolova, G., Malia, T., Gilliland, G. L., & O'Neil, K. T. (2012). Design of novel FN3 domains with high stability by a consensus sequence approach. *Protein Engineering, Design and Selection*, *25*(3), 107–117. https://doi.org/10.1093/protein/gzr064

Joffe, A. et al. (2020). Macrophage phagocytosis assay with reconstituted target particles. *Nature Protocols*, *In Press*.

Joffe, A. M., Bakalar, M. H., & Fletcher, D. A. (2020). Macrophage phagocytosis assay with reconstituted target particles. *Nature Protocols*, *15*(7), 2230–2246. https://doi.org/10.1038/s41596-020-0330-8

Kant, A. M., De, P., Peng, X., Yi, T., Rawlings, D. J., Kim, J. S., & Durden, D. L. (2002). SHP-1 regulates Fcgamma receptor-mediated phagocytosis and the activation of RAC. *Blood*, *100*(5), 1852–1859.

Kharitonenkov, A., Chen, Z., Sures, I., Wang, H., Schilling, J., & Ullrich, A. (1997). A family of proteins that inhibit signalling through tyrosine kinase receptors. *Nature*, *386*(6621), 181–186. https://doi.org/10.1038/386181a0

Kheir, W. A., Gevrey, J.-C., Yamaguchi, H., Isaac, B., & Cox, D. (2005). A WAVE2-Abi1 complex mediates CSF-1-induced F-actin-rich membrane protrusions and migration in macrophages. *Journal of Cell Science*, *118*(22), 5369–5379. https://doi.org/10.1242/jcs.02638

Kiefer, F., Brumell, J., Al-Alawi, N., Latour, S., Cheng, A., Veillette, A., Grinstein, S., & Pawson, T. (1998). The Syk Protein Tyrosine Kinase Is Essential for Fcγ Receptor Signaling in Macrophages and Neutrophils. *Molecular and Cellular Biology*, *18*(7), 4209–4220.

Köhler, K., Xiong, S., Brzostek, J., Mehrabi, M., Eissmann, P., Harrison, A., Cordoba, S.-P., Oddos, S., Miloserdov, V., Gould, K., Burroughs, N. J., van der Merwe, P. A., & Davis, D. M. (2010). Matched Sizes of Activating and Inhibitory Receptor/Ligand Pairs Are Required for Optimal Signal Integration by Human Natural Killer Cells. *PLoS ONE*, *5*(11). https://doi.org/10.1371/journal.pone.0015374

Li, P., Jiang, N., Nagarajan, S., Wohlhueter, R., Selvaraj, P., & Zhu, C. (2007). Affinity and Kinetic Analysis of Fcγ Receptor IIIa (CD16a) Binding to IgG Ligands. *Journal of Biological Chemistry*, *282*(9), 6210–6221. https://doi.org/10.1074/jbc.M609064200

Lu, J., Ellsworth, J. L., Hamacher, N., Oak, S. W., & Sun, P. D. (2011). Crystal Structure of Fcγ Receptor I and Its Implication in High Affinity γ-Immunoglobulin Binding. *Journal of Biological Chemistry*, *286*(47), 40608–40613. https://doi.org/10.1074/jbc.M111.257550

Machida, K., Thompson, C. M., Dierck, K., Jablonowski, K., Kärkkäinen, S., Liu, B., Zhang, H., Nash, P. D., Newman, D. K., Nollau, P., Pawson, T., Renkema, G. H., Saksela, K., Schiller, M. R., Shin, D.-G., & Mayer, B. J. (2007). High-Throughput Phosphotyrosine Profiling Using SH2 Domains. *Molecular Cell*, *26*(6), 899–915. https://doi.org/10.1016/j.molcel.2007.05.031

Majeti, R., Chao, M. P., Alizadeh, A. A., Pang, W. W., Jaiswal, S., Gibbs, K. D., Rooijen, N. van, & Weissman, I. L. (2009). CD47 Is an Adverse Prognostic Factor and Therapeutic Antibody Target on Human Acute Myeloid Leukemia Stem Cells. *Cell*, *138*(2), 286–299. https://doi.org/10.1016/j.cell.2009.05.045

Malarkannan, S. (2006). The balancing act: Inhibitory Ly49 regulate NKG2D-mediated NK cell functions. *Seminars in Immunology*, *18*(3), 186–192. https://doi.org/10.1016/j.smim.2006.04.002

McKeage, K., & Perry, C. M. (2002). Trastuzumab: A review of its use in the treatment of metastatic breast cancer overexpressing HER2. *Drugs*, *62*(1), 209–243. https://doi.org/10.2165/00003495-200262010-00008

McLarty, K., Cornelissen, B., Scollard, D. A., Done, S. J., Chun, K., & Reilly, R. M. (2009). Associations between the uptake of 111In-DTPA-trastuzumab, HER2 density and response to trastuzumab (Herceptin) in athymic mice bearing subcutaneous human tumour xenografts. *European Journal of Nuclear Medicine and Molecular Imaging*, *36*(1), 81–93. https://doi.org/10.1007/s00259-008-0923-x

Morrissey, M. A., Kern, N., & Vale, R. D. (2020). CD47 Ligation Repositions the Inhibitory Receptor SIRPA to Suppress Integrin Activation and Phagocytosis. *Immunity*, *53*(2), 290-302.e6. https://doi.org/10.1016/j.immuni.2020.07.008

Morrissey, M. A., & Vale, R. D. (2019). CD47 suppresses phagocytosis by repositioning SIRPA and preventing integrin activation. *BioRxiv*, 752311. https://doi.org/10.1101/752311

Mouro-Chanteloup, I., Delaunay, J., Gane, P., Nicolas, V., Johansen, M., Brown, E. J., Peters, L. L., Le Van Kim, C., Cartron, J. P., & Colin, Y. (2003). Evidence that the red cell skeleton protein 4.2 interacts with the Rh membrane complex member CD47. *Blood*, *101*(1), 338–344. https://doi.org/10.1182/blood-2002-04-1285

Neel, B. G., Gu, H., & Pao, L. (2003). The 'Shp'ing news: SH2 domain-containing tyrosine phosphatases in cell signaling. *Trends in Biochemical Sciences*, *28*(6), 284–293. https://doi.org/10.1016/S0968-0004(03)00091-4

Okazawa, H., Motegi, S., Ohyama, N., Ohnishi, H., Tomizawa, T., Kaneko, Y., Oldenborg, P.-A., Ishikawa, O., & Matozaki, T. (2005). Negative Regulation of Phagocytosis in Macrophages by the CD47-SHPS-1 System. *The Journal of Immunology*, *174*(4), 2004–2011. https://doi.org/10.4049/jimmunol.174.4.2004

Oldenborg, P.-A., Zheleznyak, A., Fang, Y.-F., Lagenaur, C. F., Gresham, H. D., & Lindberg, F. P. (2000). Role of CD47 as a Marker of Self on Red Blood Cells. *Science*, *288*(5473), 2051–2054. https://doi.org/10.1126/science.288.5473.2051

Philipsen, L., Engels, T., Schilling, K., Gurbiel, S., Fischer, K.-D., Tedford, K., Schraven, B., Gunzer, M., & Reichardt, P. (2013). Multimolecular Analysis of Stable Immunological Synapses Reveals Sustained Recruitment and Sequential Assembly of Signaling Clusters. *Molecular & Cellular Proteomics*, *12*(9), 2551–2567. https://doi.org/10.1074/mcp.M112.025205

Ren, L., Chen, X., Luechapanichkul, R., Selner, N. G., Meyer, T. M., Wavreille, A.-S., Chan, R., Iorio, C., Zhou, X., Neel, B. G., & Pei, D. (2011). Substrate specificity of protein tyrosine phosphatases 1B, RPTPα, SHP-1, and SHP-2. *Biochemistry*, *50*(12), 2339–2356. https://doi.org/10.1021/bi1014453

Russ, A., Hua, A. B., Montfort, W. R., Rahman, B., Riaz, I. B., Khalid, M. U., Carew, J. S., Nawrocki, S. T., Persky, D., & Anwer, F. (2018). Blocking 'don't eat me' signal of CD47-SIRPα in hematological malignancies, an in-depth review. *Blood Reviews*, *32*(6), 480–489. https://doi.org/10.1016/j.blre.2018.04.005

Scapini, P., Pereira, S., Zhang, H., & Lowell, C. A. (2009). Multiple Roles of Lyn Kinase in Myeloid Cell Signaling and Function. *Immunological Reviews*, *228*(1), 23–40. https://doi.org/10.1111/j.1600-065X.2008.00758.x

Schindelin, J. et al. (2012). Fiji: An open-source platform for biological-image analysis. *Nature Methods*, *9*, 676–682.

Selner, N. G., Luechapanichkul, R., Chen, X., Neel, B. G., Zhang, Z.-Y., Knapp, S., Bell, C. E., & Pei, D. (2014). Diverse Levels of Sequence Selectivity and Catalytic Efficiency of Protein-Tyrosine Phosphatases. *Biochemistry*, *53*(2), 397–412. https://doi.org/10.1021/bi401223r

Sezgin, E., Kaiser, H.-J., Baumgart, T., Schwille, P., Simons, K., & Levental, I. (2012). Elucidating membrane structure and protein behavior using giant plasma membrane vesicles. *Nature Protocols*, *7*(6), 1042–1051. https://doi.org/10.1038/nprot.2012.059

Stebbins, C. C., Watzl, C., Billadeau, D. D., Leibson, P. J., Burshtyn, D. N., & Long, E. O. (2003). Vav1 Dephosphorylation by the Tyrosine Phosphatase SHP-1 as a Mechanism for Inhibition of Cellular Cytotoxicity. *Molecular and Cellular Biology*, *23*(17), 6291–6299. https://doi.org/10.1128/MCB.23.17.6291-6299.2003

Stein, S. C., & Thiart, J. (2016). TrackNTrace: A simple and extendable open-source framework for developing single-molecule localization and tracking algorithms. *Scientific Reports*, *6*, 37947. https://doi.org/10.1038/srep37947

Theocharides, A. P. A., Jin, L., Cheng, P.-Y., Prasolava, T. K., Malko, A. V., Ho, J. M., Poeppl, A. G., van Rooijen, N., Minden, M. D., Danska, J. S., Dick, J. E., & Wang, J. C. Y. (2012). Disruption of SIRPα signaling in macrophages eliminates human acute myeloid leukemia stem cells in xenografts. *Journal of Experimental Medicine*, *209*(10), 1883–1899. https://doi.org/10.1084/jem.20120502

Thompson, K. E., Bashor, C. J., Lim, W. A., & Keating, A. E. (2012). SYNZIP Protein Interaction Toolbox: In Vitro and in Vivo Specifications of Heterospecific Coiled-Coil Interaction Domains. *ACS Synthetic Biology*, *1*(4), 118–129. https://doi.org/10.1021/sb200015u

Tsai, R. K., & Discher, D. E. (2008). Inhibition of "self" engulfment through deactivation of myosin-II at the phagocytic synapse between human cells. *The Journal of Cell Biology*, *180*(5), 989–1003. https://doi.org/10.1083/jcb.200708043

Tsang, E., Giannetti, A. M., Shaw, D., Dinh, M., Tse, J. K. Y., Gandhi, S., Ho, H., Wang, S., Papp, E., & Bradshaw, J. M. (2008). Molecular Mechanism of the Syk Activation Switch. *Journal of Biological Chemistry*, *283*(47), 32650–32659. https://doi.org/10.1074/jbc.M806340200

van de Donk, N. W. C. J., & Usmani, S. Z. (2018). CD38 Antibodies in Multiple Myeloma: Mechanisms of Action and Modes of Resistance. *Frontiers in Immunology*, *9*. https://doi.org/10.3389/fimmu.2018.02134

VanDerMeid, K. R., Elliott, M. R., Baran, A. M., Barr, P. M., Chu, C. C., & Zent, C. S. (2018). Cellular Cytotoxicity of Next-Generation CD20 Monoclonal Antibodies. *Cancer Immunology Research*, *6*(10), 1150–1160. https://doi.org/10.1158/2326-6066.CIR-18-0319

Veillette, A., Thibaudeau, E., & Latour, S. (1998). High Expression of Inhibitory Receptor SHPS-1 and Its Association with Protein-tyrosine Phosphatase SHP-1 in Macrophages. *Journal of Biological Chemistry*, *273*(35), 22719–22728. https://doi.org/10.1074/jbc.273.35.22719

Wakselman, S., Béchade, C., Roumier, A., Bernard, D., Triller, A., & Bessis, A. (2008). Developmental Neuronal Death in Hippocampus Requires the Microglial CD11b Integrin

and DAP12 Immunoreceptor. *Journal of Neuroscience*, *28*(32), 8138–8143. https://doi.org/10.1523/JNEUROSCI.1006-08.2008

Weiskopf, K., Jahchan, N. S., Schnorr, P. J., Cristea, S., Ring, A. M., Maute, R. L., Volkmer, A. K., Volkmer, J.-P., Liu, J., Lim, J. S., Yang, D., Seitz, G., Nguyen, T., Wu, D., Jude, K., Guerston, H., Barkal, A., Trapani, F., George, J., … Sage, J. (2016). CD47-blocking immunotherapies stimulate macrophage-mediated destruction of small-cell lung cancer. *The Journal of Clinical Investigation*, *126*(7), 2610–2620. https://doi.org/10.1172/JCI81603

Willingham, S. B., Volkmer, J.-P., Gentles, A. J., Sahoo, D., Dalerba, P., Mitra, S. S., Wang, J., Contreras-Trujillo, H., Martin, R., Cohen, J. D., Lovelace, P., Scheeren, F. A., Chao, M. P., Weiskopf, K., Tang, C., Volkmer, A. K., Naik, T. J., Storm, T. A., Mosley, A. R., … Weissman, I. L. (2012). The CD47-signal regulatory protein alpha (SIRPa) interaction is a therapeutic target for human solid tumors. *Proceedings of the National Academy of Sciences of the United States of America*, *109*(17), 6662–6667. https://doi.org/10.1073/pnas.1121623109

Xu, M. M., Pu, Y., Han, D., Shi, Y., Cao, X., Liang, H., Chen, X., Li, X.-D., Deng, L., Chen, Z. J., Weichselbaum, R. R., & Fu, Y.-X. (2017). Dendritic Cells but Not Macrophages Sense Tumor Mitochondrial DNA for Cross-priming through Signal Regulatory Protein α Signaling. *Immunity*, *47*(2), 363-373.e5. https://doi.org/10.1016/j.immuni.2017.07.016

Yanagita, T., Murata, Y., Tanaka, D., Motegi, S., Arai, E., Daniwijaya, E. W., Hazama, D., Washio, K., Saito, Y., Kotani, T., Ohnishi, H., Oldenborg, P.-A., Garcia, N. V., Miyasaka, M., Ishikawa, O., Kanai, Y., Komori, T., & Matozaki, T. (2017). Anti-SIRPα antibodies as a potential new tool for cancer immunotherapy. *JCI Insight*, *2*(1), e89140. https://doi.org/10.1172/jci.insight.89140

Yokosuka, T., Takamatsu, M., Kobayashi-Imanishi, W., Hashimoto-Tane, A., Azuma, M., & Saito, T. (2012). Programmed cell death 1 forms negative costimulatory microclusters that directly inhibit T cell receptor signaling by recruiting phosphatase SHP2. *The Journal of Experimental Medicine*, *209*(6), 1201–1217. https://doi.org/10.1084/jem.20112741

Chapter 3: Impact of ITAM multiplicity and ITAM/ITIM combinations on activating-inhibitory signal integration

Introduction

In macrophage phagocytosis, activating Fc receptors drive phagocytosis through phosphorylation of their cytoplasmic ITAM motifs. In humans, ITAMs on Fcγ receptors exist in two configurations (Ben Mkaddem et al., 2019). FcγRIIA and FcγRIIC are each a single transmembrane protein containing one ITAM on the cytoplasmic tail of the extracellular antibody-binding region. In contrast, FcγRIA and FcγRIIIA are complexes composed of three chains: a single alpha-chain, which contains the extracellular antibody-binding domain, and two γ-chains, each of which contain a single ITAM. Though this second category of FcγRs complexes contains two total ITAMs, each chain only contains a single ITAM in both categories.

Interestingly, this is in contrast to the T-cell receptor complex (TCR), which has 10 total ITAMs per receptor (Schamel et al., 2019). The complex consists of two zeta chains containing three ITAMs each, in addition to four chains containing a single ITAM (two ε chains, plus a γ and δ chain). Extensive study of the TCR ITAMs has demonstrated the role of the multiple ITAMs within the complex. For example, using synthetic inducible binding, James showed that while more ITAMs within the TCR didn't increase T-cell activation levels, increasing ITAMs led to more robust, reliable, and synchronized T-cell activation (James, 2018).

Further studies have shed light on the role of ITAMs and ITAM position within the TCR zeta chain specifically. In CAR-T cell studies *in vivo*, Feucht et al. showed that a single ITAM in the CAR zeta chain was sufficient to get effective tumor clearance, but that the position of that ITAM in the most membrane proximal position was critical to robust cell signaling and function (Feucht et al., 2019). This and other studies point to the important of membrane proximity of ITAMs for T-cell activity (Pitcher & van Oers, 2003).

In macrophages, a higher density of ligand drives greater enrichment of FcγRs and their associated ITAMs, and leads to more robust phagocytosis (Zhang et al., 2010). The correlation between increasing local ITAMs and increasing phagocytosis raises the question of whether additional ITAMs on phagocytic receptors could enhance phagocytosis. Recently, Kern et al. showed with synthetically constrained ligands that increasing a number of ITAMs per receptor did not compensate for reduced ligand density (Kern et al., 2021). However, this does not completely address whether and how phagocytosis scales with receptor ITAM multiplicity. Answering this question could have important implications on design and development of future phagocytic CARs and macrophage cell therapies, a rapidly growing area of clinical interest (Klichinsky et al., 2020; Morrissey et al., 2018; Poltavets et al., 2020).

Interestingly, inhibitory receptors such as SIRPα contain multiple inhibitory ITIMs on a single chain, which suggests that motif duplication within a single receptor may be impactful in phagocytic decisions (Barclay & van den Berg, 2014). Furthermore, ITAM-like and ITIM domains co-exist on the cytoplasmic domains of some receptors, such as FCRL5, but impact and regulation of this dual signaling is not understood (Li et al., 2016).

Here, we use synthetic phagocytic receptors containing different numbers of ITAMs to evaluate how ITAM multiplicity impacts phagocytosis. We then explore how inhibitory signaling via CD47-SIRPα interactions is impacted by ITAM multiplicity. Finally, we examine how signals are integrated on receptors containing both ITAM and ITIM motifs.

Results

Phagocytosis does not scale with increasing number of ITAMs on single receptor

To probe the impact of increasing ITAMs on phagocytosis, synthetic receptors were designed that consisted of a Syn18 extracellular binding domain, between 0-4 intracellular ITAM domains, and a C-terminal GFP (Figure 3.1a). The ITAM repeat domain used was from FcγRIIA, and repeats in the synthetic receptors include the 40 amino acid and 10 amino acid regions surrounding the ITAM from the FcγRIIA cytoplasmic tail. RAW 264.7 macrophage-like cell lines expressing each of these receptors were incubated with identical fluorescent target particles coated in Syn17-F3L ligand. Phagocytosis and receptor expression was evaluated per cell, and quantification showed that phagocytosis is not increased by additional ITAMs in series on a phagocytic receptor (Figure 3.1b). Cells of similar receptor expression phagocytose similar average numbers of target particles, regardless of ITAM number.

To assess whether a ITAM multiplicity was sensitive in a specific ligand density regime, we repeated the phagocytosis assay with multiple densities of Syn17-F3L ligand (Figure 3.1c). Overall, phagocytosis decreased with decreasing ligand density, demonstrating that the synthetic receptors respond similarly to endogenous FcγRs to changing antibody densities. Importantly, we see the background eating in the GFP-only control. In two of the four ligand densities, we see a slight increase between the 1xITAM and 2xITAM conditions, indicating that a second ITAM in series may modestly increase phagocytosis. However, addition of a third or fourth ITAM had no effect at any ligand density. This data shows that phagocytosis does not simply scale with ITAM number.

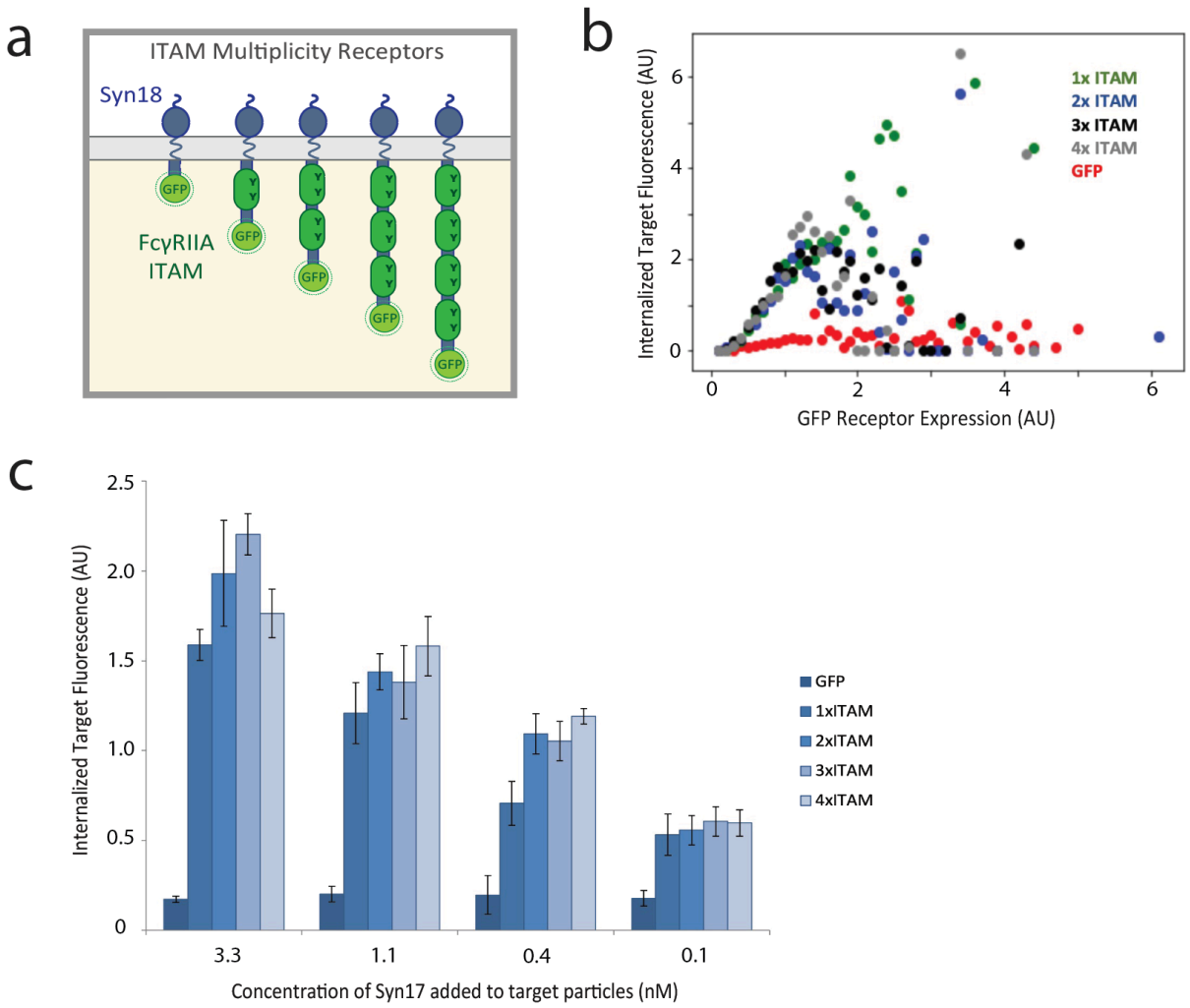

Figure 3.1. Phagocytosis by ITAM multiplicity synthetic receptors. *(a) Schematic of Syn18-ITAM-GFP multiplicity receptors (b) Quantification of phagocytosis by RAW 264.7 cells expressing ITAM multiplicity receptors. Internalized target fluorescence and receptor GFP expression was quantified per cell. Cells are binned by GFP expression, and average phagocytosis for each bin is displayed. (c) Phagocytosis by ITAM multiplicity receptors across many Syn17-F3L ligand densities. Each condition is the average of three independent experiments, representing >300 cells per condition. Bars represent mean ± s.e.m.*

ITAM multiplicity does not significantly diminish CD47 potency

Though ITAM multiplicity did not significantly enhance phagocytosis in response to activating ligand exclusively, we next wondered whether more ITAMs on phagocytic receptors could decrease the impact of inhibitory signaling. As discussed in Chapter 2, the ratio of ITAMs to ITIMs at the phagocytic interface is critical in phagocytosis decisions due their ability to recruit downstream kinases and phosphatases, respectively. Increasing the number of ITAMs on a receptor may enhance Syk recruitment and reduce the impact of SIRPα-bound phosphatases.

To test this, we incubated the ITAM multiplicity cells (with 0-4 ITAMs on synthetic receptors) with target particles containing a fixed amount of Syn17-F3L ligand and increasing densities of CD47. Upon quantifying phagocytosis, we observed that ITAM multiplicity does not enhance phagocytosis in response to CD47 (Figure 3.2). Cells phagocytosed the same number of target particles on average for a given CD47 density, regardless of the number of ITAMs.

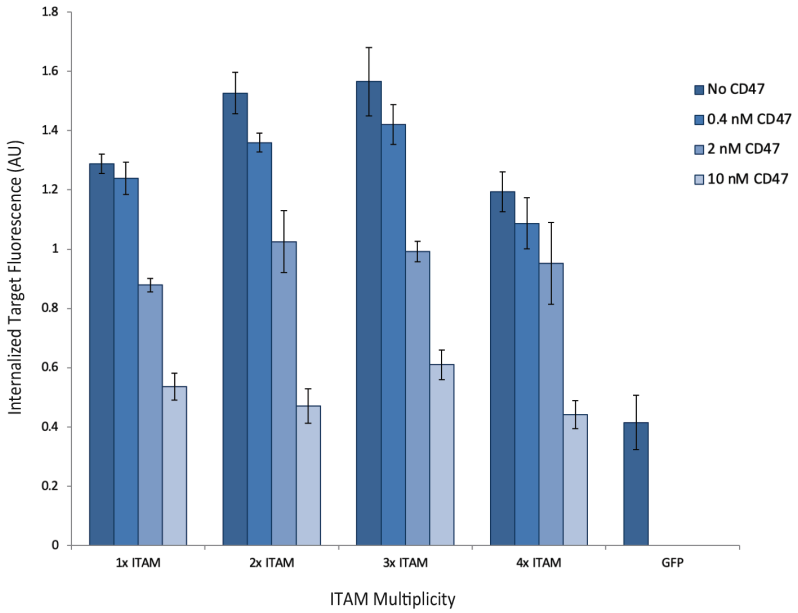

Figure 3.2. Phagocytosis by ITAM multiplicity receptors in response to increasing CD47 target density. *Macrophages were incubated with target particles of fixed Syn17-F3L density and increasing CD47. Each condition is the average of three independent experiments, representing >300 cells per condition. Bars represent mean ± s.e.m.*

Combining ITAM and ITIM motifs on single synthetic receptor ensures fixed ITAM-ITIM ratio

As described in Chapter 2, an antibody:CD47 ratio of at least 10:1 was required for target phagocytosis in our reconstituted phagocytosis assay. To further explore the idea of ITAM:ITIM ratio and motif multiplicity, we next created synthetic receptors with a combination of ITAMs and ITIMs (Figure 3.3). In addition to synthetic Syn18 receptor containing the FcγRIIA ITAM, we created receptors with SIRPα ITIMs, both FcγRIIA ITAM and SIRPα ITIMs, and SIRPα ITIMs with two FcγRIIA ITAMs. We then incubated with fluorescent targets coated in Syn17-F3L and quantified target internalization. We found that SIRPα ITIMs dominate phagocytosis in the combination ITAM/ITIM receptors with both 1xITAM and 2xITAM, which is consistent with the required ITAM:ITIM ratios previously reported. We also found that the SIRPα ITIMs dominate for either ITAM-ITIM order, as we created receptors with both the SIRPα ITIMs and FcγRIIA ITAM membrane proximal.

To test whether this behavior was sensitive to ligand density, we conducted the phagocytosis assay with three different densities of Syn17-F3L ligand. Phagocytosis trends were consistent across all ligand densities, indicating that the SIRPα ITIMs dominance was not density-dependent.

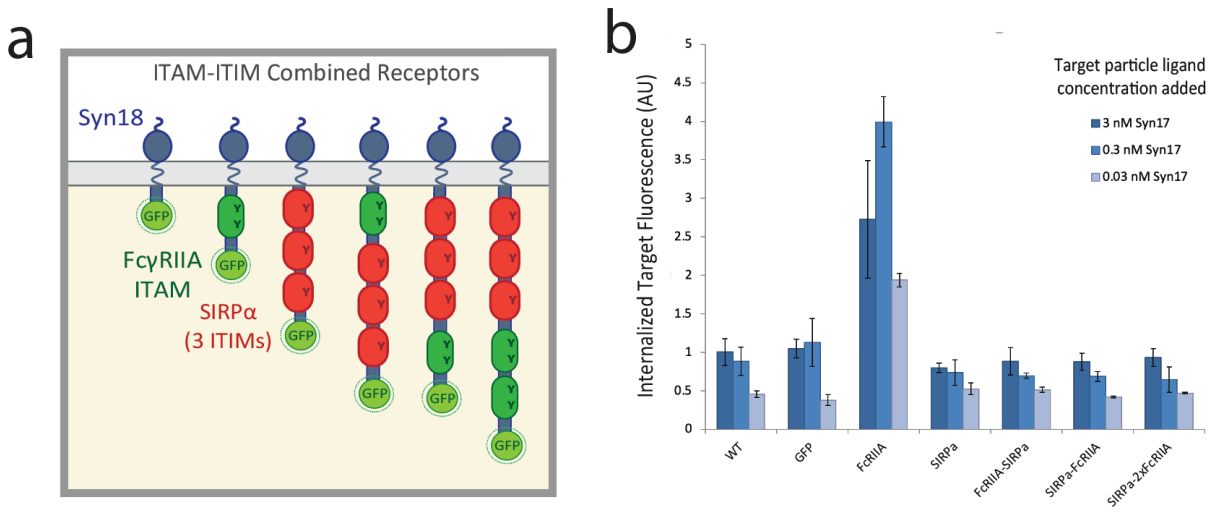

Figure 3.3. Phagocytosis by combined FcγRIIA-SIRPα ITAM-ITIM receptors. *(a) Schematic of combined FcγRIIA ITAM domains and SIRPα ITIM domains on synthetic receptors (b) Phagocytosis of target particles at different Syn17-F3L densities with macrophages expressing Syn18 receptors with varying intracellular signaling combinations. Each condition is the average of three independent experiments, representing >300 cells per condition. Bars represent mean ± s.e.m.*

SIRPα has three ITIMs in its cytoplasmic domain, which likely contributes to its potent ability to shut down FcγRIIA ITAM signaling. To assess if a different inhibitory receptor was similarly potent, we created a new panel of inhibitory and combination receptors using the ITIM domain of FcγRIIB, which contains only one ITIM, and repeated the phagocytosis assay with target particles coated in Syn17-F3L. In contrast to SIRPα receptors, receptors combining FcγRIIA ITAM and FcγRIIB ITIM showed some phagocytosis above background levels. Interestingly, phagocytosis seemed to be dependent on the order of the ITAM and ITIM motifs, as receptors with the FcγRIIA ITAM more membrane proximal phagocytosed more targets.

Finally, we created two additional synthetic receptors with FcγRIIA ITAM and FcγRIIB ITIM, but now mutated the critical tyrosine in the FcγRIIB ITIM. Mutating the ITIMs recovered phagocytosis of targets by these combination receptors, demonstrating that reduced phagocytosis can be attributed to inhibitory signaling by the FcγRIIB ITIM. Both motif orders (ITAM-mutantITIM or mutantITIM-ITAM) exhibited similar levels of phagocytosis, suggesting that the functional FcγRIIA ITAM can signal equally well in either position within the cytoplasmic tail.

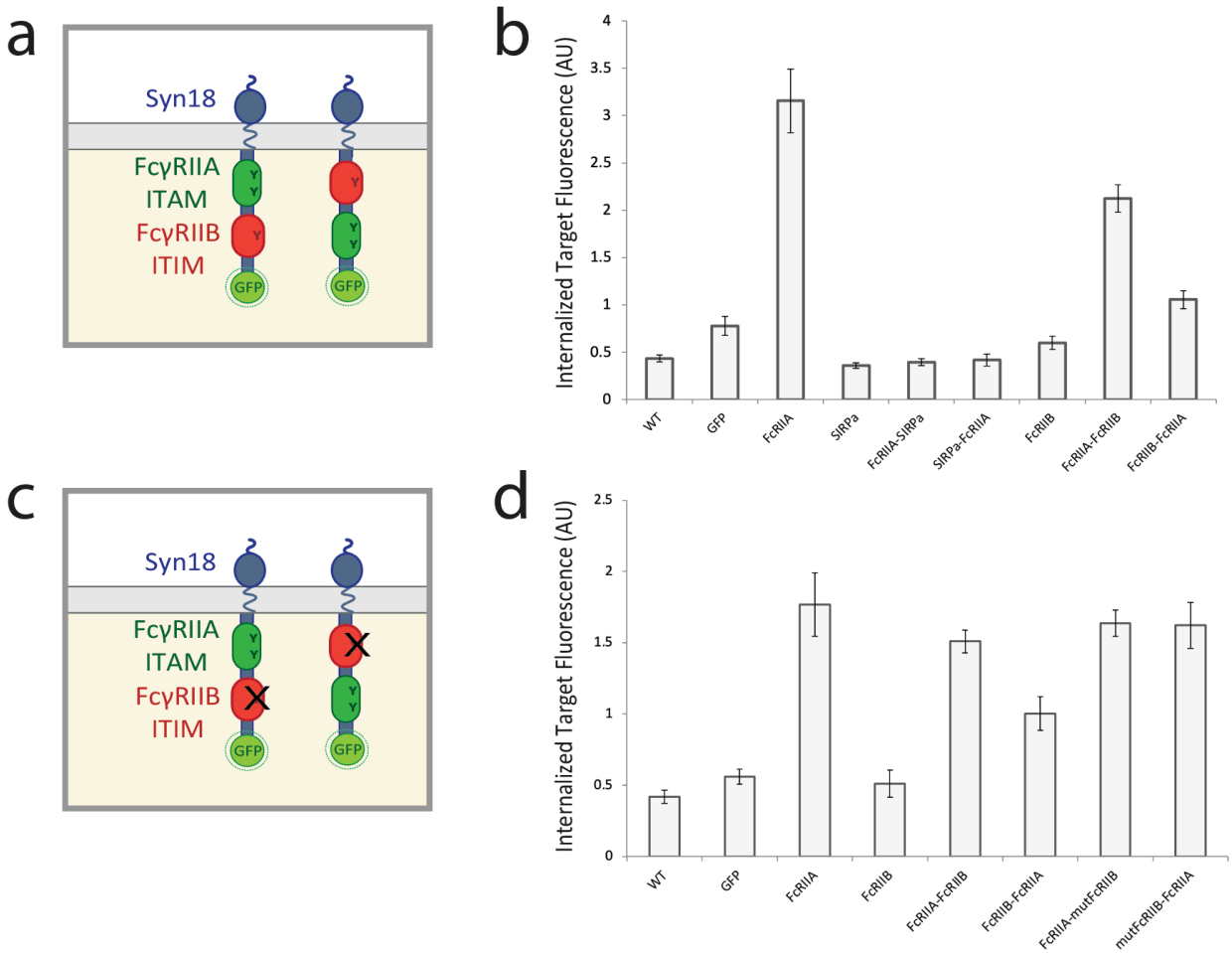

Figure 3. 4. Phagocytosis by combined FcγRIIA- FcγRIIB ITAM-ITIM receptors *(a) Schematic of FcγRIIA- FcγRIIB combined receptor (b) Phagocytosis of Syn17-F3L target particles by ITAM-ITIM receptors. Each condition is the average of three independent experiments, representing >300 cells per condition. Bars represent mean ± s.e.m. (c) Schematic of FcγRIIA- FcγRIIB combined receptors with mutated ITIM tyrosine (b) Phagocytosis of Syn17-F3L target particles by mutant ITAM-ITIM receptors. Each condition is the average of three independent experiments, representing >300 cells per condition. Bars represent mean ± s.e.m.*

Conclusions and Ongoing work

Though it has been examined at length in the context of TCR signaling, ITAM multiplicity is largely unstudied in the context of phagocytic FcγRs. These results demonstrate that phagocytosis does not scale directly with additional ITAMs in series, and that ITAMs in series cannot be used to better overcome inhibitory signaling. Our results with combination ITAM-ITIM receptors also support our previous findings that SIRPα dominates FcγR ITAMs at certain ratios.

The combination receptors containing the FcγRIIA ITAM and FcγRIIB ITIM present an interesting hypothesis on why additional ITAMs in series do not increase phagocytosis. When the FcγRIIA ITAM was closer to the membrane, the macrophages phagocytosed more targets, while macrophages phagocytosed less when FcγRIIB ITIM was closer to the membrane. This suggests that the more membrane proximal domain is more potent. In macrophages, both ITAMs and ITIMs are phosphorylated by membrane by kinase Lyn (Mkaddem et al., 2017). Lyn must be able to access the tyrosines in these motifs, and we might speculate that the further away from the membrane the motif is, the less likely it is to interact with Lyn and hence less likely to become phosphorylated. If ITAMs that are further from the membrane are not phosphorylated, they cannot recruit Syk and will not contribute to downstream phagocytic signaling.

Ongoing experiments aim to test this hypothesis more directly in two ways. First, we will ask if the C-terminus distance from the membrane increases significantly as additional ITAMs are added to the cytoplasmic domain. Using cell surface optical profilometry (CSOP)—a technique developed in our lab for measuring protein height to nm accuracy—we will measure the distance of the C-terminal GFP on our ITAM multiplicity receptors to the membrane (Son et al., 2020). Based on our hypothesis, we expect to see that the C-terminus gets further away from the membrane, thus making it less likely to become phosphorylated.

Second, we will ask if mutating membrane proximal ITAMs changes phagocytosis levels in our multiple ITAM receptors. To do this, we will create additional versions of our 1-4xITAM receptors in which only the C-terminal (furthest from the membrane) ITAM is functional (Figure 3.5a). The rest will have mutated ITAM tyrosines, rendering them non-functional. We expect to see phagocytosis decrease as the sole functional ITAM gets further from the membrane. Additionally, if we fix macrophages interacting with targets and stain for phosphorylation, we expect to see phosphorylation per receptor decrease as the functional ITAM gets further from the membrane.

Should the results of these experiments support our hypothesis, we then hope to develop alternative strategies for increasing ITAMs at a phagocytic interface. Increasing ITAMs at an interface could be an important tool for developing macrophage-based cell therapies, particularly in instances of low target ligand density. Instead of simply chaining more ITAMs in series, we hope to explore at least two additional strategies of increasing ITAM density while keeping ITAMs close to the membrane (Figure 3.5b). First, we will artificially increase ITAMs through lateral clustering. A first attempt at this will involve induced FRB-FKBP dimerization through addition of rapamycin. Second, we will artificially increase membrane proximal ITAM density by introducing a membrane anchor to the C-terminal end of a cytoplasmic ITAM chain. The

membrane anchor would create a cytoplasmic loop, bringing C-terminal ITAMs close to the membrane and increasing their chances of phosphorylation.

In summary, these results begin to suggest a phagocytic paradigm that relies on membrane proximal signaling motifs. We hope that future experiments continue to shed light on this mechanism and provide guidance for leveraging and manipulating phagocytic signaling as a therapeutic strategy.

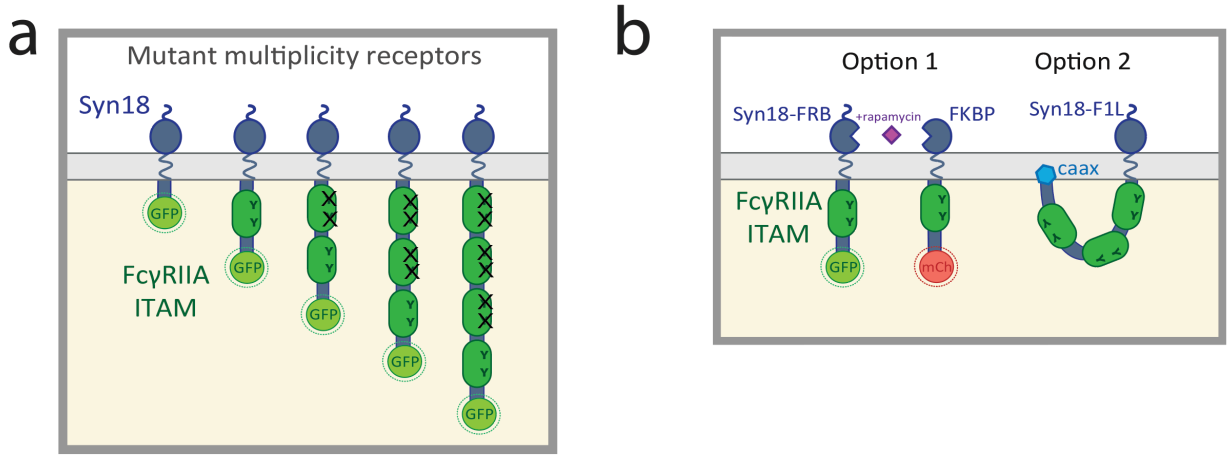

Figure 3.5. Proposed experiments for exploring ITAM multiplicity *(a) Mutating membrane proximal ITAMs will clarify if and how impactful ITAM membrane proximity is. (b) Use of small molecules (option 1) or membrane anchors (option 2) could increase ITAM density while maintaining close ITAM proximity to the membrane.*

Materials and methods

Cell culture

For information on macrophage cell culture, please reference Experimental Models and Subject Details in Chapter 2.

Generation of cell lines

All cell lines were generated in RAW 264.7 macrophage-like cells. For each synthetic receptor design, the 41 amino acid sequence of Syn18 was placed N-terminally to one FNIII domain (Jacobs et al., 2012) to control the height above the membrane of the synthetic receptor protein. The extracellular part was followed by the transmembrane domain of mouse SIRPα (Accession #P97797, amino acid 374-394), followed by intracellular regions of FcγRIIA (Accession #P12318, amino acid 240-317), SIRPα (Accession #P97797, amino acid 395-513), and FcγRIIB (Accession #P08101, amino acid 232-330). In receptors with multiple intracellular ITAM or ITIM domains in series, domain sequences were separated by a six amino acid GGSGGS linker.

For additional methods information, please reference in-depth STAR Method Details in Chapter 2 as follows:

- For receptor design, reference *"Design of synthetic receptors"*
- For macrophage receptor expression, reference *"Generation of stable cell lines"*

Formation of target particles

Please reference in-depth STAR Method Details in Chapter 2 as follows:

- For ligand design and purification, reference *"Purification of Syn17-F3L"*
- For formation of target particles, reference *"Preparation of cell-like reconstituted target particles"*

Phagocytosis of target particles

For method information, please reference *"Target particle phagocytosis assay"* within the STAR Method Details in Chapter 2. Note that to generate data in Figure 3.1b, CellTracker Green was not added to macrophages for imaging. Instead, GFP of the synthetic receptors was imaged and quantified per cell using CellProfiler.

References

Barclay, A. N., & van den Berg, T. K. (2014). The Interaction Between Signal Regulatory Protein Alpha (SIRPα) and CD47: Structure, Function, and Therapeutic Target. *Annual Review of Immunology*, *32*(1), 25–50. https://doi.org/10.1146/annurev-immunol-032713-120142

Ben Mkaddem, S., Benhamou, M., & Monteiro, R. C. (2019). Understanding Fc Receptor Involvement in Inflammatory Diseases: From Mechanisms to New Therapeutic Tools. *Frontiers in Immunology*, *10*. https://doi.org/10.3389/fimmu.2019.00811

Feucht, J., Sun, J., Eyquem, J., Ho, Y.-J., Zhao, Z., Leibold, J., Dobrin, A., Cabriolu, A., Hamieh, M., & Sadelain, M. (2019). Calibration of CAR activation potential directs alternative T cell fates and therapeutic potency. *Nature Medicine*, *25*(1), 82–88. https://doi.org/10.1038/s41591-018-0290-5

Jacobs, S. A., Diem, M. D., Luo, J., Teplyakov, A., Obmolova, G., Malia, T., Gilliland, G. L., & O'Neil, K. T. (2012). Design of novel FN3 domains with high stability by a consensus sequence approach. *Protein Engineering, Design and Selection*, *25*(3), 107–117. https://doi.org/10.1093/protein/gzr064

James, J. R. (2018). Tuning ITAM multiplicity on T cell receptors can control potency and selectivity to ligand density. *Science Signaling*, *11*(531), eaan1088. https://doi.org/10.1126/scisignal.aan1088

Kern, N., Dong, R., Douglas, S. M., Vale, R. D., & Morrissey, M. A. (2021). Tight nanoscale clustering of Fcγ receptors using DNA origami promotes phagocytosis. *ELife*, *10*, e68311. https://doi.org/10.7554/eLife.68311

Klichinsky, M., Ruella, M., Shestova, O., Lu, X. M., Best, A., Zeeman, M., Schmierer, M., Gabrusiewicz, K., Anderson, N. R., Petty, N. E., Cummins, K. D., Shen, F., Shan, X., Veliz, K., Blouch, K., Yashiro-Ohtani, Y., Kenderian, S. S., Kim, M. Y., O'Connor, R. S., … Gill, S. (2020). Human chimeric antigen receptor macrophages for cancer immunotherapy. *Nature Biotechnology*, *38*(8), 947–953. https://doi.org/10.1038/s41587-020-0462-y

Li, H., Borrego, F., Nagata, S., & Tolnay, M. (2016). Fc Receptor–like 5 Expression Distinguishes Two Distinct Subsets of Human Circulating Tissue–like Memory B Cells. *The Journal of Immunology*, *196*(10), 4064–4074. https://doi.org/10.4049/jimmunol.1501027

Mkaddem, S. B., Murua, A., Flament, H., Titeca-Beauport, D., Bounaix, C., Danelli, L., Launay, P., Benhamou, M., Blank, U., Daugas, E., Charles, N., & Monteiro, R. C. (2017). Lyn and Fyn function as molecular switches that control immunoreceptors to direct homeostasis or inflammation. *Nature Communications*, *8*(1), 246. https://doi.org/10.1038/s41467-017-00294-0

Morrissey, M. A., Williamson, A. P., Steinbach, A. M., Roberts, E. W., Kern, N., Headley, M. B., & Vale, R. D. (2018). Chimeric antigen receptors that trigger phagocytosis. *ELife*, *7*, e36688. https://doi.org/10.7554/eLife.36688

Pitcher, L. A., & van Oers, N. S. C. (2003). T-cell receptor signal transmission: Who gives an ITAM? *Trends in Immunology*, *24*(10), 554–560. https://doi.org/10.1016/j.it.2003.08.003

Poltavets, A. S., Vishnyakova, P. A., Elchaninov, A. V., Sukhikh, G. T., & Fatkhudinov, T. Kh. (2020). Macrophage Modification Strategies for Efficient Cell Therapy. *Cells*, *9*(6), 1535. https://doi.org/10.3390/cells9061535

Schamel, W. W., Alarcon, B., & Minguet, S. (2019). The TCR is an allosterically regulated macromolecular machinery changing its conformation while working. *Immunological Reviews*, *291*(1), 8–25. https://doi.org/10.1111/imr.12788

Son, S., Takatori, S. C., Belardi, B., Podolski, M., Bakalar, M. H., & Fletcher, D. A. (2020). Molecular height measurement by cell surface optical profilometry (CSOP). *Proceedings of the National Academy of Sciences*, *117*(25), 14209–14219. https://doi.org/10.1073/pnas.1922626117

Zhang, Y., Hoppe, A. D., & Swanson, J. A. (2010). Coordination of Fc receptor signaling regulates cellular commitment to phagocytosis. *Proceedings of the National Academy of Sciences of the United States of America*, *107*(45), 19332–19337. https://doi.org/10.1073/pnas.1008248107

Chapter 4: Spatial control of signaling through size-dependent re-organization

Introduction

Phagocytic interfaces are facilitated by receptor-ligand interactions, and the size and organization of these receptor-ligand pairs, as well as non-binding proteins and glycoproteins, is critical for phagocytic signaling (Allard et al., 2012; Bakalar et al., 2018; Freeman et al., 2016; Goodridge et al., 2011). Previous work by our lab has demonstrated how short antigens facilitate more efficient phagocytosis: FcRs engaged to short antigen-bound antibodies create a narrower cell-cell interface between the macrophage and the target, thus more efficiently driving exclusion of the tall inhibitory phosphatase CD45 (Bakalar et al., 2018). Interestingly, as described in Chapter 2, the SIRPα-CD47 interface is similarly small (~13 nm), meaning that inhibitory signaling is tuned to be engaged and colocalized to optimal activating signaling interfaces.

Importantly, our work and other previous studies have shown that inhibitory receptors such as SIRPα must be engaged at the phagocytic interface to effectively shut down phagocytosis. By manipulating the extracellular domain of SIRPα, Morrissey et al. showed that the presence of SIRPα at the interface was critical for its inhibitory function, and that increasing SIRPα at an interface could decrease phagocytosis even if SIRPα was not engaged (Morrissey et al., 2020). Hence, proactively removing SIRPα from a phagocytic interface presents an interesting strategy to increase phagocytosis.

Blocking of the SIRPα-CD47 inhibitory checkpoint has become a key target in cancer immunotherapy development (Logtenberg et al., 2020; Russ et al., 2018; Yanagita et al., 2017). More specifically, SIRPα blocking antibodies in development prevent engagement of SIRPα to CD47, thus preventing accumulation of SIRPα at the phagocytic interface. However, this strategy may not actually eliminate phagocytic inhibition due to tonic signaling—or constitutive signaling in a resting state—by SIRPα ITIMs still present at the interface (Fernandes et al., 2020). To eliminate local tonic signaling, SIRPα may need to be completely excluded from the signaling interface.

However, no existing therapies explicitly aim to leverage extracellular size or manipulate spatial organization within a phagocytic interface. Here, we present preliminary results using extracellular size to manipulate spatial organization within an interface and propose a bispecific antibody strategy to exploit this therapeutically.

Results

Addition of tall molecules can drive reorganization of short surface proteins

Previous work from our lab showed that a short non-binding protein can co-exist at synthetic membrane interfaces with receptor-ligand pairs of comparable or greater height (Schmid et al., 2016). However, it is energetically unfavorable for a tall non-binding protein to remain within a short interface, and the tall non-binding protein will move out of the short interface and be segregated from the receptor-ligand pair.

We first asked if addition of a tall molecule to a transmembrane protein with a short extracellular domain could drive the segregation of that short protein from a narrow cell-cell interface. To do this, we created a synthetic receptor consisting of an extracellular Syn18 binding domain and intracellular GFP and expressed this receptor in RAW 264.7 macrophages. The extracellular domain of the synthetic receptor is estimated to extend ~4 nm above the cell surface. When the macrophages were settled on a supported lipid bilayer (SLB) coated in antibody bound to biotinylated lipids, the Syn18-GFP receptor stayed within the interface created by FcγR-antibody interactions (~13 nm tall, Figure 4.1a). The exclusion ratio—the ratio of GFP fluorescence outside the interface footprint to that within the footprint—is approximately 1, showing that there is no significant exclusion of the short GFP receptor.

However, upon addition of a purified tall protein that binds to the synthetic receptor, Syn17-F5L labeled with AlexaFluor555, the short Syn18-GFP receptor moved out of the interface (Figure 4.1b). Syn17-F5L, with its five Fibcon repeats, is estimated to increase the height of the receptor by 15 nm to ~20 nm. The exclusion ratio of the Syn18-GFP receptor increased to 1.9 with the addition of the tall Syn17-F5L, and the exclusion ratio of the Syn17-F5L was over 2.5, highlighting how very little of the tall molecule localized within the footprint (Figure 4.1c). The Syn18-GFP exclusion is lower than the Syn17-F5L because some of the Syn18-GFP receptor is not bound to the tall ligand, and therefore is not excluded. This result was additionally demonstrated using giant plasma membrane vesicles (GPMVs), which allow examination of membrane protein organization without the complexity and contribution of any cytoskeletal activity. These results demonstrate that the addition of tall binders can be used to manipulate membrane protein localization.

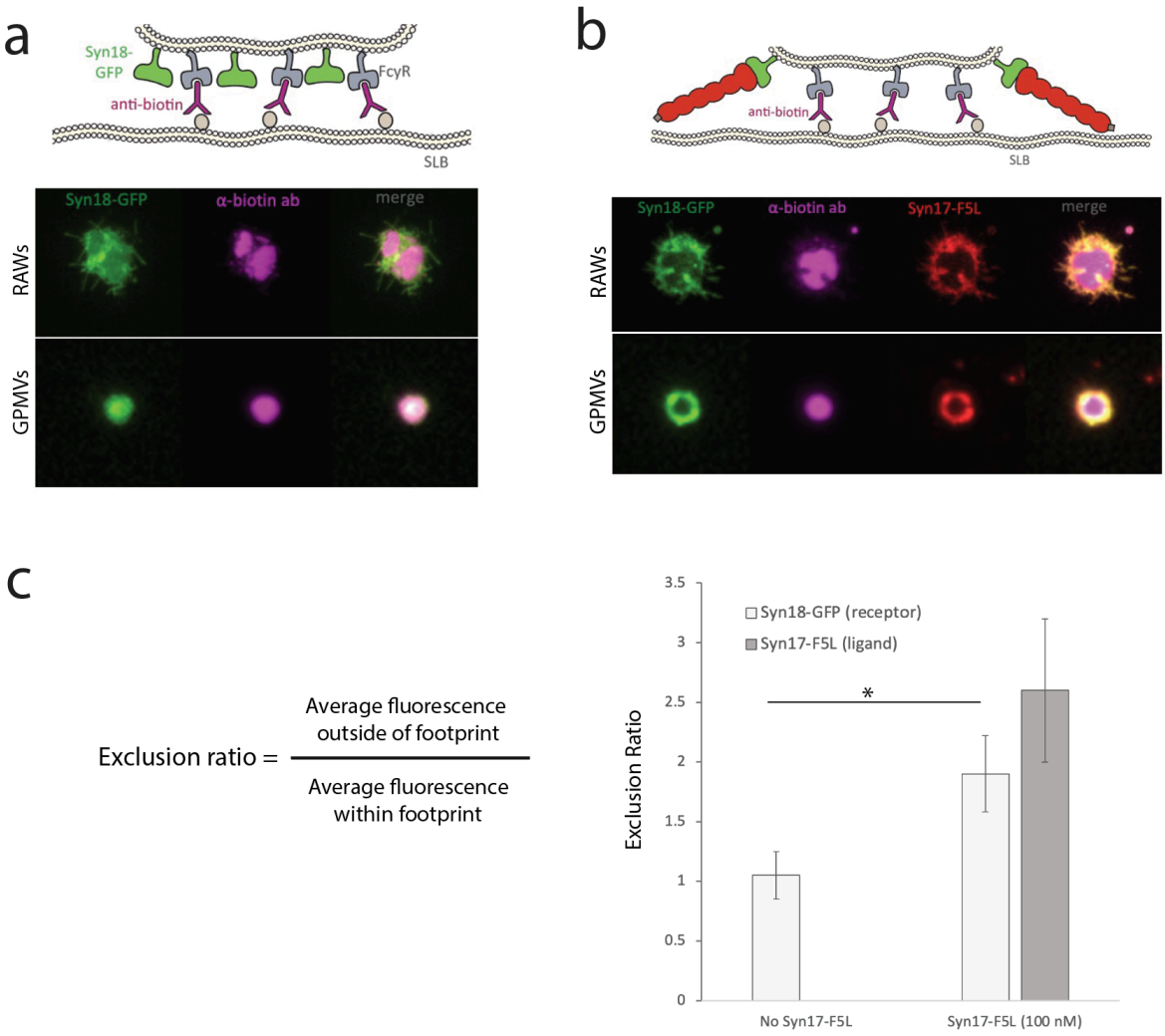

Figure 4.1. Manipulation of protein exclusion from an interface *(a) Cell and GPMV footprints on antibody-coated SLB. Endogenous FcRs engage antibody (magenta) while Syn18-GFP remains unbound. (b) Cell and GPMV footprints on antibody SLB with addition of tall Syn17-F5L binder (red). (c) Quantification of exclusion of GFP and mCherry from cell footprints. Each condition is average of 20 cells. Bars represent mean ± standard deviation.* Conditions were compared with two-tailed student's *t* test, with (*) denoting $p<0.05$.

Coupling of tall and short surface proteins drives reorganization of the short proteins

Next, we wanted to probe whether a tall molecule that is segregated from an interface could shift the localization of a short protein to which it was coupled. To test this, we created two new transmembrane proteins that could be dimerized with addition of the small molecule rapamycin (Figure 4.2a). The first protein was similar to the receptor previously used, a Syn18-GFP receptor, but now with an FRB domain C-terminal to the GFP. The second transmembrane protein had a non-functional F1L extracellular domain and intracellular mCherry, followed by a FKBP domain. These two proteins were co-expressed in RAW 264.7 macrophages. Rapamycin-

induced binding was validated using anti-GFP beads: only in the presence of rapamycin was the mCherry pulled down with the beads (Figure 4.2b).

As above, tall Syn17-F5L (now unlabeled) was added to increase the height of the Syn18-GFP-FRB receptor, and macrophages were settled onto an antibody-coated SLB. With no drug added, the F1L-mCherry-FKBP had an average exclusion ratio of 1.25, indicating that it remained largely in the footprint created by the FcR-antibody interaction. With addition of rapamycin, the F1L-mCherry-FKBP was segregated to the edge of the footprint and the exclusion ratio increased to 1.85 (Figure 4.2c-d), . Though these systems require more thorough characterization, these results support the idea that a short protein could be coupled to a tall protein to move it out of a narrow cell-cell interface where it would normally not be excluded.

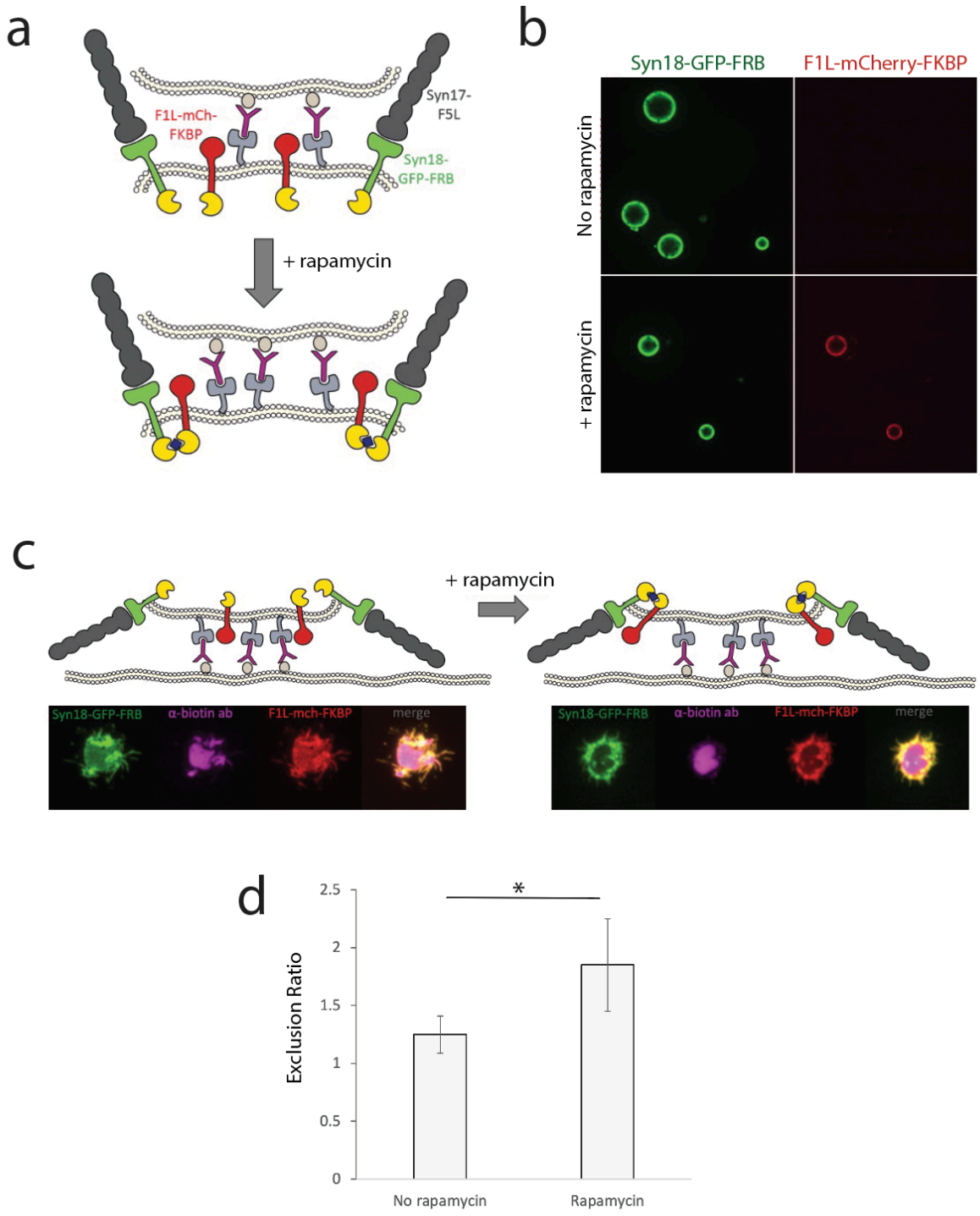

Figure 4. 2. Manipulation of short non-binding proteins within an interface *(a) Schematic of synthetic dimerization system (b) Validation of dimerization via anti-GFP bead binding. Addition of 1 µM rapamycin induces dimerization. (c) Synthetic receptor localization on SLB footprints, ± addition of 1 µM rapamycin (d) Quantification of exclusion of mCherry from cell footprints. Each condition is average of 20 cells. Bars represent mean ± standard deviation.* Conditions were compared with two-tailed student's *t* test, with (*) denoting $p<0.05$.

Design of bi-specific molecules

SIRPα is a relatively short (~10 nm) inhibitory receptor, and upon binding its ligand CD47, the SIRPα-CD47 interface excludes the tall phosphatase CD45 (see Chapter 2). Blocking SIRPα engagement with blocking antibodies or engineered CD47 are important strategies in reducing inhibition in cancer immunotherapy. However, though they prevent engagement, each of these strategies don't prevent SIRPα localization within a phagocytic interface. They also necessitate development of a strong blockers at the CD47 binding site on SIRPα, which eliminates the utility of tight binders of SIRPα that are non-blocking.

Working with collaborators at Aduro Biotech, we designed bispecific antibodies to couple SIRPα to CD45 to actively remove it from phagocytic interfaces (Figure 4.3a). Bispecific combinations were formed from four different monoclonal antibodies. Two different anti-SIRPα clones were used: 18a, which blocks CD47 binding, and 20, which only partially blocks CD47 binding. Using both clones will enable us to answer what role blocking plays in the effectiveness of this strategy. These SIRPα antibodies were combined with anti-CD45 (clone M1/9.3.4.HL.2), as well as a non-binding "dummy" antibody known as B12. Bispecific antibodies were created by Aduro Biotech using Genmab's DuoBody technology. The complete set of monoclonal and bispecific antibodies are shown in Figure 4.3b. Each monoclonal and bispecific antibody has been validated for binding specificity using purified protein targets.

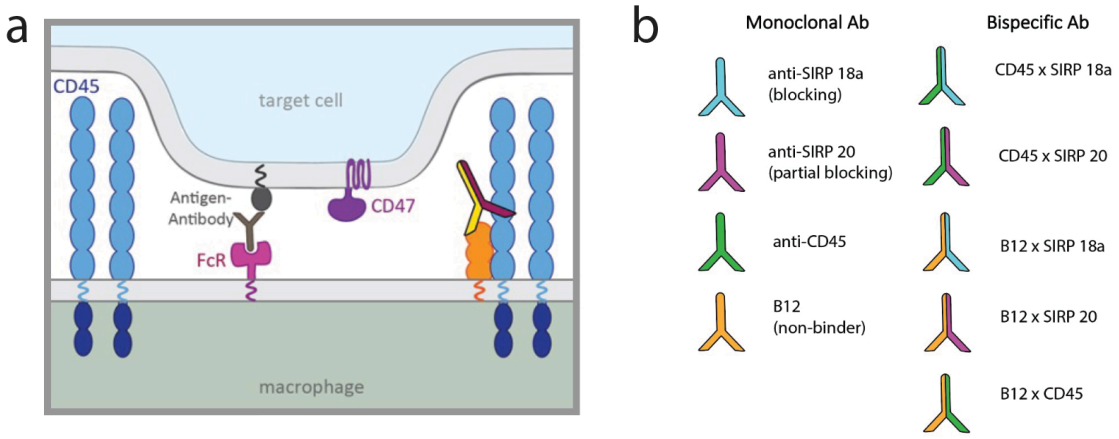

Figure 4.3. SIRPα spatial manipualtion using bispecific antibodies *(a) Schematic of desired clinical effect using SIRPα-CD45 bispecific strategy (b) Schematic of monoclonal and bispecific antibdodies developed in collaboration with Aduro Biotech*

Conclusions and Ongoing work

Using a set of synthetic receptor and protein tools, our results demonstrate that making short extracellular domains taller can change their localization within a cell-cell interface. Furthermore, tethering a protein with a short extracellular domain to a protein with a tall extracellular domain can change the localization of the short protein, driving its exclusion from an interface that it would otherwise remain in. Leveraging this idea, we created a set of bispecific antibodies to couple SIRPα to CD45, promoting SIRPα removal from a phagocytic interface.

Testing and characterization of the bispecific antibodies is ongoing. Broadly, the strategy for evaluating their impact on phagocytosis is:

1. *Determine saturating concentrations of antibody on surface of macrophages:* To do this, we will create saturation curves of antibody on the surface of macrophages. This will help dictate appropriate antibody dosages to utilize in phagocytosis assays.
2. *Assess impact of bispecific on phagocytosis of target particles:* To do this, we will incubate macrophages with target particles coated in antibody and CD47, with and without bispecific antibodies. We will explore a range of antibody-CD47 ratios on these targets, hoping to characterize the range of molecular densities in which this strategy is effective.
3. *Evaluate localization of SIRPα within interface:* To do this, we image bispecific localization when macrophages and macrophage-derived GPMVs are forming an antibody-mediated interface on an SLB.
4. *Assess impact of bispecific on phagocytosis of target cells:* Ultimately, we would like to demonstrate that this bispecific strategy improves clearance of tumor cells. To do this, we will incubate macrophages with hHER2-expressing MC38 cells and quantify phagocytosis with and without bispecific antibodies.

Notably, these experiments must be conducted with bone marrow derived macrophages (BMDMs) from a B6 mouse background because the 18a antibody is specific to B6 SIRPα. The 18a antibody is a poor binder of SIRPα from BALB/c mouse background, from which RAW 264.7 macrophages are derived.

This testing plan will help identify the therapeutic potential of these molecules and help understand if and how they are shifting spatial organization at macrophage-target interfaces. Should they be successful, this presents an interesting new strategy of leveraging extracellular size for manipulating immune interfaces and overcoming inhibitory checkpoints.

Recently, work by Fernandes et al. demonstrated that coupling a different inhibitory receptor, PD-1, to CD45 reduces tonic inhibitory signaling in T-cells by forcing the ITIM next to CD45's phosphatase domain (Fernandes et al., 2020). While the authors show some improvement in phagocytosis using their bispecific molecule (called RIPR) to target SIRPα, they did not examine the receptor localization or deeply probe the potential of this strategy in macrophages. As such, much more investigation is warranted to understand if, how, and why SIRPα-CD45 coupling can be a viable clinically.

Materials and methods

Cell culture

For information on macrophage cell culture, please reference Experimental Models and Subject Details in Chapter 2.

Generation of cell lines

All cell lines were generated in RAW 264.7 macrophage-like cells. For methods information, please reference in-depth STAR Method Details in Chapter 2 as follows:

- For receptor design, reference *"Design of synthetic receptors"*
- For macrophage receptor expression, reference *"Generation of stable cell lines"*

Formation and imaging on SLB

For methods information, please reference in-depth STAR Method Details in Chapter 2 as follows:

- For SLB creation, reference *"Formation of planar SLBs"*
- For GPMV creation, reference *"GPMV formation"*
- For interface imaging, reference *"TIRF imaging of GPMV and cell interfaces"*
- For microscope set-up details, reference *"Imaging techniques"*

Acknowledgements

Eva Schmid contributed greatly to this work through experimental design and idea generation for bispecific antibody development. Many colleagues at Aduro Biotech helped make the bispecific molecules, but we owe a special thank you to Sander van Duijnhoven and Erik Voets.

References

Allard, J. F., Dushek, O., Coombs, D., & Anton van der Merwe, P. (2012). Mechanical Modulation of Receptor-Ligand Interactions at Cell-Cell Interfaces. *Biophysical Journal*, *102*(6), 1265–1273. https://doi.org/10.1016/j.bpj.2012.02.006

Bakalar, M. H., Joffe, A. M., Schmid, E. M., Son, S., Podolski, M., & Fletcher, D. A. (2018). Size-Dependent Segregation Controls Macrophage Phagocytosis of Antibody-Opsonized Targets. *Cell*, *174*(1), 131-142.e13. https://doi.org/10.1016/j.cell.2018.05.059

Fernandes, R. A., Su, L., Nishiga, Y., Ren, J., Bhuiyan, A. M., Cheng, N., Kuo, C. J., Picton, L. K., Ohtsuki, S., Majzner, R. G., Rietberg, S. P., Mackall, C. L., Yin, Q., Ali, L. R., Yang, X., Savvides, C. S., Sage, J., Dougan, M., & Garcia, K. C. (2020). Immune receptor inhibition through enforced phosphatase recruitment. *Nature*, *586*(7831), 779–784. https://doi.org/10.1038/s41586-020-2851-2

Freeman, S. A., Goyette, J., Furuya, W., Woods, E. C., Bertozzi, C. R., Bergmeier, W., Hinz, B., van der Merwe, P. A., Das, R., & Grinstein, S. (2016). Integrins Form an Expanding Diffusional Barrier that Coordinates Phagocytosis. *Cell*, *164*(1), 128–140. https://doi.org/10.1016/j.cell.2015.11.048

Goodridge, H. S., Reyes, C. N., Becker, C. A., Katsumoto, T. R., Ma, J., Wolf, A. J., Bose, N., Chan, A. S. H., Magee, A. S., Danielson, M. E., Weiss, A., Vasilakos, J. P., & Underhill, D. M. (2011). Activation of the innate immune receptor Dectin-1 upon formation of a 'phagocytic synapse.' *Nature*, *472*(7344), 471–475. https://doi.org/10.1038/nature10071

Logtenberg, M. E. W., Scheeren, F. A., & Schumacher, T. N. (2020). The CD47-SIRPα Immune Checkpoint. *Immunity*, *52*(5), 742–752. https://doi.org/10.1016/j.immuni.2020.04.011

Morrissey, M. A., Kern, N., & Vale, R. D. (2020). CD47 Ligation Repositions the Inhibitory Receptor SIRPA to Suppress Integrin Activation and Phagocytosis. *Immunity*, *53*(2), 290-302.e6. https://doi.org/10.1016/j.immuni.2020.07.008

Russ, A., Hua, A. B., Montfort, W. R., Rahman, B., Riaz, I. B., Khalid, M. U., Carew, J. S., Nawrocki, S. T., Persky, D., & Anwer, F. (2018). Blocking 'don't eat me' signal of CD47-SIRPα in hematological malignancies, an in-depth review. *Blood Reviews*, *32*(6), 480–489. https://doi.org/10.1016/j.blre.2018.04.005

Schmid, E. M., Bakalar, M. H., Choudhuri, K., Weichsel, J., Ann, H. S., Geissler, P. L., Dustin, M. L., & Fletcher, D. A. (2016). Size-dependent protein segregation at membrane interfaces. *Nature Physics*, *12*(7), 704–711. https://doi.org/10.1038/nphys3678

Yanagita, T., Murata, Y., Tanaka, D., Motegi, S., Arai, E., Daniwijaya, E. W., Hazama, D., Washio, K., Saito, Y., Kotani, T., Ohnishi, H., Oldenborg, P.-A., Garcia, N. V., Miyasaka, M., Ishikawa, O., Kanai, Y., Komori, T., & Matozaki, T. (2017). Anti-SIRPα antibodies as a potential new tool for cancer immunotherapy. *JCI Insight*, *2*(1), e89140. https://doi.org/10.1172/jci.insight.89140

Chapter 5: Local vs. global signal integration in macrophage phagocytosis

Introduction

Engulfment of a particle in the process of macrophage phagocytosis by definition must occur at the site of the particle itself. Macrophage engagement with the target and subsequent maturation and extension of the phagocytic cup ultimately leads to internalization of the target. As such, it is clear that critical signaling rapidly happens directly at the target interface and that phagocytic cup extension occurs in a highly directional manner (Jaumouillé & Waterman, 2020).

However, it is also known that a macrophage's microenvironment can have important impacts on its overall activity. A prime example of this is the immune-dampening tumor microenvironment (TME), which shifts macrophages to an M2 polarization (Boutilier & Elsawa, 2021). However, these are relatively long-term effects, occurring over the course of many hours or days after macrophages enter the TME. Changes in polarization are also largely driven by immunosuppressive cytokines, such as IL-10 and IL-4, known to be secreted into the TME (Wang et al., 2014).

In addition to polarization-induced changes to Fcγ receptor expression and suppression of effector function (Mendoza-Coronel & Ortega, 2017), macrophage phagocytosis is directly inhibited by engagement of inhibitory receptors, such as SIRPα, which binds to CD47 and shuts down phagocytosis, as described in previous chapters. Less well studied is whether phagocytic efficiency at one target interface is affected by the macrophage's direct contact with inhibitory ligands at another interface. Also poorly understood is whether shorter term inhibitory interactions (on the order of minutes) are impactful. We might expect to see this timescale of cellular interaction from a macrophage migrating through a tissue or into a site of inflammation. Unlike the TME, which acts on long-term resident macrophages, do these transient cell-cell contacts impact a macrophages ability to respond to additional threats? Put differently, is there any evidence of global signal integration happening across many cell-cell contacts, or is phagocytic signal integration only occurring locally, directly at the target site?

To address this question, we use reconstituted cell-like target particles to probe whether the presence of inhibitory target interfaces shifts the ability of macrophages to respond to activating targets. Understanding how macrophages integrate multiple simultaneous stimuli can provide greater understanding of macrophage phagocytosis in a crowded tissue or TME context.

Results

Presence of CD47-coated target particles does not inhibit phagocytosis of antibody-coated target particles, regardless of antibody concentration

To spatially segregate activating and inhibitory signals, we created two populations of target particles with different surface compositions. The activating targets were coated on an SLB containing a biotinylated lipid, to which an anti-biotin antibody was targeted as a pro-phagocytic ligand. The inhibitory targets were coated on an SLB containing a Ni-NTA-conjugated lipid, to which a His-tagged CD47 molecule was attached as an inhibitory ligand (Figure 5.1a). The SLB on the activating particles contained an AlexaFluor-647-labeled lipid, while the SLB on the inhibitory particles contained an LISS-Rhodamine-labeled lipid, so the two target populations could be distinguished when mixed.

The two types of target particle were mixed in equal amounts and added simultaneously to RAW 264.7 cells seeded in 96-well plates. As a control, phagocytosis was also quantified for target populations missing either the activating antibody, the inhibitory CD47, or both. After incubation, cells were imaged, and phagocytosis was quantified by measuring the internalized fluorescence of each bead population. There was no significant change in phagocytosis of activating beads in the presence or absence of CD47-coated targets, indicating that the simultaneous addition of inhibitory targets did not affect the macrophage ability to phagocytose (Figure 5.1b).

To probe whether the effects of inhibitory targets was more potent at low ligand density, we created additional target particles with approximately one third the antibody density. Though overall phagocytosis was lower due to lower ligand density, the presence of CD47-coated targets did not decrease phagocytosis of antibody-coated targets, consistent with previous results (Figure 5.1b).

a

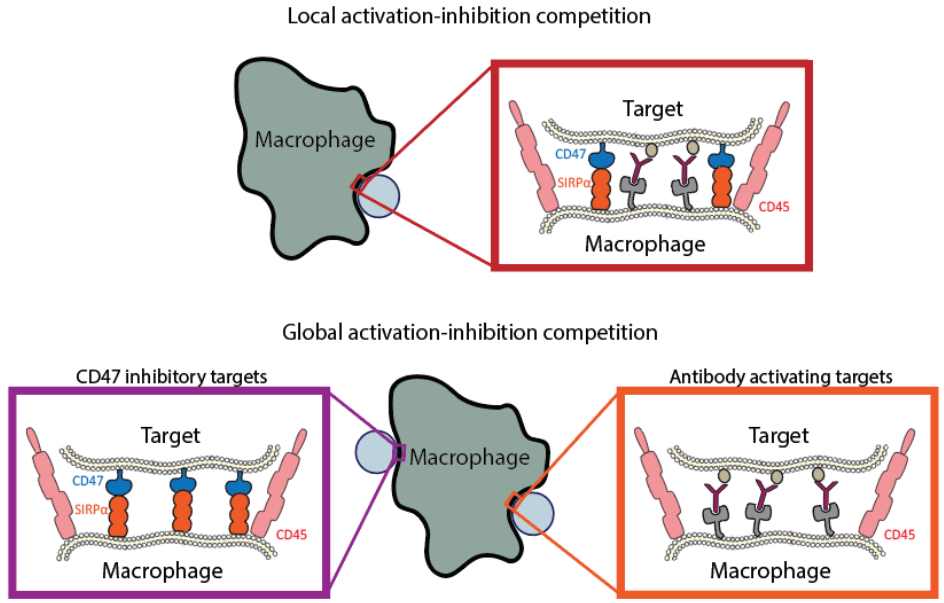
Local activation-inhibition competition
Macrophage
Target
CD47
SIRPα
CD45
Macrophage
Global activation-inhibition competition
CD47 inhibitory targets
Target
CD47
SIRPα
CD45
Macrophage
Macrophage
Antibody activating targets
Target
CD45
Macrophage

b

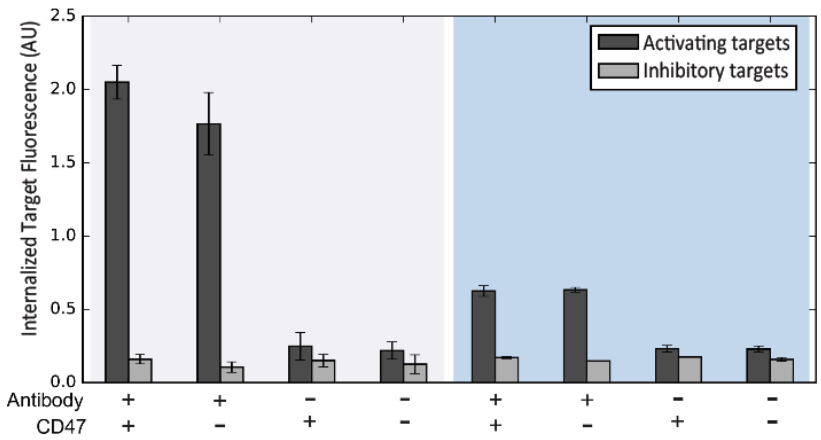
Activating targets
Inhibitory targets
Internalized Target Fluorescence (AU)
2.5
2.0
1.5
1.0
0.5
0.0
Antibody + + − − + + − −
CD47 + − + − + − + −

c

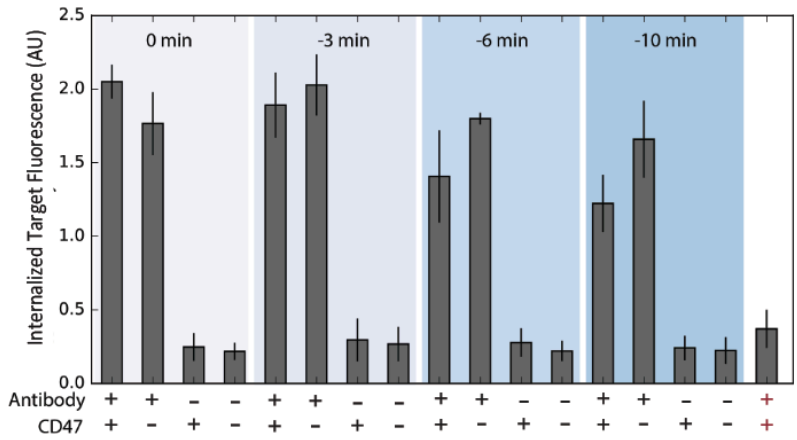
0 min
-3 min
-6 min
-10 min
Internalized Target Fluorescence (AU)
2.5
2.0
1.5
1.0
0.5
0.0
Antibody + + − − + + − − + + − − + + − − +
CD47 + − + − + − + − + − + − + − + − +

Figure 5.1. Phagocytosis of activating targets in the presence of inhibitory targets *(a) Schematic of local versus global activating-inhibitory signal integration (b) Phagocytosis with simultaneous activating and inhibitory target addition. Both activating and inhibitory target internalization is quantified. Left half (light blue) is antibody-coated targets made with 1% biotinylated lipids, while the right half (dark blue) is antibody targets made with 0.33% biotinylated lipids. Each condition is the average of three independent experiments, representing >300 cells per condition. Bars represent mean ± s.e.m. (c) Phagocytosis with staggered activating and inhibitory target addition. Only activating beads are quantified. Activating beads were added 0-10 minutes after inhibitory CD47 beads. Each condition is the average of three independent experiments, representing >300 cells per condition. Bars represent mean ± s.e.m.*

Pre-incubation of inhibitory beads may decrease eating of activating beads in a time-dependent manner

If any global inhibitory effect of a CD47 interface is not immediate, then simultaneous addition of activating and inhibitory targets may enable rapid phagocytosis of activating targets before engagement and inhibition of CD47-coated targets. To examine whether there is a time dependence of inhibitory impact, we staggered the bead addition of CD47- and antibody-coated targets. CD47-coated targets were added to macrophages 0, 3, 6, and 10 minutes prior to addition of antibody-coated targets. Though phagocytosis of antibody-coated targets did fall slightly with longer pre-incubations, there was no significant difference between phagocytosis with and without CD47-coated targets (Figure 5.1c). We hypothesize that this decrease could be due in part to high numbers of bound CD47-coated targets (as many as 15 per macrophage) that limited accessible plasma membrane on the outside of the macrophage.

Importantly, we compared these levels of phagocytosis to that of targets that have both antibody and CD47. These combined targets contained antibody and CD47 in approximately the densities they exist separately on different beads. As expected, phagocytosis of these combined targets was dramatically lower than phagocytosis of antibody-only targets in the presence of CD47 targets, confirming the highly localized inhibitory effect of CD47.

Exposure to CD47 via an SLB does not significantly alter phagocytosis of antibody-coated targets

To eliminate the risk of reduced membrane accessibility by antibody-coated targets as well as increase the time and surface area exposure to CD47, we next exposed macrophages to CD47 via a planar supported lipid bilayer (SLB). CD47 was attached to the planar SLB via Ni-NTA functionalized lipid, as was done with the inhibitory targets. Macrophages were settled onto SLBs with and without CD47 and incubated for 30 minutes prior to the addition of antibody-coated targets (Figure 5.2a). Quantification of fluorescent antibody targets showed no significant difference in phagocytosis when macrophages were exposed to CD47 (Figure 5.2b).

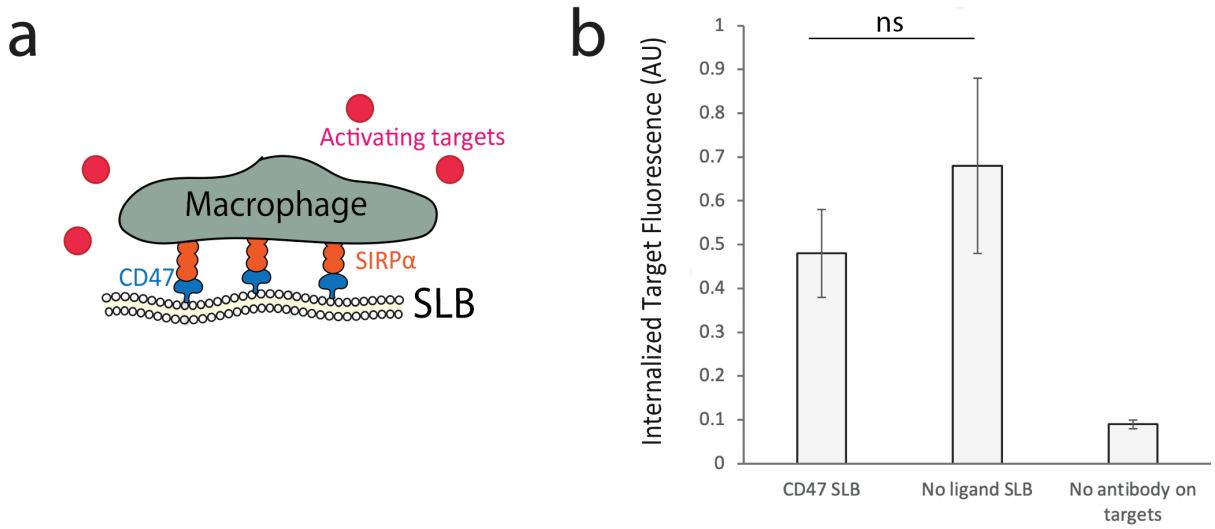

Figure 5.2. Phagocytosis of targets on an SLB *(a) Schematic of target particle addition to cells settled on a CD47-coated SLB (b) Phagocytosis of activating targets while macrophages are engaged on inhibitory or non-signaling SLB. Each condition is the average of three independent experiments, representing >45 cells per condition. Bars represent mean ± s.e.m.* . Conditions were compared with two-tailed student's *t* test.

Conclusions

Macrophage phagocytosis research primarily centers around the formation of a phagocytic cup and internalization of a specific target, but little research has been done on how adjacent or additional target interfaces my impact other phagocytosis events. Our results demonstrate the potency of local signal integration in macrophage phagocytosis. Consistent with research presented in Chapter 2, these results reinforce that macrophage decisions are made locally at each target interface. This conclusion would be further bolstered by additional experiments on SLBs and with longer incubation times with CD47 prior to antibody-coated target addition.

Physiologically, it makes sense in that macrophages need to be able to mobilize defenses directionally and selectively towards diseased or pathogenic cells that pose a threat. Inhibition by adjacent interfaces could jeopardize the macrophage's ability to appropriately clear dangerous entities from tissues. These results also point to the fact that therapeutic manipulation should focus primarily on the local phagocytic interface. Though longer-term changes in receptor expression or polarization are impactful on phagocytosis levels, short term therapeutic interventions should be directed at altering activation-inhibition ratios directly at the target interface.

Materials and methods

Cell culture

For information on macrophage cell culture, please reference Experimental Models and Subject Details in Chapter 2.

Formation of target particles

For in-depth descriptions, please reference STAR Method Details in Chapter 2 as follows:

- For ligand design and purification, reference *"Purification of Syn17-F3L"*
- For formation of target particles, reference *"Preparation of cell-like reconstituted target particles"*

Note that as described above, LISS-Rhodamine lipids were added to fluorescently label activating target particles coated in antibody. Separately, DOPE-647 lipids were used to label inhibitory targets coated in CD47.

Phagocytosis of target particles

For method information, please reference *"Target particle phagocytosis assay"* within the STAR Method Details in Chapter 2. Note that in this Chapter, two colors of target particles—647 for inhibitory and Rhodamine for activating—were imaged. Fluorescence intensity in both channels was quantified using CellProfiler.

Formation and imaging on SLB

For methods information, please reference in-depth STAR Method Details in Chapter 2 as follows:

- For SLB creation, reference *"Formation of planar SLBs"*
- For microscope set-up details, reference *"Imaging techniques"*

References

Boutilier, A. J., & Elsawa, S. F. (2021). Macrophage Polarization States in the Tumor Microenvironment. *International Journal of Molecular Sciences*, *22*(13), 6995. https://doi.org/10.3390/ijms22136995

Jaumouillé, V., & Waterman, C. M. (2020). Physical Constraints and Forces Involved in Phagocytosis. *Frontiers in Immunology*, *11*, 1097. https://doi.org/10.3389/fimmu.2020.01097

Mendoza-Coronel, E., & Ortega, E. (2017). Macrophage Polarization Modulates FcγR- and CD13-Mediated Phagocytosis and Reactive Oxygen Species Production, Independently of Receptor Membrane Expression. *Frontiers in Immunology*, *8*, 303. https://doi.org/10.3389/fimmu.2017.00303

Wang, N., Liang, H., & Zen, K. (2014). Molecular mechanisms that influence the macrophage m1-m2 polarization balance. *Frontiers in Immunology*, *5*, 614. https://doi.org/10.3389/fimmu.2014.00614

Chapter 6: Mapping ITAM phosphorylation states using Syk-SH2 domain kinetics

Introduction

Fc receptors activate phagocytic signaling through phosphorylation of two tyrosines in the FcR ITAM domains (Figure 6.1), which then recruit Syk kinase and initiate downstream signaling (Crowley et al., 1997; Tsang et al., 2008). Each of Syk's two SH2 domains engage with a single ITAM phosphotyrosine, and a flexible linker between the SH2 domains accommodates different spacing between tyrosines within an ITAM (Mócsai et al., 2010). Syk binding to the ITAM releases the kinase domain from its autoinhibited state, enabling it to phosphorylate important downstream molecules in phagocytic machinery.

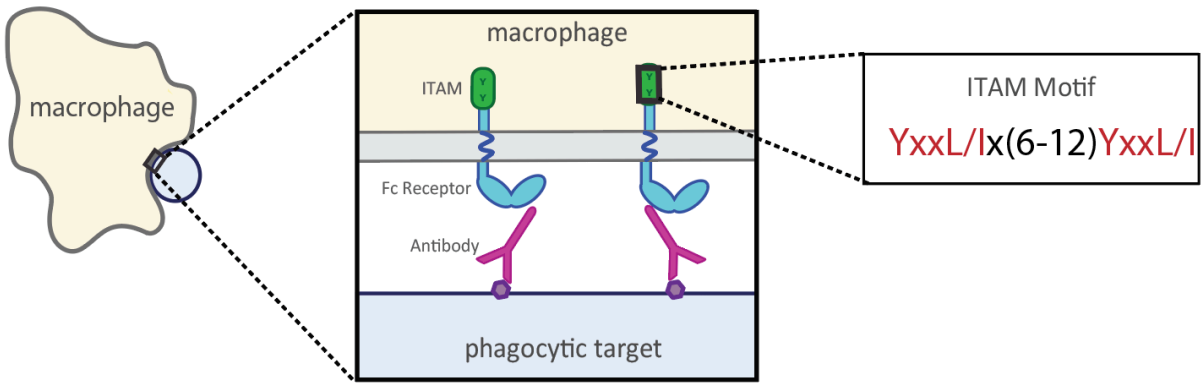

Figure 6.1. Canonical ITAM sequence that facilitates FcR-mediated phagocytosis.

Previous research in the field has characterized Syk SH2 interactions with ITAM sequences. By mutating Syk SH2 domains or by limiting ITAM phosphorylation to specific tyrosines, multiple studies have demonstrated that the Syk SH2 interaction with N-terminal tyrosine is higher affinity than the C-terminal tyrosine, at least for the subset of ITAMs tested (Chen et al., 1996; Fütterer et al., 1998; Shiue et al., 1995). Additionally, Feng and Post used purified SH2 domains to characterize k_{on} and k_{off} of each SH2 domain to individual ITAM tyrosines, and found that the N-terminal tyrosine was almost 6-fold higher affinity than the C-terminal tyrosine in the ITAM (Feng & Post, 2016).

Importantly, mutating ITAM tyrosines have functional consequences in phagocytosis. Mutating either the N- or C-terminal tyrosine dramatically decreases phagocytosis (Mitchell, Marilyn et al., 1994). Additionally, mutating the N-terminal tyrosine has been shown to reduce target particle engagement and FcR clustering (Sobota et al., 2005). Together, these binding and functional studies show that both ITAM tyrosines and both Syk SH2 domains are necessary for

maximal phagocytosis, and that interactions between Syk SH2 domains and ITAM tyrosines are kinetically distinct.

Why are there two tyrosines on the ITAM and why are they kinetically distinct? This question prompted us to wonder whether differential phosphorylation of each ITAM tyrosine could act as a sort of kinetic proofreading. Focused primarily on T cell receptor (TCR) signaling, the idea of kinetic proofreading in immune signaling proposes that T cells can discriminate between targets not just by ligand-TCR engagement but also by monitoring the dynamics of those binding events as well as the dynamics of downstream signaling events (Fehervari, 2019). For example, upon binding, the TCR receptor initiates LAT phosphorylation. LAT has multiple phosphorylation sites, most of which exhibit fast phosphorylation kinetics. However, a glycine at the -1 position to Y132 tyrosine in LAT slows phosphorylation, enabling phosphorylation to happen only when the TCR-ligand interaction is tight enough to maintain a stable complex for a long time (Lo et al., 2019). T cells rely on this slow phosphorylation step to accurately discriminate between self and non-self.

In the context of phagocytosis, we wondered whether the second ITAM tyrosine could be playing this role. FcR-antibody interactions must be strong enough to maintain FcR localization in an interface long enough for membrane-bound kinase Lyn to phosphorylate not just one, but two tyrosine sites. A weak FcR-antibody interaction or a weak antibody-antigen interaction may not maintain that interface long enough for dual phosphorylation to occur. In this case, Syk binding and activation would decrease dramatically, ultimately reducing phagocytosis.

To begin to address this question, we set out to map the phosphorylation states of ITAMs within a phagocytic interface. It is well characterized that FcRs cluster, become phosphorylated, and recruit Syk within the interface, but no attempt has been made to our knowledge to map the distribution of N- versus C- versus dual-phosphorylation of ITAMs within an interface. A spatial map with primarily N-terminal phosphorylation could support the idea of kinetic proofreading by alluding to slower kinetics of C-terminal phosphorylation. Examining phosphorylation differences between tight and weak FcR-antibody engagement could futher shed light on this mechanism.

The lack of phosphorylation mapping is likely in part because distinguishing between phosphorylation states is non-trivial. Staining with commonly used phosphotyrosine antibodies does not provide necessary single receptor resolution, and creating mutant FcRs to isolate phosphorylation states likely alters endogenous phosphorylation patterns.

An alternative strategy is to leverage the kinetic behavior of Syk itself for substrate discrimination. In Figure 6.2, generic protein A binds to protein B, dwells for some period, and then unbinds. By quantifying these parameters, we can enumerate binding events and create a distribution of dwell times. Now, if the state of B changes to B' or B*, protein A will now interact with B differently, and we will alter the binding rate and dwell time distribution of A. If these distributions are distinct enough, we can use this kinetic information to discriminate between states of B.

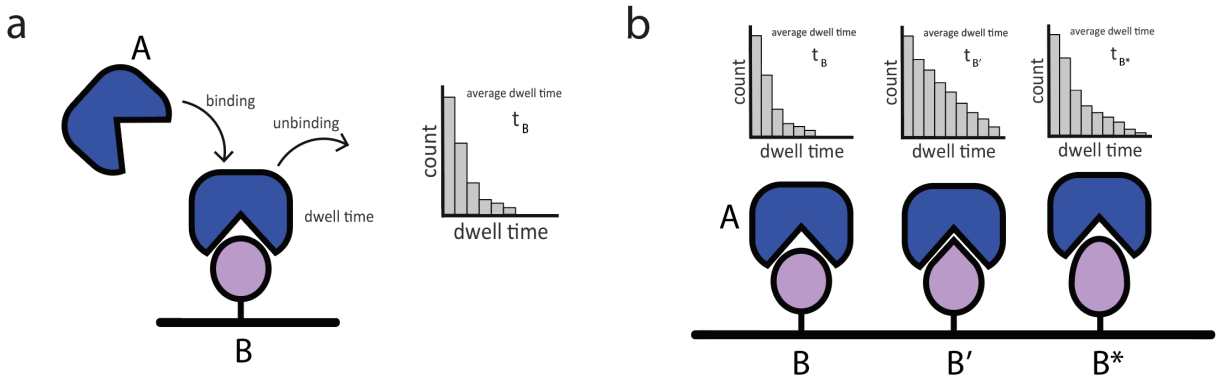

Figure 6.2. Kinetic discrimination between substrate states *(a) Protein A binds protein B at some rate and for a distribution of dwell times (b) Changes to the state of protein B to B' or B* change the binding kinetics of protein A.*

As described previously, the dual Syk SH2 domains have been shown to exhibit distinct kinetic behavior in binding to various ITAM phosphorylation states. Therefore, by quantifying Syk binding kinetics to individual ITAMs, we can theoretically discriminate between phosphorylation states, even in a mixed population of various phosphorylation states. Here, we propose a strategy combining single molecule resolution with kinetic information for mapping phosphorylation within a phagocytic interface. Creation of this map will not only provide insight into phosphorylation distribution within clusters and regions of the phagocytic cup, but it can also help elucidate if and how kinetic proofreading plays a role in FcR signaling and phagocytic efficiency.

Results

ITAM phosphorylation state yields different Syk-SH2 binding profile

The cornerstone of these experiments is the ability to image individual Syk molecules binding and unbinding. To do this, we first purified murine dual Syk-SH2 domains and labeled them with AlexaFluor 555. Notably, we removed the Syk kinase domain for ease of purification and to remove any possibility that the kinase could change phosphorylation state of adjacent receptors during experiments.

Ultimately, we aim to map phosphorylation of endogenous FcRs within a cellular context, but first we must validate that different ITAM phosphorylation states actually yield different kinetics. To do this, we designed four different versions of the same purified ITAM peptide, with each combination of phosphorylation state: YY (no phosphorylation), pYY (N-terminal phosphorylation only), YpY (C-terminal phosphorylation only), and pYpY (dual phosphorylation. Each peptide was manufactured with a biotin on the N-terminus to anchor it to a substrate (Figure 6.3a).

To image Syk binding to the various peptides, we created planar supported lipid bilayers (SLBs) containing biotinylated lipids (Figure 6.3b). Streptavidin was attached to biotinylated lipids, and then peptides were added, followed by fluorescently labeled Syk. Peptides were added at 10-fold lower concentration than streptavidin to limit ITAM clustering from multiple peptides engaging with a single streptavidin. Binding events were imaged using TIRF microscopy at a fast frame rate (100 fps) to obtain high time resolution for binding events. Timelapse images were acquired for all four peptides, plus multiple no-peptide controls (SLB, Syk, and streptavidin only) to aid in removal of background events (Figure 6.3c).

To analyze binding events, timelapse images were imported into Matlab TrackNTrace package. Particle trajectories more than 100 frames or above the mean intensity were then removed, as they were assumed to be non-specific background binding events or clumps of multiple Syk molecules. Dwell time and binding events for each condition were then quantified (Figure 6.1d-e).

Analysis of binding events showed very low background binding in non-peptide controls. Across peptides, a modest increase (~10%) in average dwell time was seen between YpY and pYY, with a greater increase (~60%) occurring between YpY and pYpY dual phosphorylated peptide (Figure 6.1f). However, the more dramatic difference across peptides was seen in the number of binding events, with the pYpY dual phosphorylation increase by 97% of the YY no phosphorylation peptide (Figure 6.1g). This data suggests that dwell time may be less effective at distinguishing between phosphorylation states than binding count.

a

Four purified peptides from GenScript:

- **YY:** *ERPPPVPNPD**Y**EPIRKGQRDL**Y**SGLNQR
- **pYY:** *ERPPPVPNPD(**pY**)EPIRKGQRDL**Y**SGLNQR
- **YpY:** *ERPPPVPNPD**Y**EPIRKGQRDL(**pY**)SGLNQR
- **pYpY:** *ERPPPVPNPD(**pY**)EPIRKGQRDL(**pY**)SGLNQR

Canonical ITAM:
ERPPPVPNPD**YEPIRKGQRDLYSGL**NQR

b

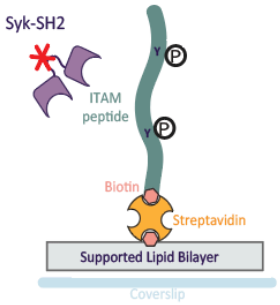

c

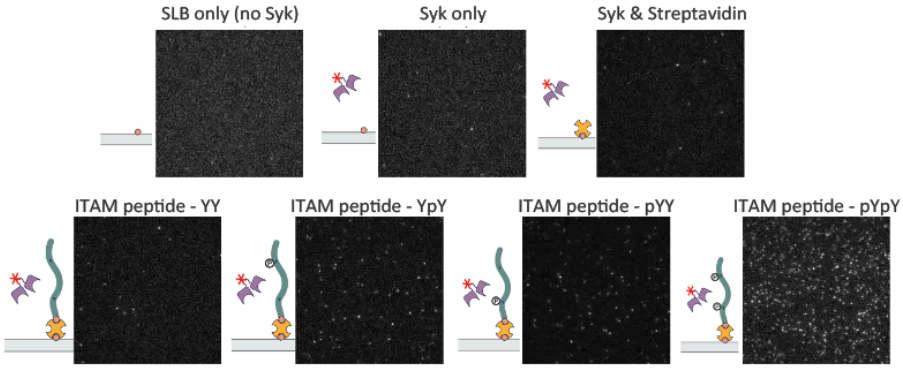

d

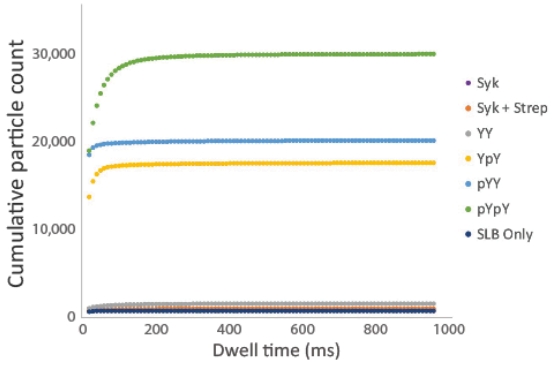

e

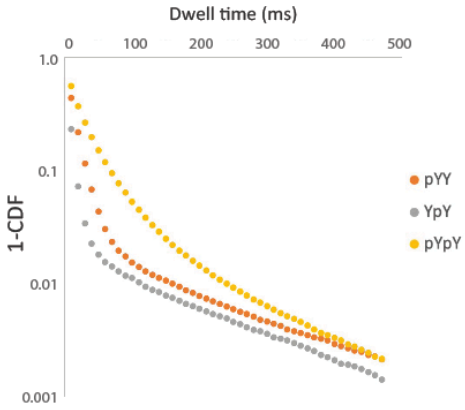

f

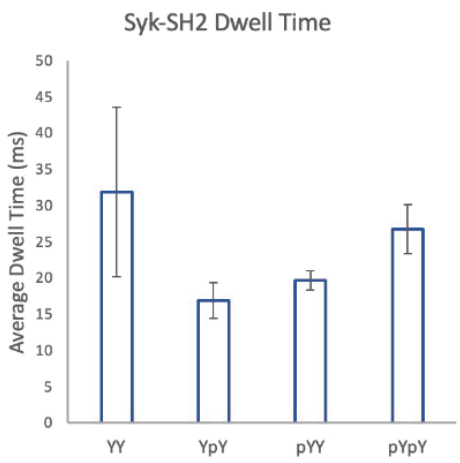

g

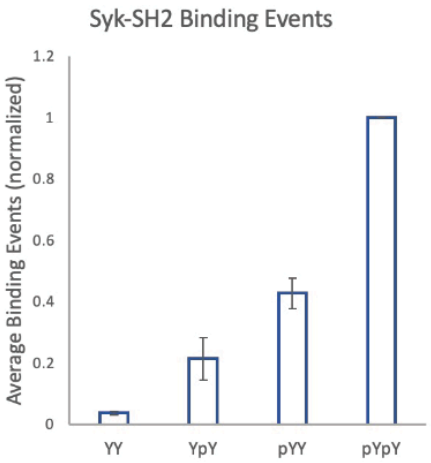

Figure 6.3. Single molecule Syk binding to purified ITAM peptides *(a) Purified peptide sequences. Sequences include some of the surrounding cytoplasmic domain and are biotinylated at the N-terminal end (indicated with *). (b) Schematic of purified peptide experimental set-up on biotin-containing SLB (c) Example frames from peptide binding timelapses, acquired with TIRF microscopy (d) Cumulative binding events per phosphorylation state (e) Cumulative distribution function of dwell times for each phosphorylation state. No phosphorylation YY peptide was omitted due to low event count. (f) Average dwell time of Syk-SH2 to phosphopeptides. Each condition is the average of three independent experiments, representing >3000 binding events. Bars are mean ± s.e.m. (g) Average number of binding events of Syk-SH2 per field of view. Each condition is the average of three independent experiments, representing >30 FOVs. Bars are mean ± s.e.m.*

ITAM phosphorylation state can be validated in fixed macrophages with synthetic ITAM receptors

Next, we sought to test whether phosphorylation state *in vivo* can be distinguished using Syk kinetics. This is difficult to validate using endogenous receptors, since we expect a mixed population of receptors and their phosphorylation states. To reduce some of this complexity, we developed a panel of synthetic receptors with different combinations of ITAM tyrosines mutated to phenylalanine: YY (unmutated), YF (C-terminal tyrosine mutated), FY (N-terminal tyrosine mutated), and FF (both tyrosines mutated). Like previously describe synthetic receptors, the outside of the receptor was a Syn18 binding domain (Figure 6.4a). Each of these receptors was expressed in RAW 264.7 macrophages.

First, to validate the receptors, we conducted a phagocytosis assay, incubating macrophages with target particles coated in Syn17-F3L ligand. Consistent with previous studies, mutation of both tyrosines (Syn18-ITAM-FF) dropped phagocytosis to background levels, while unmutated ITAM receptor (Syn18-ITAM-YY) showed robust phagocytosis (Figure 6.4b). Interestingly, while the N-terminal mutant (Syn18-ITAM-FY) exhibited a decrease in phagocytosis, the C-terminal mutant (Syn18-ITAM-YF) did not decrease from the unmutated receptor. This differs from previously reported studies, that showed mutation of either tyrosine decreases phagocytosis. We speculate this could be due to the fact that the Syn18-Syn17 pair has a higher affinity than endogenous FcR-antibody interactions.

To then probe Syk binding to these receptors, we settled macrophages onto SLBs coated in Syn17-F3L ligand. Cells were fixed on the SLB after 10 minutes, permeabilized, and incubated with purified Syk-SH2-555. Binding events at the cell-SLB interface were then imaged in TIRF.

Analysis of these events showed no significant different in average dwell time across cells expressing the different receptors, with the exception of the C-terminal mutant (Figure 6.4c). We initially expected the trend to follow that of the purified peptides, with the Syn18-ITAM-FY mirroring the YpY peptide and the Syn18-ITAM-YF mirroring the pYY peptide. While dwell time comparisons appear less consistent, quantification of Syk-SH2 binding count more closely mirrors the trend seen with the purified peptides, with increasing binding events from Syn18-

ITAM-FY to -YF to -YY (Figure 6.4d). This data further supports the idea that binding events may be a more accurate way than dwell time to distinguish between ITAM phosphorylation state. More broadly, these experiments also demonstrate that Syk-SH2 binding kinetics is a viable strategy for quantifying receptor phosphorylation in fixed cells.

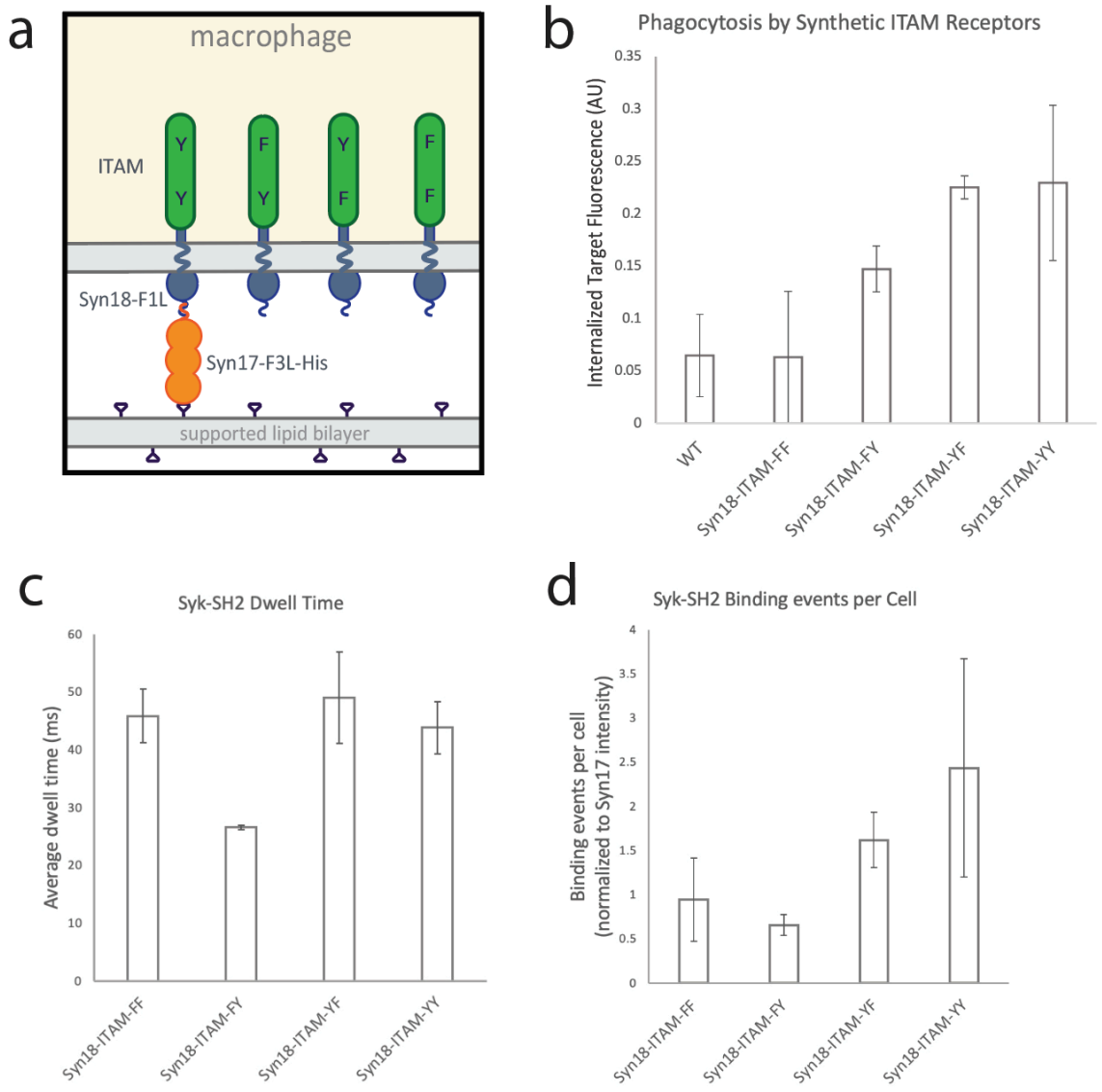

Figure 6.4. Single molecule Syk binding to synthetic ITAM receptors *(a) Schematic of ITAM mutant receptors. Tyrosines were selectively mutated to restrict phosphorylation states. (b) Phagocytosis of Syn17-F3L particles with ITAM-mutant receptors. Each condition is the average of three independent experiments, representing >300 cells per condition. Bars represent mean ± s.e.m. (c) Average dwell time of Syk-SH2 to phosphopeptides. Each condition is the average of three independent experiments, representing >4000 binding events in*

10 cells. Bars are mean ± s.e.m. (d) Average number of binding events of Syk-SH2 per cell. Each condition is the average of three independent experiments, representing >10 cells. Bars are mean ± s.e.m.

ITAM phosphorylation map of endogenous FcRs could yield insight into phagocytic signaling clusters

Lastly, we sought to map phosphorylation state of endogenous FcR ITAMs. To do this, we incubated WT macrophages on antibody coated SLBs, then fixed, permeabilized, and incubated with Syk-SH2-555 (Figure 6.5a-b). In order to distinguish phosphorylation state for individual receptors, we must acquire many binding events per receptor to accurately quantify either dwell time distributions or binding count. As such, we imaged continuously for 3 minutes, acquiring roughly 15,000 frames.

During analysis of these images, instead of simply grouping and averaging all binding events within a frame or cell as was done previously, location of each binding event was mapped to a pixel. Importantly, pixel-based mapping is a first step in developing this pipeline. Future analysis would aim to achieve sub-pixel mapping.

Preliminary maps show the potential of this technique. In Figure 6.5c, each pixel displays the number of binding events that occurred in that pixel, and those binding events can be then further analyzed for additional kinetic parameters such as dwell time (Figure 6.5d). Example pixel clusters also show interesting spatial distribution, with pixels of low Syk binding count surrounding pixels of high Syk binding counts (Figure 6.5e). This points to the idea that this mapping strategy may be useful in understanding phosphorylation within FcR clusters.

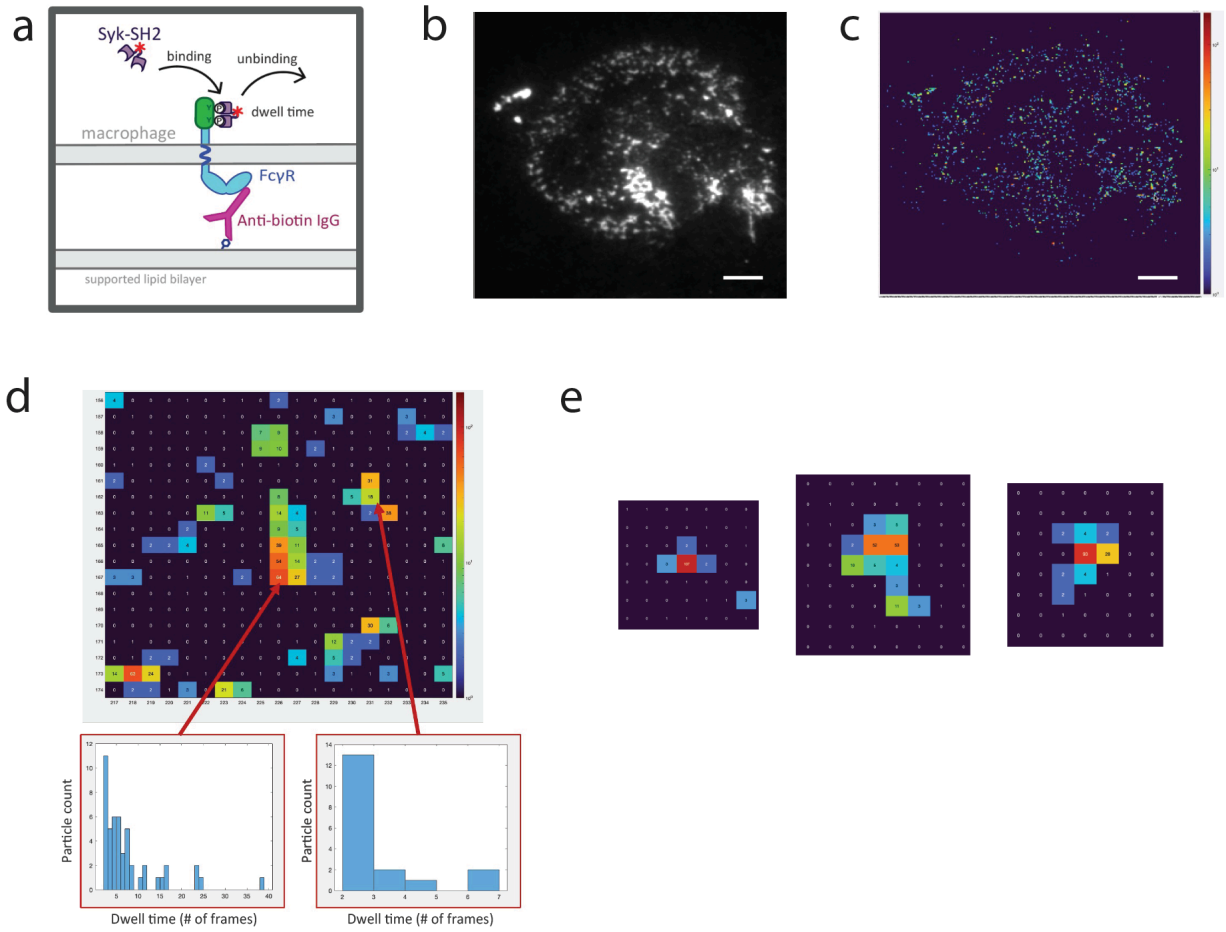

Figure 6.5. Mapping phosphorylation of endogenous ITAMs *(a) Schematic of ITAM Syk interaction at an interface mediated by FcR-antibody interactions. (b) Antibody enriched within macrophage footprint on an antibody-coated SLB. Scale bar is 5 μm. (c) Heatmap of binding event count within the macrophage footprint on the antibody-coated SLB. Binding events are binned to the closest pixel. Heatmap generated in Matlab. Scale bar is 5 μm. (D) Example dwell time distributions from specific pixels. Histograms of dwell time can be plotted from the particles associated to each pixel. (E) Example pixel clusters show spatial variability in binding event count.*

Conclusions and Ongoing work

These results represent an initial proof-of-concept that single molecule imaging can be combined with kinetic information to map variation in a substrate. Phosphorylation of ITAMs is critical to FcR-mediated phagocytosis, and understanding where and when phosphorylation of each ITAM tyrosine occurs could be incredibly helpful in understanding phagocytic machinery.

However, this technique is still very much in its infancy, and key technical challenges need to be overcome. Correcting for stage drift in long timelapses will be critical for accurately associating binding events to the right pixel. Most notably perhaps, a better characterization of the tradeoffs between resolution, dwell time, and various imaging parameters must be conducted to ensure we are obtaining and mapping our highest achievable resolution.

Importantly, we also need to reflect on the viability and utility of this technique for this particular biological question, specifically with regards to resolution and dwell time distributions. First, with respect to resolution, Kern et al. recently showed using DNA origami to artificially define ligand organization that phagocytic receptors showed increased sensitivity down to 3.5 nm spacing (Kern et al., 2021). While spacing within native FcR clusters has not been measured, it is unlikely that single molecule localization techniques, including ours, could identify individual receptors within a cluster of that size. Hence, we need to revisit how we then aggregate binding events for multiple receptors and what insights we can draw from that analysis.

Second, with respect to dwell time, we need to reflect on whether a measure of binding events is sufficient for discrimination between phosphorylation states. The original vision of the project was to differentiate between phosphorylation states based on distinct distributions of dwell time, but it is unclear whether these distributions are distinct enough to distinguish state reliably within a mixed state population. Further analysis and characterization of binding kinetics in purified peptides and synthetic receptors is necessary before proceeding with endogenous receptor mapping.

If more thorough analysis and characterization of this technique proves promising in mapping phosphorylation within a phagocytic interface, we might logically next ask how inhibitory signaling shifts this phosphorylation distribution. We know from our work in Chapter 2 that adjacent ITIM-associated phosphatases dephosphorylate ITAMs. This mapping technique could further that understanding on a highly spatial and molecular scale, providing new and interesting insight into the mechanism of inhibitory signaling.

Materials and methods

Cell culture

For information on macrophage cell culture, please reference Experimental Models and Subject Details in Chapter 2.

Generation of cell lines

All cell lines were generated in RAW 264.7 macrophage-like cells. For methods information, please reference in-depth STAR Method Details in Chapter 2 as follows:

- For receptor design, reference *"Design of synthetic receptors"*
- For macrophage receptor expression, reference *"Generation of stable cell lines"*

Formation and imaging on SLB

For methods information, please reference in-depth STAR Method Details in Chapter 2 as follows:

- For SLB creation, reference *"Formation of planar SLBs"*
- For microscope set-up details, reference *"Imaging techniques"*

ITAM peptide single molecule Syk binding

To conduct ITAM peptide single molecule binding experiments, SLBs were formed from POPC SUVs containing 1% biotinylated lipid. After SLB formation, 20 μg/mL streptavidin in PBS was added to wells and incubated for 5 minutes. Wells were rinsed 4 times with gel filtration buffer (GFB, 20 mM Tris-HCl, 150 mM KCl, 0.5 mM TCEP, 0.1 mM EDTA, pH 7.5). Lyophilized peptides purchased from Genscript were rehydrated in MilliQ water to 2 mg/mL, then diluted to 2 μg/mL in GFB. Peptides were added to wells and incubated for 5 minutes. Wells were then washed 4 times with GFB. Non-specific binding in wells was then blocked using 100 μg/mL casein in GFB, incubated for 5 minutes. Lastly, 0.5 nM Syk-SH2-555 was added with 100 μg/mL casein in GFB.

Wells were imaged immediately after Syk-SH2-55 addition. Timelapse images using a 10 ms exposure were acquired for each peptide condition.

Single molecule tracking analysis

Single molecule binding events were identified and tracked frame-over-frame using Matlab's TrackNTrace package (Stein & Thiart, 2016). Custom Matlab script was then used for post-processing and to calculate dwell times. Post-processing primarily involved the following: a.) removing any tracks that lasted more than 100 frames, as these were assumed to be non-specific adsorption of Syk to the surface or bilayer, b.) removal of binding events that were brighter than one standard deviation above the mean particle brightness, assumed to be clumps of Syk-SH2 protein, and c.) removing any binding events outside of a user-defined ROI. For ITAM peptide biding experiments, no ROI was defined and binding events within the entire field were measured. For cell-based experiments, ROIs were defined around individual cells.

Formation of target particles

Please reference in-depth STAR Method Details in Chapter 2 as follows:

- For ligand design and purification, reference *"Purification of Syn17-F3L"*
- For formation of target particles, reference *"Preparation of cell-like reconstituted target particles"*

Phagocytosis of target particles

For method information, please reference *"Target particle phagocytosis assay"* within the STAR Method Details in Chapter 2.

Macrophage receptor single molecule Syk binding

To image single molecule binding events in cells, macrophages were dropped onto an SLB containing the appropriate ligand (antibody in the case of WT macrophages, Syn17-F3L in the case of Syn18-ITAM receptors). Macrophages were incubated on the SLB for 10 minutes, then fixed with 4% paraformaldehyde in PBS for 10 minutes. Wells were rinsed 5 times with PBS,

then cells were permeabilized with 0.2% Tween-20 in PBS for 10 minutes. After 5 rinses with PBS, non-specific binding was then blocked with 3% BSA and 100 μg/mL casein in GFB for at least 30 minutes. Lastly, 0.5 nM Syk-SH2-555 was added with 100 μg/mL casein in GFB.

Acknowledgements

This work would not have been possible without the scientific and experimental guidance of Andrew Harris. The concept of mapping substrate variation using kinetic differences originate with Andrew, and he contributed greatly to the experimental design and data processing pipelines described above.

References

Chen, T., Repetto, B., Chizzonite, R., Pullar, C., Burghardt, C., Dharm, E., Zhao, Z., Carroll, R., Nunes, P., Basu, M., Danho, W., Visnick, M., Kochan, J., Waugh, D., & Gilfillan, A. M. (1996). Interaction of Phosphorylated FcεRIγ Immunoglobulin Receptor Tyrosine Activation Motif-based Peptides with Dual and Single SH2 Domains of p72syk. *Journal of Biological Chemistry*, *271*(41), 25308–25315. https://doi.org/10.1074/jbc.271.41.25308

Crowley, M. T., Costello, P. S., Fitzer-Attas, C. J., Turner, M., Meng, F., Lowell, C., Tybulewicz, V. L. J., & DeFranco, A. L. (1997). A Critical Role for Syk in Signal Transduction and Phagocytosis Mediated by Fcγ Receptors on Macrophages. *The Journal of Experimental Medicine*, *186*(7), 1027–1039.

Fehervari, Z. (2019). Proving kinetic proofreading. *Nature Immunology*, *20*(6), 665–665. https://doi.org/10.1038/s41590-019-0413-2

Feng, C., & Post, C. B. (2016). Insights into the allosteric regulation of Syk association with receptor ITAM, a multi-state equilibrium. *Physical Chemistry Chemical Physics*, *18*(8), 5807–5818. https://doi.org/10.1039/C5CP05417F

Fütterer, K., Wong, J., Grucza, R. A., Chan, A. C., & Waksman, G. (1998). Structural basis for syk tyrosine kinase ubiquity in signal transduction pathways revealed by the crystal structure of its regulatory SH2 domains bound to a dually phosphorylated ITAM peptide11Edited by D. Rees. *Journal of Molecular Biology*, *281*(3), 523–537. https://doi.org/10.1006/jmbi.1998.1964

Kern, N., Dong, R., Douglas, S. M., Vale, R. D., & Morrissey, M. A. (2021). Tight nanoscale clustering of Fcγ receptors using DNA origami promotes phagocytosis. *ELife*, *10*, e68311. https://doi.org/10.7554/eLife.68311

Lo, W.-L., Shah, N. H., Rubin, S. A., Zhang, W., Horkova, V., Fallahee, I. R., Stepanek, O., Zon, L. I., Kuriyan, J., & Weiss, A. (2019). Slow phosphorylation of a tyrosine residue in LAT optimizes T cell ligand discrimination. *Nature Immunology*, *20*(11), 1481–1493. https://doi.org/10.1038/s41590-019-0502-2

Mitchell, Marilyn, Min-Mei Huang, Paul Chien, & Alan Schreiber. (1994). Substitutions and deletions in the cytoplasmic domain of the phagocytic receptor Fc gamma RIIA: effect on receptor tyrosine phosphorylation and phagocytosis. *Blood*, *84*(9), 3252.

Mócsai, A., Ruland, J., & Tybulewicz, V. L. J. (2010). The SYK tyrosine kinase: A crucial player in diverse biological functions. *Nature Reviews Immunology*, *10*(6), 387–402. https://doi.org/10.1038/nri2765

Shiue, L., Zoller, M. J., & Brugge, J. S. (1995). Syk Is Activated by Phosphotyrosine-containing Peptides Representing the Tyrosine-based Activation Motifs of the High Affinity Receptor for IgE *. *Journal of Biological Chemistry*, *270*(18), 10498–10502. https://doi.org/10.1074/jbc.270.18.10498

Sobota, A., Strzelecka-Kiliszek, A., Gładkowska, E., Yoshida, K., Mrozińska, K., & Kwiatkowska, K. (2005). Binding of IgG-Opsonized Particles to FcγR Is an Active Stage of Phagocytosis That Involves Receptor Clustering and Phosphorylation. *The Journal of Immunology*, *175*(7), 4450–4457. https://doi.org/10.4049/jimmunol.175.7.4450

Stein, S. C., & Thiart, J. (2016). TrackNTrace: A simple and extendable open-source framework for developing single-molecule localization and tracking algorithms. *Scientific Reports*, *6*, 37947. https://doi.org/10.1038/srep37947

Tsang, E., Giannetti, A. M., Shaw, D., Dinh, M., Tse, J. K. Y., Gandhi, S., Ho, H., Wang, S., Papp, E., & Bradshaw, J. M. (2008). Molecular Mechanism of the Syk Activation Switch. *Journal of Biological Chemistry*, *283*(47), 32650–32659. https://doi.org/10.1074/jbc.M806340200

Chapter 7: Concluding Remarks

Immune cells throughout our body are faced with the difficult challenge of identifying and reacting selectively to threats or diseased cells, while minimizing off-target damage to surrounding tissues. As some of the first responders of the innate immune system, macrophages are critical for ridding the body of foreign invaders that could cause disease. Antibody-mediated macrophage phagocytosis is particularly powerful as it provides an important link between the adaptive and innate immune systems, combining the swift action of innate responses with the tuned specificity of antibody selectivity.

The overarching goal of this dissertation has been to better understand the rules that govern macrophage antibody-mediated phagocytic signaling and decisions. In Chapter 2, I describe how we used reconstitution to elucidate ratio-dependent rules that govern ITAM-ITIM signal integration. We further showed that therapeutic antibodies can be leveraged to manipulate that ratio and promote cancer cell clearance. In Chapter 3, I explore how and why additional ITAMs in a phagocytic receptor do not significantly improve phagocytic efficiency. Expanding on these preliminary results could help create important rules for design and development of synthetic phagocytic receptors. In Chapter 4, I propose a strategy to spatially manipulate phagocytic interfaces to enhance phagocytosis, and in Chapter 5, my results demonstrate how local signal integration dominates phagocytic decisions. Lastly, in Chapter 6, I examine ITAM phosphorylation on a single molecule level, presenting initial results for mapping phosphorylation in a phagocytic interface.

Central to many studies within this dissertation was the ability to explore a single biological process—macrophage phagocytosis—across many length scales. Chapter 2, for example, investigates phagocytosis of whole tumor cells, while Chapter 6 dives into Syk signaling at sub-pixel resolution. The ability to span these different scales has enabled me to effectively link molecular mechanism to whole cell functional output in a way that has been enlightening and highly enjoyable.

Similarly, the ability to probe questions on macrophage phagocytosis using many different levels of complexity has allowed for quantitative and mechanistic analysis that would not have been possible otherwise. Reducing complex target cells to reconstituted target particles and simplifying cell-cell interfaces with use of planar SLBs facilitated many of the conclusions drawn here. In Chapter 5, for example, the ability to isolate activating and inhibitory signals to different particles enabled clear interpretation of phagocytosis results that may have been muddled by more complex targets. Importantly, with each study, I was certain to relate simplified systems to more complex physiologically relevant scenarios. This was showcased particularly in Chapter 6, where ITAM complexity increased from purified peptide to synthetic receptors to endogenous FcRs. Examining phagocytosis on these various levels has enabled conclusions that would have been challenging to study solely in native biological systems.

I hope that the work presented here will provide a valuable contribution to the study of macrophage phagocytosis and that it will ultimately help in improving public health. Additionally, I hope that many of the ideas and systems will be expanded and applied to

additional immune cell types and ITAM- or ITIM-bearing receptors. In the remainder of this chapter, I will briefly address ideas or observations that have not yet been discussed that could provide interesting future directions in the study of macrophage phagocytosis.

Macrophage heterogeneity

Throughout this dissertation, I quantify how macrophage phagocytosis behavior changes in response to various stimuli. On average, population trends are very responsive to ligand density, spatial organization, and blocking antibodies. However, within each phagocytosis experiment, heterogeneity exists across macrophages exposed to identical targets. Within a single well, many macrophages will be stuffed with target particles (as many as 30 or more!) while others just a few microns away may have phagocytosed only a few.

There are few potential explanations for this variation. First, the simplest is that exposure to targets is not uniform across the well, and some macrophages simply do not have access to that many targets in the relatively short (20 minute) phagocytosis incubation time. This explanation is unattractive, however, because targets are adding at least a 10-fold excess of macrophages and form an almost continuous layer of targets over much of the well, indicating that access is likely not limited.

More likely, fundamental differences across macrophages in the population is a key source of this variation. Differences in receptor expression, cell cycle state, or adhesion could all contribute to differences in phagocytosis. We can also ask whether heterogeneity across a population is random or whether heterogeneity within a population arises through some coordinated means – and whether it is beneficial in some circumstances. For example, if macrophages are sorted based on level of phagocytosis and then re-challenged with new targets, do high eaters stay as high eaters? Or does some distribution in phagocytosis arise from a previously homogeneous population of high eaters? Exploring these questions could yield interesting insights into macrophage biology.

Macrophage spatial exploration

Through much of this dissertation, I examine phagocytosis as an endpoint—how many particles were eaten after a certain period? What is not captured here is the dynamic process through which macrophages locate and engage target particles in the first place.

Macrophages are extremely active cells, constantly extending long membrane processes into the space around them. Interestingly, these long membrane extensions are capable of initiating phagocytosis. Through timelapse imaging, I have observed macrophages engaging targets up to 15 microns away from the main cell body, and subsequently retracting, pulling the particle, and ultimately engulfing it. These types of observations beg the question of how, where, and why does the macrophage explore the space around it. Is it random or systematic in some way? What

coordinates extension and retraction of this membrane, and how does this machinery change upon engaging a target. Perhaps most importantly, how does this behavior change in a dense, tissue-like environment versus just culture media?

Pilot experiments conducted by Physiology Course students at the Marine Biological Laboratory in Woods Hole, MA, during the summer of 2021 suggested that while actin networks driving the phagocytic cup are known to be Arp2/3-mediated, exploratory macrophage membrane processes may be formin-mediated. However, much more careful study is necessary to describe a definitive mechanism. The preliminary results do, however, point to the possibility that examination of how macrophages find and initiate target engagement could provide important physiological insight into phagocytic decisions.

Alternative phagocytic receptors

FcR-antibody interactions are a key driver of phagocytosis, but additional phagocytic pathways are also critical in ridding the body of threats and maintaining tissue homeostasis (Gordon, 2016). The lipid phosphatidylserine (PS), which is exposed to the outer membrane leaflet in apoptotic cells, is an important mediator for clearance of dead cells. Complement receptors drive phagocytosis of complement-opsonized particles, and pattern recognition receptors engage bacterial ligands, driving their engulfment and clearance. Interestingly, not all these receptors contain the canonical ITAM sequence, indicating that other pathways and molecular players can also drive phagocytosis (Flannagan et al., 2012).

The reconstituted target particles used throughout this dissertation provide a flexible platform to probe alternative phagocytic mechanisms. Preliminary results coating targets in PS-containing SLBs show that macrophages phagocytose target particles in a PS-dependent manner, highlighting that surface composition and activating ligand can be modulated to explore additional pathways. This provides a powerful tool to quantitatively ask if and how different pathways are distinct from Fc-mediated phagocytosis.

Macrophage therapeutic potential

Synthetic macrophage receptors provided a useful tool to isolate and examine phagocytic signaling throughout my dissertation. But engineered phagocytic receptors are also being designed and harnessed in clinical settings as well. In fact, due to their phagocytic abilities, the potential for antigen presentation, manipulatable phenotypes, and tissue penetration, macrophages have become an important focus of various clinical strategies.

Perhaps most exciting is the utilization of macrophages in cell therapy. Chimeric antigen receptor (CAR) T cell therapies have proved to be an effective way to treat various hematologic cancers, but poor tissue penetration by T cells means that these cell therapies fail to clear solid tumors efficiently. In contrast, macrophage ability to enter tissues including tumors makes them

a prime candidate for the next generation of cell therapies. Recently, Klichinsky et al. demonstrated the first use of CAR macrophages directed against human HER2-expressing tumor models in mice (Klichinsky et al., 2020). Based on the success of this study, the first CAR macrophage clinical trial began in February 2021 (ClinicalTrials.gov Identifier: NCT04660929). Results from this trial will certainly influence the future and trajectory of engineered macrophage CAR strategies.

Macrophage receptors drive specificity and effector function, but macrophage polarization is also of key importance in cell therapies (Poltavets et al., 2020). The tumor microenvironment (TME) has been shown to shift macrophages toward anti-inflammatory and immunosuppressive M2 polarization. Ongoing laboratory and clinical research is exploring the possibility of shifting macrophages in the TME from M2 to pro-inflammatory M1 polarization, in the hopes that this stimulates better tumor recognition and clearance. A study by Lee et al. also explored delivery of a pro-apoptotic peptide to M2-polarized macrophages in the TME, selectively killing these detrimental immune cells (Lee et al., 2019). In contrast, promoting M2 polarization may be desirable in mitigating autoimmune diseases, such as atherosclerosis (Bi et al., 2019). Secretion of anti-inflammatory factors by M2 macrophages, such as IL-10 and TGF-b, promotes tissue repair, reduces inflammation, and is associated with atherosclerosis regression.

Interestingly, macrophage polarization is being harnessed as an asset for cell therapy, not only in cancer clearance but also in cancer detection. Aalipour et al. engineered macrophages to produce a synthetic reporter upon adoption of a tumor-associated M2 polarization (Aalipour et al., 2019). The high sensitivity of this cell-based sensor enabled earlier detection of smaller tumors than current clinically-used biomarkers.

Taken together, this sampling of clinical applications highlights the diverse therapeutic utility macrophages could have. As mechanisms of phagocytosis and other key macrophage effector functions become clearer and clearer, our scientific community gains increasing control and better tools to harness these functions in a clinical setting. I have enjoyed being able to contribute to this effort and look forward to continued participation within this community in the future.

References

Aalipour, A., Chuang, H.-Y., Murty, S., D'Souza, A. L., Park, S., Gulati, G. S., Patel, C. B., Beinat, C., Simonetta, F., Martinić, I., Gowrishankar, G., Robinson, E. R., Aalipour, E., Zhian, Z., & Gambhir, S. S. (2019). Engineered immune cells as highly sensitive cancer diagnostics. *Nature Biotechnology*, *37*(5), 531–539. https://doi.org/10.1038/s41587-019-0064-8

Bi, Y., Chen, J., Hu, F., Liu, J., Li, M., & Zhao, L. (2019). M2 Macrophages as a Potential Target for Antiatherosclerosis Treatment. *Neural Plasticity*, *2019*, 6724903. https://doi.org/10.1155/2019/6724903

Flannagan, R. S., Jaumouillé, V., & Grinstein, S. (2012). The cell biology of phagocytosis. *Annual Review of Pathology*, *7*, 61–98. https://doi.org/10.1146/annurev-pathol-011811-132445

Gordon, S. (2016). Phagocytosis: An Immunobiologic Process. *Immunity*, *44*(3), 463–475. https://doi.org/10.1016/j.immuni.2016.02.026

Klichinsky, M., Ruella, M., Shestova, O., Lu, X. M., Best, A., Zeeman, M., Schmierer, M., Gabrusiewicz, K., Anderson, N. R., Petty, N. E., Cummins, K. D., Shen, F., Shan, X., Veliz, K., Blouch, K., Yashiro-Ohtani, Y., Kenderian, S. S., Kim, M. Y., O'Connor, R. S., … Gill, S. (2020). Human chimeric antigen receptor macrophages for cancer immunotherapy. *Nature Biotechnology*, *38*(8), 947–953. https://doi.org/10.1038/s41587-020-0462-y

Lee, C., Jeong, H., Bae, Y., Shin, K., Kang, S., Kim, H., Oh, J., & Bae, H. (2019). Targeting of M2-like tumor-associated macrophages with a melittin-based pro-apoptotic peptide. *Journal for Immunotherapy of Cancer*, *7*, 147. https://doi.org/10.1186/s40425-019-0610-4

Poltavets, A. S., Vishnyakova, P. A., Elchaninov, A. V., Sukhikh, G. T., & Fatkhudinov, T. Kh. (2020). Macrophage Modification Strategies for Efficient Cell Therapy. *Cells*, *9*(6), 1535. https://doi.org/10.3390/cells9061535